2016

Adeno-associated virus-VEGF-165 Mediated Modification of Adipose Derived Stem Cells for Cell Therapy

Upasana Niyogi
Wright State University

Adeno-associated virus-VEGF-165 Mediated Modification of Adipose Derived Stem Cells for Cell Therapy

A thesis submitted in partial fulfillment
of the requirements for the degree of
Master of Science

By

Upasana Niyogi
B.E., M. S. Ramaiah Institute of Technology, Bangalore, India

---

2016
Wright State University

WRIGHT STATE UNIVERSITY
GRADUATE SCHOOL

July 25, 2016

I HEREBY RECOMMEND THAT THESIS PREPARED UNDER MY SUPERVISION BY Upasana Niyogi ENTITLED Adeno-associated virus–VEGF-165 mediated modification of adipose derived stem cells for cell therapy BE ACCEPTED IN PARTIAL FULFILLMENT OF THE REQUIREMENTS FOR THE DEGREE OF Master of Science.

_____

Katherine J.D.A. Excoffon, PhD

Dissertation Director

_____

Barbara Hull, Ph.D.

Director, Microbiology and Immunology

M.S. Program

College of Science and Mathematics

Committee on Final Examination

_____

Katherine JDA Excoffon, Ph.D.

_____

Barbara Hull, Ph.D.

_____

R. Michael Johnson, M.D., FACS.

_____

Robert E. W. Fyffe, Ph.D.

Vice President for Research and

Dean of the Graduate School

ABSTRACT

Upasana Niyogi. M.S. Department of Microbiology and Immunology, Wright State University, 2016. Adeno-associated virus–VEGF-165 mediated modification of adipose derived stem cells for cell therapy

Chronic wounds have become a major clinical and economic burden in our society. New approaches that accelerate wound healing are desperately needed. Angiogenesis and vascularization play a critical role in healing. One of the essential angiogenic factors that promote the formation of vascular beds is vascular endothelial growth factor (VEGF). Moreover, adipose-derived stem cells (ASC), through their regeneration and differentiation properties, may promote healing when transplanted into a wound bed. I have proposed to develop a novel organotypic wound model to facilitate the study of wound healing process. I hypothesize that administration of genetically-modified ASC secreting VEGF via an adeno-associated viral vector serotype (AAV5) directly into the wound site will accelerate rejuvenation of ischemic tissue. To test this hypothesis, the VEGF-165 gene was synthesized (IDT) and cloned (Clontech) into two AAV5 plasmids, pAAV5-CMV-GFP and pAAV5-CAG-GFP and transfected in HEK293, Cos-7 and primary ASC cells for gene expression. Based on the higher transfection efficiency and VEGF secretion in pAAV5-CAG-VEGF-GFP, AAV5-CAG-VEGF-GFP virus was produced by the University of Iowa using the Baculovirus system. I used AAV5-CAG-VEGF-GFP and AAV5-CMV-GFP (control virus) to transduce the ASC. Wound healing assays *in vitro* measured by scratch assay were performed on monolayers of ASC and were observed for healing. *In vivo* wound healing assay was performed on 2mm or 3mm

organotypic wound models by treating them with ASC-AAV5-CAG-VEGF-GFP, ASC-AAV5-CMV-GFP, non-transduced ASC or ASC media. *In vitro* wound healing assays showed complete closure of non-transduced ASC in three days whereas the ASC-AAV5-CAG-VEGF-GFP healed within two days indicating the efficiency of VEGF in accelerating closure. *In vivo* wound healing assays on organotypic wounds showed some closure in wounds treated with ASC compared to control wounds treated with media alone. However wounds treated with ASC-AAV5-CAG-VEGF-GFP facilitated enhanced in complete closure compared to non-transduced ASC-treated wounds. No significant difference was observed between ASC-AAV5-CMV-GFP or non-transduced ASC treated wounds. We observed similar results in both 2 mm or 3 mm wounded models and with autologous or allogenic stem cells. Moreover, red light therapy (670 nm) also caused partial closure of wounds. Future studies should involve personalization of the wound model system depending on patient's disease condition and developing ASC therapy with a cocktail of growth factors that can facilitate complete wound closure.

Table of Contents

Table of Figures

ACKNOWLEDGMENTS

I would like to thank Dr. Katherine Excoffon for her tremendous support, guidance, care and concern for completion of my project and my successful future. I would also like to thank all of my thesis committee members, Dr. Katherine Excoffon, Dr. Barbara Hull and Dr. R. Michael Johnson for providing valuable guidance and suggestions. I would like to express my gratitude to Dr. Michael Johnson and his lab members from Miami Valley Hospital, especially Greg Gould and Filip Polanokovic for providing me with the adipose derived stem cells and the wound models which formed the base of my thesis. I would also like to acknowledge Dr. Sunishka M. Wimalawansa and Greg Gould for training me in flow cytometry technique. I would like to thank all of Dr. Excoffon laboratory members, Dr. Priyanka Sharma, Mahmoud Alghamri, James Mathew Readler, Ibrahim Alkhomsi, Nathan Andrew Northern, Timothy Lee Williamson, past members, Jonathan Bowers and Shon Jergens and summer stream student, Andrew Mogga for their help and suggestions. I would specially like to thank Dr. Priyanka Sharma for guiding me in each step of my thesis and training me in the techniques used in the project. I would like to thank my family and all my friends for their immense support. Last but not the least, my acknowledgement goes to Microbiology and Immunology M.S. program, Biological Sciences Department , College of Science and Mathematics, Boonshoft School of Medical Science and the Plastic Surgery Foundation for funding parts of this research.

DEDICATION

This is dedicated to

My parents, ***Sanjay Kumar Niyogi & Arpita Niyogi***

My grandparents: ***Late Dr. Saroj Kumar Niyogi, Mrs. Rekha Niyogi***

Mr. Gurusadaya Sur & Pratima Sur

And

My love, ***Satya Sai Sudhir Ayyagari***

You make all the sacrifice worth it

Chapter 1: Introduction

1.1. Human Skin

The human skin is the largest organ in the body with a surface area of 1.8 m^2 and accounting for almost 15% of the total human body weight (Kanitakis *et al*., 2002). The primary function of skin is for thermoregulatory maintenance of the body temperature and also as a physical barrier protecting the body from chemicals, ultraviolet radiation, toxins, microorganisms, trauma and injury (Elias *et al*., 2005). Skin also plays a role in sensing touch, pain, temperature and in immune regulation.

Skin consists of two layers epidermis and dermis separated by the basement membrane (shown in figure 1). The epidermis is the outer layer of the skin which is constantly shedding and regenerating and acts as a protective barrier. The inner layer of the skin, the dermis, is embedded in the third layer and acts as an insulator, providing structural support to the skin (Breitkreutz *et al.*, 2013).

1.1.1. Epidermis

Epidermis is the outer layer of the skin made up of multilayered epithelium. The five distinct sublayers of the epidermis are called the stratum corneum, stratum lucidum, stratum granulosum, stratum spinosum, and stratum basale. The predominant cells of the epidermis are keratinocytes that synthesize keratin. Under normal circumstances the only mitotically active layer of the epidermis is the basal layer (Blanpain *et al.*, 2006).

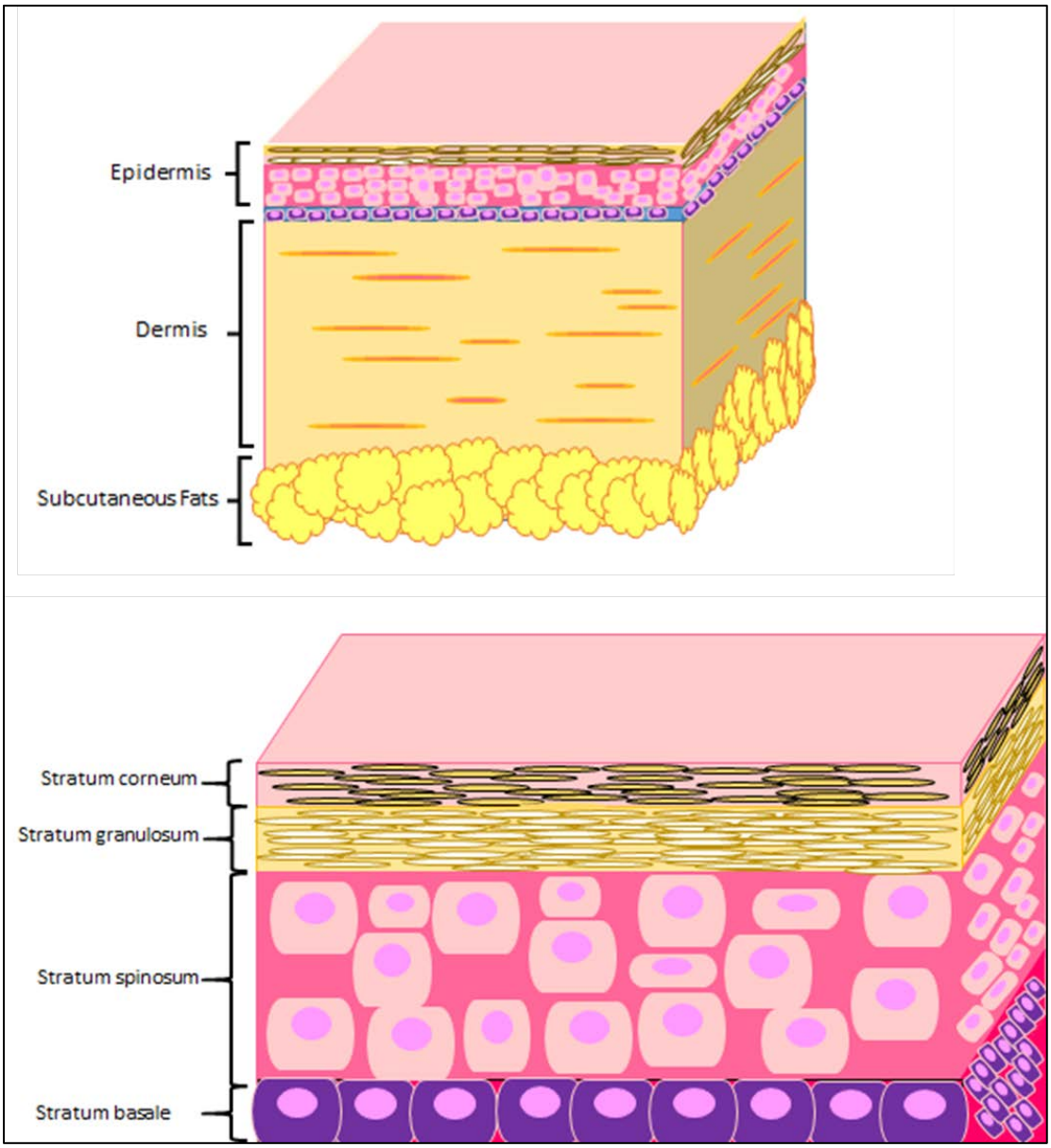

Figure 1: Anatomy of skin

Schematic representation of the layers of human skin along with sublayers and appendages.

The superficial epidermis consists of dead cells that are constantly shed and replaced by new sets of keratinocytes that migrate from the basal layer to the surface of the skin by a process known as keratinization.

In thick skin, the *stratum corneum* is the topmost layer of the skin and mainly consists of about 20-30 layers of horny cells or corneocytes, and is rich in proteins and low in lipids. The thick layer acts as a protective layer and also prevents loss of water from the skin. The next layer, *stratum lucidum* is mainly present in the soles of the hands and feet, also preventing water loss from the skin. *Stratum granulosum* is the granular layer made up of one to three layers of stratified squamous cells and consists of lamellar granules and tonofibrils. It is present in the soles of feet and the palms of hands. The fourth layer *stratum spinosum*, also known as the spinous layer lies just above the basal layer and are connected by desmosomes which appear as prickles under a microscope. (Chu, 2008). The basal layer also known as the *stratum germinativim*, is single layered and mainly consists of the dividing and non-dividing keratinocytes that attach to the basement membrane. It is also attached to the suprabasal squamous cells by desmosomes. The basal layer also consists of melanocytes, which protect the body from UV radiation and chronic light. Lastly, the basal layer contains Merkel cells, which play a role in perception of touch.

1.1.2. Basement membrane

The epidermis and dermis are separated from each other by the basal lamina or the basement membrane, which acts as a gate keeper and controls cell trafficking. It is through this layer that the nutrients diffuse into the epidermis. The basement membrane binds to many cytokines and releases them under conditions of physiological remodeling.

The structure of the basement membrane is very irregular and flattens with age. It links the basal keratinocytes to the dermis. The basal lamina is made up of type IV collagen, anchoring fibrils and dermal microfilaments. It provides support to the epidermis, establishes cell polarity, and organizes the arrangement of cytoskeleton in basal cells (Breitkreutz *et al.*, 2013).

1.1.3. Dermis

The inner layer of skin is the dermis which consists mostly of fibroblasts, mast cells and histiocytes. The dermis provides elasticity and tensile strength to skin, protecting it from mechanical injury (Burr *et al.*, 2005). The dermis consists of two layers: the papillary layer and the reticular layer. The papillary layer contains nerves and capillaries which provide nutrients to the epidermis while the reticular layer consists of collagen and elastin that allow the dermis to stretch and contract. With age the amount of collagen and elastin decrease, while elastin also loses its elastic nature. This loss of elasticity appears as wrinkles on skin. (Tortora *et al.*, 2009). The dermis also consists of eccrine glands, apocrine glands, sebaceous glands, ceruminous glands, blood vessels, and hair follicles especially in the forehead, palm, in groin, and axillae.

1.2. Wounds

A wound is defined as an injury in the skin thereby causing disruption or damage to skin. It can be a simple break in the epidermis layer or a deeper injury or cut in the dermal and the subcutaneous fat layer (Velnar *et al.*, 2009). It can be caused due to burns, traumatic lacerations, infections, radiation, pressure ulcers, diabetic ulcers, ischemia or other dermatologic conditions A completely healed wound is the one where the skin has regained its normal anatomy and function (Velnar *et al.*, 2009).

1.2.1. Classification of wounds

Wounds, depending on the type, can take variable time to heal (Falanga, 2005). Wounds can be categorized as acute or chronic wounds depending on the time they take to heal. Acute wounds are defined as the wounds which heal in an orderly and timely manner within a month and restore the normal integrity and anatomical functions of the skin membrane (Velnar *et al.*, 2009). By contrast, chronic wounds are defined as those that fail to heal or regain the structural and functional integrity of the skin in an orderly process within a period of three months (Mustoe *et al.*, 2006).

1.2.2. Chronic wounds

Chronic wounds are a major burden on our society. Nearly, 6.5 million Americans suffer from wounds that do not heal, costing healthcare almost $25 billion a year (Sen *et al.*, 2009). Though the onset of chronic wounds is via acute wounds, factors like impaired neovascularization, prolonged inflammation, persistent infection, desiccation, reduced growth factors, drug resistance, diabetes, immune status, and nutritional status can compromise healing (Falanga *et al.*, 2005).

1.2.3. Wound healing process

The normal wound healing process consists of four phases: hemostasis, inflammatory phase, proliferative phase and matrix remodeling, and scar formation. (Broughton *et al.*, 2009). Wound healing is a complex process requiring a regulated combination of cell proliferation and migration, vascularization, angiogenesis, re-epithelization, extracellular matrix deposition, and remodeling (Guo *et al.*, 2010). The first phase hemostasis starts immediately after injury, when the blood vessels constrict to protect the vascular system. Fibrins prevent blood loss and protect the damaged area from

bacterial entry (Velnar *et al.*, 2009). Proinflammatory cytokines and growth factors like FGF (fibroblast growth factor), TGF (transforming growth factor), EGF (epithelial growth factor), and PDGF (platelet derived growth factor) are released into the wound site. Once the bleeding is controlled, inflammatory cells such as macrophages and neutrophils are attracted to the wound site. Previously constricted blood vessels now open up by vasodilation and allow macrophages to enter. Neutrophils clear out the invading microbes and the macrophages clear the apoptotic cells including the neutrophils (Guo *et al.*, 2010). The inflammatory and proliferative phases overlap with one another. The proliferative phase is characterized by the entry of fibroblasts into the wounds and deposition of collagen, glycosaminoglycans, and proteoglycans, which are important components of extracellular matrix (ECM) (Guo *et al.*, 2010). In the last phase, the wound enters the remodeling phase, where collagen is re-arranged, new blood vessels are formed to strengthen vascular capillaries, scarring continues and the tensile strength of the new skin gradually improves (Falanga *et al.*, 2005).

1.2.4. Factors affecting wound healing

Various factors contribute to impaired wound healing. These include local factors which directly affect the healing process and systemic factors like the overall health or the nutritional status of the individual (Guo *et al.*, 2010). Examples of local factors are infection and oxygenation. Oxygenation plays an important role in wound healing. Hypoxic conditions in healthy patients can initiate the wound healing process by angiogenesis and secretion of growth factors. However, unhealthy patients with chronic wounds or microvascular insufficiency are not able to respond physiologically to hypoxia to promote healing. Wound infection typically occur a week or so after injury. The

majority of the infections are bacterial. Rarely fungal or viral infection can be seen in immunocompromised patients.

Systemic factors include age, sex hormones, stress, nutrition, disease, alcoholism, and smoking (Guo *et al.*, 2010). Elderly people are more prone to suffering from chronic wounds because of delays in epithelialization, collagen synthesis, and angiogenesis. Aged males are more susceptible to impaired chronic wound healing because androgens negatively regulate wound healing, whereas estrogen in aged females positively regulate wound healing by upregulating regeneration, matrix production, epidermal function, (Gilliver *et al.*, 2007). Stress can substantially delay wound healing by upregulating the level of glucocorticoids and by decreasing secretion of proinflammatory cytokines, macrophages, and neutrophils in the wound site. Alcohol consumption and smoking exposes patients to heart and vascular disease, stroke, lung disease, and also to higher risk of infection by decreasing host resistance (Guo *et al.*, 2010). Carbohydrates, fats, proteins, vitamins, minerals are all necessary to facilitate proper healing, and deficiency in any of these can contribute to impaired wound healing (Falanga *et al.*, 2005).

1.2.5. Treatments for chronic wounds

Current approaches towards the treatment of chronic wounds include skin grafting, hyperbaric oxygenation, and amputation. However, therapeutic limitations of these traditional approaches include tendon adhesions, nerve entrapment, and neuropathies inflicting further functional deficits and atrophy to a wounded extremity (Diegelmann *et al.*, 2004). Hence, new strategies for therapy have to be developed.

1.3. Skin substitutes

Skin substitutes are heterogenous materials used to cover skin defects thereby aiding in temporary or permanent wound healing (Singh *et al.*, 2012). Skin substitutes can be classified into biological and synthetic substitutes. These should be easily available, easy to store and use, should be able to prevent infection, survive in hypoxic conditions and also be cost effective (Nathoo *et al.*, 2014).

1.3.1. Biological skin substitutes

Biological skin substitutes have an intact extracellular matrix thus promoting enhanced epithelialization and dermis formation. However, they take a longer time to become vascularized because of its slow integration process (Halim *et al.*, 2010). Some of the widely used biological skin substitutes include xenografts, allografts, and autografts.

Autografts are tissues grafted from the patient's body. They can be partial thickness (with the epidermis and a part of the dermis layer) or full thickness (with the entire epidermis and dermis layer).

Biosynthetic skin products

Xenografts are tissues obtained from other species and are often used as a wound covering material. They can temporarily cover partial thickness burns, but there are eventually rejected by the host (Halim *et al.*, 2010). Allografts are tissues obtained from another individual of the same species. They can be vascularized, promote angiogenesis, secrete cytokines and growth factors, and prevent bacterial colony formation and desiccation of wound beds (Singh *et al.*, 2012).

1.3.2. Synthetic skin substitutes

Synthetic skin substitutes can be either cellular or acellular, and are obtained from natural or synthetic sources. Natural sources include cadaveric skin free of cellular components, but containing proteins and collagen (Singh *et al.*, 2012) Synthetic sources can be in the form of a degradable polymer, with types including Biobrane®, Integra®, Alloderm®, Apligraft®, Matriderm®.

Biobrane® is a bi-laminated membrane made of nylon mesh (acting as the dermal layer) and a silicone membrane (as the epidermal layer) embedded into the collagen matrix (Halim *et al.*, 2010). It is used as a temporary skin substitute and is readily available and easy to use, but it brings along some risks of infection (Alrubaiy *et al.*, 2009). Integra® is a bi-layered skin substitute made of silicone as the epidermal layer, and bovine collagen and shark chondroitin-6-sulphate glycosaminoglycan as the dermal layer. It leads to revascularization of wounds within three weeks of implantation, but can also cause accumulation of fluid near wound site thus leading to a chance of infection (Nathoo *et al.*, 2014). Alloderm® is made from cadaveric skin wherein the epidermis and the cellular components are removed, but it provides a good matrix for growth of fibroblast and endothelial cells (Alrubaiy *et al.*, 2009). Apligraft® is bi-layered and is made up of type I bovine collagen and allogenic keratinocyte and neonatal fibroblast. When used with autografts it shows the best results. It can be used for burns, partial thickness wounds, or full thickness wounds. A limitation of Apligraft® is that it has a shelf life of only 5 days, hence it has to be prepared fresh before use. (Singh *et al.*, 2012).

1.4. Stem cells in wound healing

Stem cells play a pivotal role in wound healing by promoting tissue regeneration. Epidermal stem cells, which are present in the epidermis and the bulge of hair follicles, promote keratinocyte migration and promote epithelialization. (Gue *et al.*, 2010). Mesenchymal stem cells differentiate into different lineages such as osteoblasts, chondrocytes, adipocytes, keratinocytes, and fibroblasts, as well as promoting wound healing (Falanga *et al.*, 2005). Hematopoietic stem cells differentiate into blood cells and near the wound site they regulate proliferation and migration of epithelial and dermal MSC thus inducing wound healing (Wu *et al.*, 2007).

1.5. Adipose derived stem cells

Adipose derived stem cells (ASCs), through their regenerative properties, induce healing of a wound when transplanted onto the wound bed of mice models. ASCs are multipotent in nature, secrete growth factors, promote angiogenesis, and differentiate into multiple lineages upon induction (Kim *et al.*, 2007). The benefits of ASCs over bone marrow stem cells include achievement of higher yields upon isolation from the donor (nearly 40 fold) and a procedure that is overall less invasive to the patient, resulting in less donor morbidity (Zuk *et al.*, 2002, Kern *et al.*, 2006). Their ease of isolation, longtime preservation, and capacity to survive in hypoxic conditions makes them ideal cell therapeutic candidates (Gonda *et al.*, 2008). Moreover, since they are isolated from the patient's own body, the chance of immune rejection extremely low.

1.5.1. Localization and characterization of adipose derived stem cells

ASCs are typically obtained from liposuction or lipectomy, are digested with collagenase, and subjected to centrifugation (Figure 2). The stromal vascular

fraction thus obtained, are seeded and expanded in culture (Hassan *et al.*, 2014). The growth and differentiation capacity of the ASCs depends on the site from where they are extracted. ASCs obtained from superficial abdominal layer are more susceptible to differentiation than ASCs obtained from subcutaneous fats. Additionally, ASCs differentiating potential is higher in younger people than the elderly (Scripper *et al.*, 2008). ASCs characterization is analyzed by the expression of positive surface markers like CD13, CD34, CD36, CD44, CD73, CD90, CD105, Stro-1 and by negative markers like CD31, CD45, and CD106. (Musina *et al.*, 2005). By their autocrine activity ASCs promote re-epithelialization and fibroblast proliferation (Kim *et al.*, 2007).

1.5.2. ASC as a regenerative medicine for wound healing

ASCs induce wound healing by stimulating collagen production, keratinocyte and fibroblast proliferation, angiogenesis, epithelialization to potentiate wound healing (Kim *et al.*, 2007). ASCs administration in diabetic mice accelerates wound healing by neovascularization and angiogenesis. (Ebrahimian *et al.*, 2009). ASCs when co-cultured with fibroblasts increase the migration capacity of the fibroblasts and thus potentiate wound healing (Kim *et al.*, 2007). Hypoxic conditions upregulate ASCs activity by enhancing angiogenesis, secretion of growth factors and anti-apoptotic factors (Hassan *et al.*, 2014). ASCs promote tissue regeneration and neovessel formation in severely radiation-damaged tissues (Rigotti *et al.*, 2007). ASCs also secrete growth factors like EGF, FGF, PDGF, KGF, and VEGF, which potentiate healing in acute and chronic wounds (Galliano *et al.*, 2004).

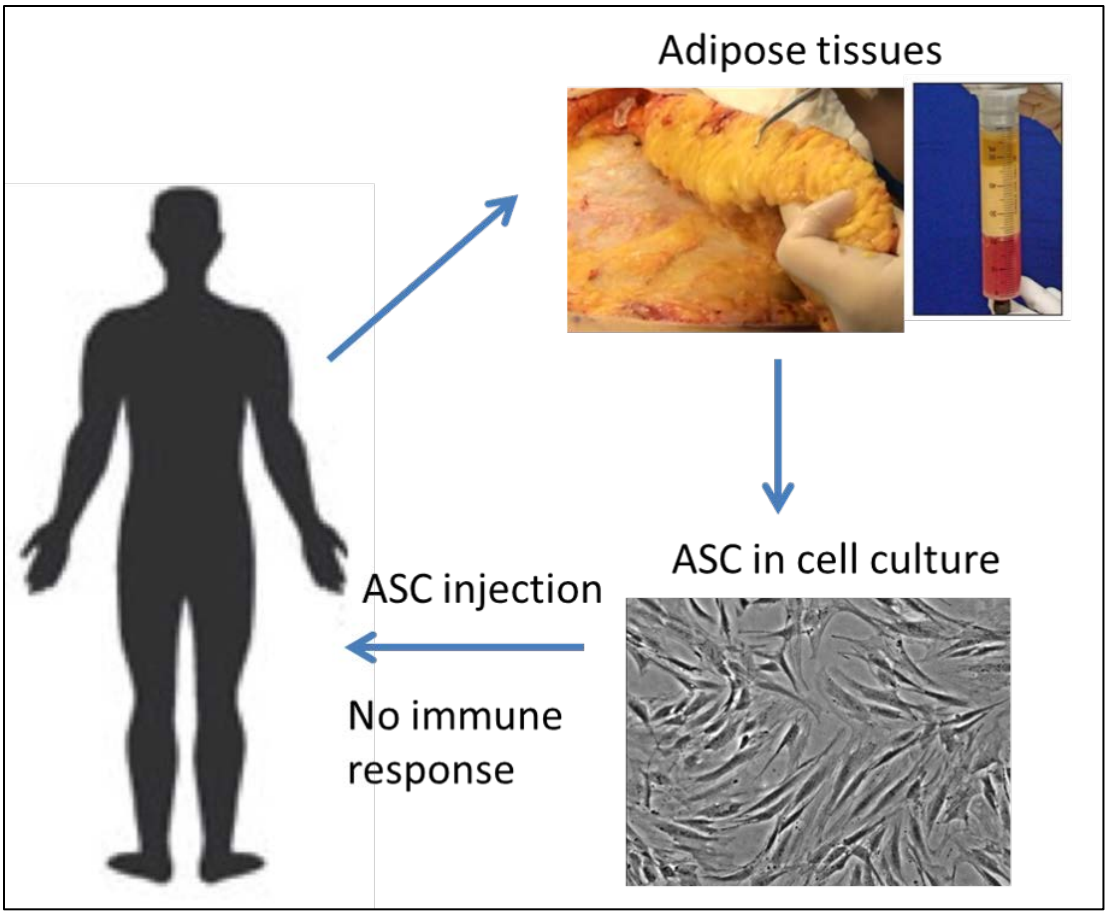

Figure 2: Schematic representation of extraction of ASCs from a patient's body and expansion in cell culture for transplantation into patients.

1.6. Vascular endothelial growth factor (VEGF)

Angiogenesis and vascularization play a critical role in healing, especially in the proliferative phase of wound healing, resulting in the formation of new blood vessels that deliver oxygen, nutrients, and essential growth factors to injured tissues (Jacobi *et al.*, 2004). Vascular endothelial growth factor (VEGF), also known as vascular permeability factor (VPF) is one of the essential angiogenic factors promoting the development of the capillary network in ischemic tissues (Jacobi *et al.*, 2004). VEGF is considered to be one of the most potent factors in the formation of blood vessels. It is a 34-42 kDa homodimer protein. It plays a role in proliferation and differentiation of endothelial cells, degradation of basement membranes, and lumen formation (Leung *et al.,* 1989 as reviewed by Bryne *et al.,* 2005). VEGF is also a chemotactic agent for macrophages and monocytes, thereby attracting them to the site of inflammation (Clauss *et al.,* 1990 as reviewed by Bryne *et al.,* 2005). VEGF is produced by macrophages, platelets, neutrophils, endothelial cells, fibroblasts and smooth muscle cells (Nissen *et al.,* 1998 as reviewed by Bao *et al.,* 2009).

1.6.1. VEGF isoforms

The amino acid structure of VEGF shares approximately 20% of its homology with the PDGF superfamily (Neufeld *et al.,* 1999 as reviewed by Bryne *et al.,* 2005). The VEGF family consists of VEGF-A, VEGF-B, VEGF-C, VEGF–D, VEGF-E and PLGF. Exons 1-5 are conserved in all VEGF-A forms (Figure 3). Alternative splicing in the exon 6 and 7 of the VEGF mRNA shows that there are 5 isoforms of VEGF, namely $VEGF_{121}$, $VEGF_{145}$, $VEGF_{165}$, $VEGF_{189}$, and $VEGF_{206}$ consisting of 121, 145, 165, 189 and 206 amino acids respectively (Tischer *et al.,* 1991 as cited by Bryne *et al.,* 2005) (shown in figure 3). $VEGF_{121}$ is freely secreted because of the absence of both exon 6 and

7. $VEGF_{165}$ and $VEGF_{145}$, are moderately bound as $VEGF_{165}$, lacks only exon 6 whereas $VEGF_{145}$ lacks exon 7. $VEGF_{189}$, and $VEGF_{206}$ are tightly bound to the heparin residues due to the presence of exon 6 (Hoeben *et al.,* 2004 as reviewed by Bao *et al.,* 2009). Most recently identified is $VEGF_{165b,}$ which, unlike the other VEGF isoforms, is an angiogenesis inhibitor. $VEGF_{165b}$ differs from $VEGF_{165}$ by the six amino acids in the carboxyl terminal (Woolard *et al.,* 2004 as reviewed by Bryne *et al.,* 2005). Of all the isoforms of VEGF, $VEGF_{165}$ is the most abundant isoform with highest biological activity.

1.6.2. VEGF receptors

The binding of VEGF to a receptor depends on the isoform (figure 4). VEGF-A binds to both VEGFR-1 (Flt-1) and VEGFR-2 (KDR) (Bao *et al.,* 2009) while VEGF-B shows high binding affinity to VEGFR-1. VEGF-C and VEGF-D bind to VEGFR-3 and also induce tyrosine phosphorylation of VEGFR-2 and VEGFR-3 (Bryne *et al.,* 2005). VEGF-E specifically binds to VEGFR-2 (Bryne *et al.,* 2005).

1.6.3. VEGF Signaling

The binding affinity of VEGF to the VEGFR1 receptor is higher than to the VEGFR2 receptor, however the ability to induce tyrosine kinase activity is 10 fold higher in the VEGFR2 than the VEGFR1 receptor (Gille *et al.,* 2001). VEGFR2 can induce phosphorylation of the ERK-1, ERK-2 and MAPK protein, whereas the VEGFR1 shows minimal expression of the phosphorylated ERK-2 (Figure 5). VEGF stimulates cell proliferation via Ras-Raf-MEK-ERK pathway. VEGFR2 induces production of p38MAPK protein and aids in cell proliferation. (Bryne *et al.,* 2005). Under stress conditions, the PI3-Kinase pathway (PI3K) and the Akt/protein kinase B (PKB) pathway

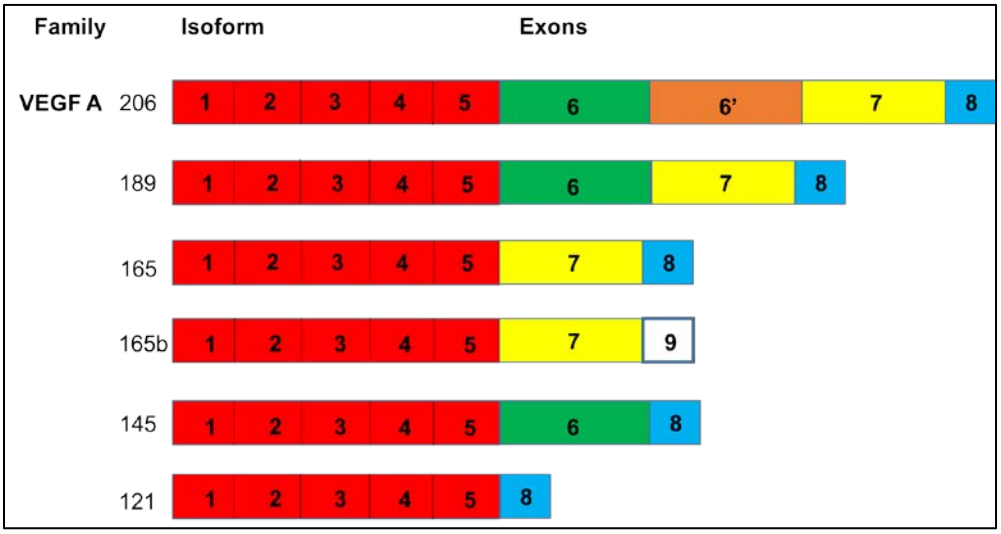

Figure 3: Isoforms of VEGF-A.

Schematic representation of different isoforms of VEGF-A.

is activated by VEGFR2 to promote cell survival. VEGF also aids in cell migration via the focal adhesion kinase (FAK) and Paxillin, and by the phosphatidylinositol-3-phosphate (PI3) Kinase/Akt pathway (Koch *et al.*, 2012).

1.6.4. VEGF as an angiogenic factor

VEGF acts as an important angiogenic factor and also aids in increasing vascular permeability in sites of tumors or chronic wounds. $VEGFR1^{-/-}$ deficient mice can die due to over production of endothelial cells and blood vessel formation, whereas $VEGFR2^{-/-}$ deficient mice can die due to lack of blood vessel formation, thus indicating that VEGFR2 positively regulates signal transduction while VEGFR1 negatively regulates it (Takahashi *et al.*, 2005).

1.7. Viral vectors for gene therapy

Viral vector mediated gene therapy, using adenovirus, retrovirus, lentivirus, or adeno-associated virus (AAV), is one of the most efficient ways for delivering a gene of interest into the locale of wound and enhancing wound healing (Gauglitz *et al.*, 2011). Viral vectors can be lytic or non-lytic depending on their ability to interact with the host cell. Lytic vectors break the host cell membrane to release virions as seen in adenovirus, adeno associated virus, and herpes simplex virus. Non-lytic viruses like retroviruses or lentiviruses keep the cell membrane intact after releasing its virions (Branski *et al.*, 2007).

1.7.1. Retrovirus

Retroviruses are single stranded RNA viruses. Retroviral gene expression is long term and is mostly tissue specific, although retroviruses are capable of transducing

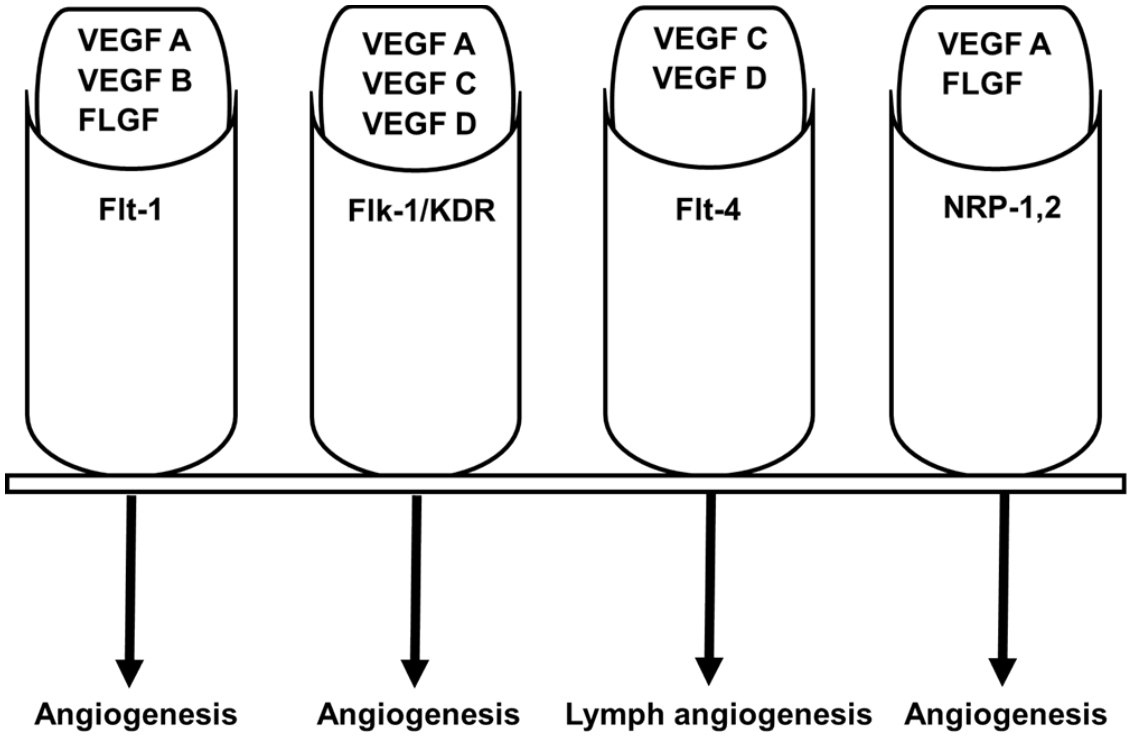

Figure 4: Binding of VEGF ligands to the VEGF receptors and their functions.

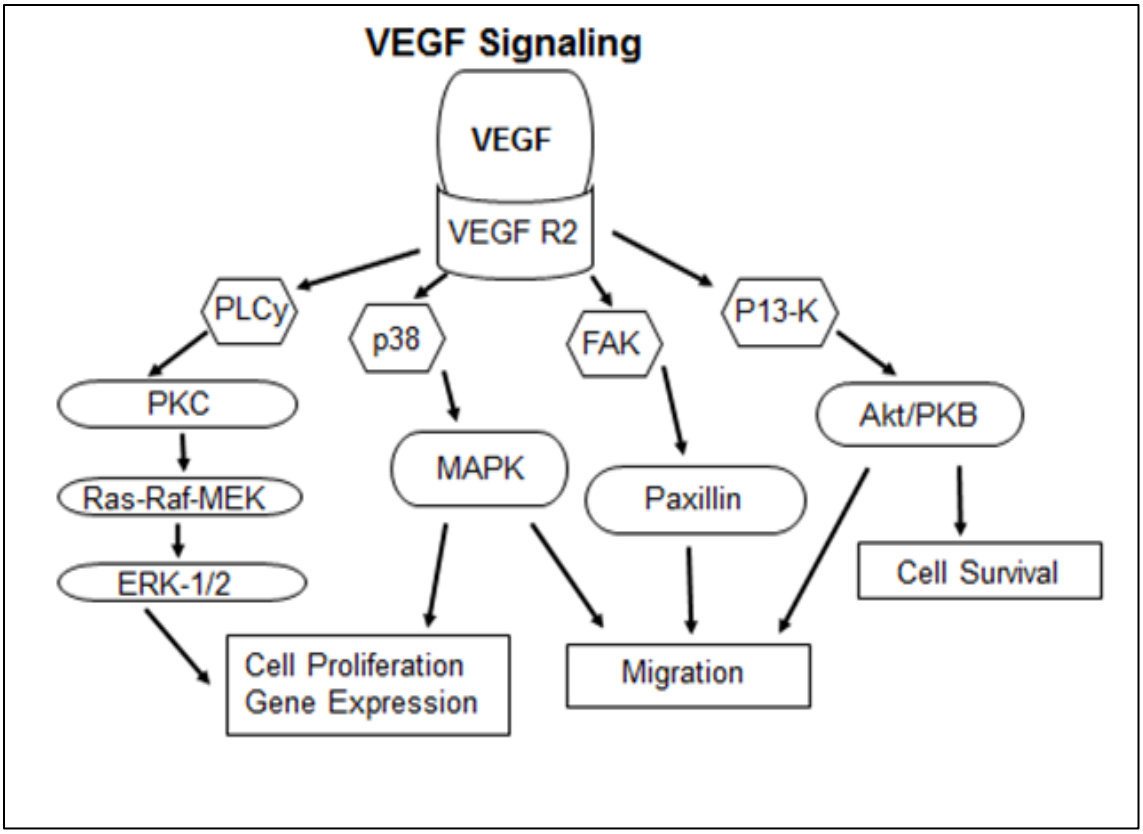

Figure 5: Signaling pathway of the VEGF activated by VEGFR2 receptor

VEGF activation by VEGFR2 regulates cell proliferation, cell migration, and cell survival.

In these recombinant viruses viral genes for replication and assembling are removed and a gene of interest is inserted into the viral vectors (Branski *et al.*, 2009).

only dividing cells with low efficiency (Anson *et al*., 2004). However, gene insertion through retroviruses is permanent as they integrate into the host cell chromosome and express the gene of interest. As a result, there are chances of non-specific integration into the chromosome, causing abnormal expression of the nearby host genes or insertional mutagenesis leading to expression of oncogenes (Yi *et al.*, 2011).

1.7.2. Adenovirus

Adenoviruses are double stranded DNA viruses being investigated for gene therapy. These are lytic viruses and have a genome size of 36kb. Adenoviral gene transduction is cell specific, stable, and can transduce both dividing and non-dividing cells (Branski *et al.*, 2009). The viral genome does not integrate into the chromosome of the host cell, so transgene expression is transient (Silman *et al.*, 2000). However, gene expression through adenovirus can cause an inflammatory response (Ritter *et al.*, 2002).

1.7.3. Adeno-associated virus

Adeno-associated viruses (AAVs) are non-enveloped single stranded DNA viruses belonging to the Parvoviridae family. These are dependoviruses which usually depend on a helper virus like adenovirus or herpes simplex virus for a productive infection (Zhijian et al, 2006). AAVs can also infect cells and stay as a provirus in the absence of the helper virus. AAVs were discovered as a contaminant of an adenovirus isolate (Atchison RW, 1965). AAV is not very immunogenic and does not cause any known disease in humans (Samulski *et al.*, 1987).

1.7.3.1. AAV Structure

The viral capsid of AAV is about 25 nm in diameter and consists of 4.7 kbp of single stranded DNA flanked by 145 bp ITRs (inverted terminal repeats) on both ends. The ITRs are the cis-acting elements which are required for the packaging of the virus. The first 120 base pairs of the ITR is the palindromic region, which folds itself to increase base pairing and forms a T-shaped hairpin structure. The next 25 bp section called the D sequence is usually unpaired. AAVs consist of two ORF (open reading frames), the left ORF consisting of four replication proteins Rep78, Rep68, Rep52, and Rep40 that are always trans acting. Rep78 and Rep68 are produced from the p5 promoter from unspliced and spliced transcripts and are involved in DNA replication. These proteins are also involved in site-specific integration, nicking and positive/negative regulation of the AAV gene expression. The smaller replication proteins Rep52 and Rep40 from the p19 promoter are from unspliced and spliced transcripts, respectively, and are involved in the packaging of the DNA in the capsid. The other ORF, the right ORF, consists of the three capsid proteins (VP1, VP2 and VP3) produced by alternative splicing from the p40 promoter. The unspliced transcript forms the largest capsid protein VP1 (87 kDa). VP2 (72kDa) and VP3 (62kDa) are produced from the spliced transcript. These capsid proteins are present in a 1:1:10 molar ratio in the virion shell. (Daya *et al.*, 2008).

1.7.3.2. AAV serotypes

There are 9 serotypes of AAV named as AAV1 – 9, and over 100 additional isolates (Zincarelli *et al.*, 2008). AAV1 – 6 were isolated as a contaminant of adenovirus in the lab, whereas the AAV7 – 9 were discovered by a novel PCR strategy where a

variable region of the capsid was analyzed to screen for isolates. AAV2, 3 and 5 are from humans, whereas AAV4 is from non-human primate. It is not known whether AAV1 is from a human or non-human primate as the neutralizing antibody for AAV1 is obtained from a monkey, but AAV1 was obtained from human tissue. AAV6 is considered to be a hybrid between AAV1 and AAV2, as the structure of the left ITR and the p5 promoter is similar to that of AAV2 while the remaining portions of the AAV6 is similar to AAV1 (Wu et al, 2006).

1.7.3.3. AAV Life cycle

AAV can enter into lytic or lysogenic phases depending on the presence or absence of a helper virus, respectively (figure 6). Lysogenic infection takes place in the absence of a helper virus and the AAV gene expression is repressed. Wild type AAV then latently integrates into chromosome 19 by site specific integration with the help of cis acting ITR, Rep78 or Rep68 and 138 bp integration efficiency element (IEE) or 16 bp Rep binding element (RBE) present in the p5 promoter (Daya *et al.,* 2008). Latent AAV infection is nonpathogenic because of the negative feedback regulation of the Rep proteins. Site specific integration of the AAV potentially makes safe and stable transgene expression; however, as the Rep and Cap sequences are deleted from recombinant AAV, very little integration is observed (Goncalves, 2005).

In the presence of the helper virus (adenovirus or HSV), the AAV genome enters into lytic infection phase and replicates, producing virions and expressing genes of interest. Adenovirus provides E1a, E1b, E2a, E4, and VA RNA helper genes to facilitate infection. E1a functions as a trans-activator, regulating activity of Ad genes and Rep and

Cap genes. E1b and E4 function together in transport of mRNA, and E2a along with VA RNA facilitates and stabilizes AAV mRNA translation. (Coura *et al.*, 2008). HSV mediates infection via DNA polymerase and helicase activity (Daya *et al.*, 2008). Lytic infection can also be initiated in the absence of the helper virus via inhibitors or DNA damaging agents like UV radiation. However, his process of induction is not efficient (Golcalves *et al*., 2005).

1.7.3.4. AAV tissue tropism

The efficiency of AAV transduction in tissues varies from serotype to serotype. AAV1 is very efficient in transducing skeletal muscles. AAV2 can transduce the liver, kidney, skeletal muscle, and central nervous system (CNS). AAV4 can transduce specific cell types in CNS like ependyma and astrocytes, as well as retinal pigmented epithelium (RPE) optimally. AAV5 is efficient in transducing CNS, RPE and photoreceptor cells. AAV6 transduces skeletal muscle and liver with a higher efficiency than AAV1 and AAV2. AAV7 transduces skeletal muscles with very high efficiency. AAV8 can efficiently transduce wide range of tissues like the liver, skeletal muscle, pancreas, diaphragm, and cardiac muscle. Tissue specificity for AAV9 is similar to AAV2, but AAV9 transduces tissues with much higher efficiency. (Wu *et al.*, 2006).

1.7.3.5. Recombinant AAV as a gene therapy vector

AAV is one of the ideal gene therapy vectors because of its ability to target the tissue and express the gene of interest. Depending on the tissue and cellular replication, expression can be long term (e.g. muscle) or for a limited period of time being degraded over time (e.g. liver). Due to the lack of the Rep and Cap gene and the cis acting IEE, AAV does not integrate into the chromosome; as a result it is nontoxic to the cells and

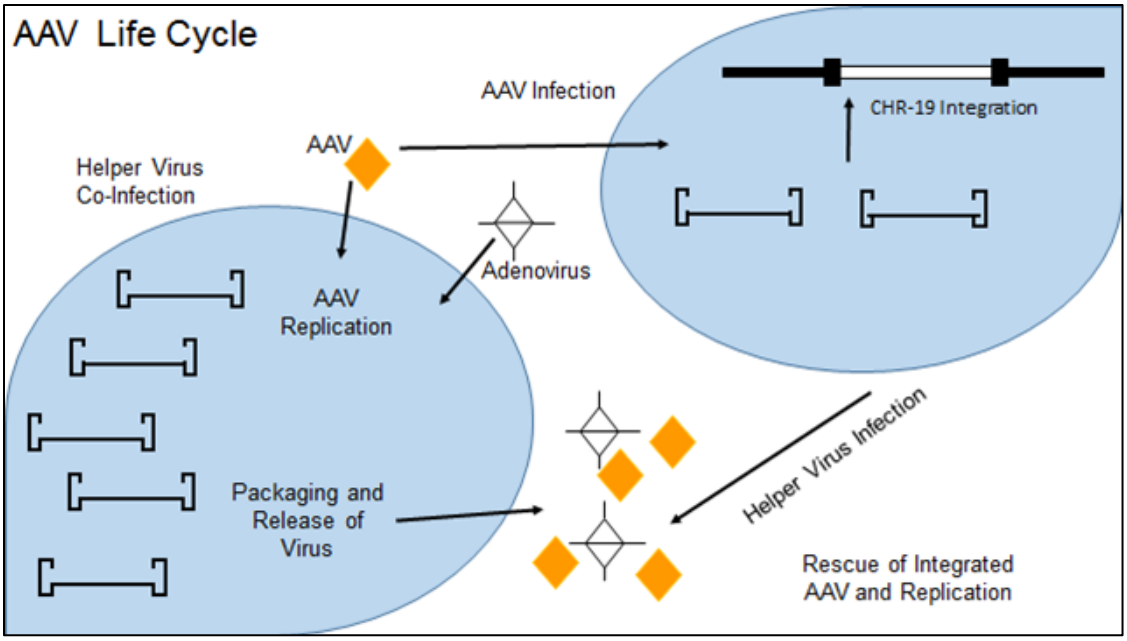

Figure 6: Life cycle of AAV

Lytic or lysogenic life cycle of AAV depending on the presence or absence of helper adenovirus. In the presence of a helper virus, AAV genome replication, gene expression and packaging, and release of virus takes place. When the helper virus is absent, AAV integrates into chromosome 9. The integrated AAV is then rescued and undergoes replication upon superinfection of adenovirus.

tissues (Daya *et al.*, 2008). Recombinant AAV is made by designing the AAV vector with the promoter region, the gene of interest, and flanked by 145 bp ITR on both sides. For efficient packaging of the AAV vector, the size of the promoter and the gene of interest is generally between 4.1 to 4.9 kb. Packaging becomes less efficient when the size of vectors exceeds 5 kb. (Pacak *et al.*, 2011). The plasmid vector is then co-transfected with the helper plasmid containing the Rep and Cap genes and the adenovirus gene of interest in mammalian cells. The recombinant AAV genome is then released from the AAV plasmid and undergoes transcription. Rep 78 and Rep 68 participate in accumulating the replicates, and Rep 52 and Rep 40 are involved in the packaging of the single stranded replicates into the viral capsid formed by VP1, VP2 and VP3 (Golcalves, 2005). The recombinant virions are then released from the cells along with the Ad particles. Due to the difference in density and temperature sensitivity between the Ad particles and the rAAV virions, the Ad particles are removed by heat inactivation at 56°C and isopycnic cesium chloride density ultracentrifugation.

The efficiency with which the rAAV can transduce tissue or cells depends on binding and entry of AAV into the cell, viral trafficking, entry into the nucleus, uncoating of capsid to release single stranded AAV, and finally synthesis of double stranded DNA. Each of these steps can act as a rate limiting step in gene expression (Daya *et al.*, 2008). Thus, to enhance AAV gene expression, trans-splicing AAVs have been designed. These trans-splicing AAV form head to tail concatemers by recombination of AAV ITR, and can deliver genes up to 9 kb in size (Yan *et al.*, 2000). Another category of the AAV is the self-complementary AAV (scAAV) which is designed specifically to reduce the lag phase time required for second strand synthesis. These scAAV can fold to synthesize the

second strand. However, a disadvantage of scAAV is that the transgene size is reduced to less than 3kb (Wu *et al.*, 2006)

Thus, AAV because of its non-immunogenic and non-pathogenic nature and its wide tissue tropism is a prime vector for gene modification (Coura *et al*., 2008).

1.8. Red light therapy

Red light therapy was discovered long ago in 1960, but only recently is it being widely used in nerve and tissue regeneration, wound healing, reduction in pain and inflammation (Avci *et al.*, 2014). It uses a red light (670 nm) laser or red light emitting diodes (LED) or a combination of both to promote bio-stimulatory effects on cellular, molecular and tissue level (Amid *et al.*, 2013). *In vitro* studies have shown better survivability and viability of ASCs, and increased level of growth factor secretion by ASCs with exposure to red light (Kim *et al.*, 2012).

1.8.1. Mechanism of action

The mechanism by which red light therapy functions is not known, but it appears that the absorption of red light by photo-acceptors in the plasma membrane of cells and cytochrome C oxidase, a mitochondrial chromophore, leads to photo dissociation of nitric oxide thereby causing an increase in energy level, mitochondrial activity, electron transport, ATP production. It also positively regulates the activity of transcription factors involved with cell migration, cell proliferation, cell adhesion (Avci *et al.*, 2013).

1.8.2. Secretion of growth factors and cytokines upon red light exposure

Exposure of damaged skin tissue to red light leads to an increased secretion of fibroblast growth factor (FGF), platelet derived growth factor (PDGF),

vascular endothelial growth factor (VEGF), transforming growth factor β (TGF-β1), IL-1β, TNF-α, and increased mRNA level of ICAM-1, connexin 43 (Cx43), and decreased secretion of IL-6. Secretion of IL-1β, TNF-α in the damaged site recruits matrix metalloproteinases (MMP) to remove the damaged collagen fibers and synthesize new fibers. Later, tissue inhibitors of metalloproteinases (TIPMs) further protect the newly formed collagen fibers by inhibiting MMPs. Cx43 then enhances cell to cell communication between dermal fibroblasts and further enhances collagen production.

1.8.3. Concern with red light therapy

Red light therapy is also highly dose dependent. Low dose of red light results in inefficient healing and high level exposure can lead to the damage of tissue. Thus the correct dosimetry parameter has to be known to perform such therapy (Avci *et al.*, 2012).

1.9. Hypothesis, Objective and Specific Aims of this thesis

The inability to heal wounds, leading to chronic wounds, is a growing problem in our society and new treatments are needed. The overall hypothesis is that adipose derived stem cells (ASCs) expressing VEGF-165, via delivery by an AAV-VEGF-165 vector, will neutralize the chronic wound environment and enhance neovascularization and wound closure in an in vitro 3D wound culture. Also exposure to red light (670nm) will enhance wound closure.

The overall objective of this thesis is to develop an organotypic wound model to study chronic wound healing and test therapeutic strategies to close the wound using (1) ASCs expressing VEGF-165, via delivery by an AAV-VEGF-165 vector, or (2) red light

therapies, which are predicted to neutralize the chronic wound environment, enhance neovascularization, and facilitate wound closure.

To achieve these objectives, I have proposed three specific aims.

Aim 1:

Develop a 3D organotypic human skin wound model system.

Aim 2:

Construct and test AAV-VEGF transduction in ASCs and test the efficiency of ASCs transduced with AAV-VEGF to induce the closure of wounds in a 3D organotypic human skin wound model system.

Aim 3:

Determine the effect of red light on cell growth and wound healing.

Together this work will provide new insights into the mechanisms that prevent wound healing, provide a novel way to test potential therapies, and offer improvements to current stem cell therapy approaches.

Chapter 2: Material and Methods

2.1. Isolation and culture of ASCs

Adipose derived stem cells (ASCs) were isolated from lipectomy or lipoaspirate specimens under the IRB protocol from the Miami Valley Hospital. The specimens were washed three times with PBS and digested with Collagenase I and incubated at 37ºC for 30 minutes with gentle mixing every 2 minutes to separate out the stromal vascular fraction (SVF) which contains ASCs. Next the specimens were centrifuged at 1200 x g for 10 minutes. The supernatant was discarded and the cellular pellet was re-suspended in ASC medium (Dulbecco's modified Eagles medium, 10% fetal calf serum, 1% Antibiotic Antimycotic Solution). Cells were counted and seeded at a density of 10^5 /ml cells in T75 flasks. Medium was changed the next day to remove the non-adherent cells. The cells were maintained at 37ºC and 5% CO_2 and medium was changed every alternate day. Upon 90% confluence, the cells were detached using TrypLE and underwent 3 rounds of passaging at 1:2 dilution before experiments. The viability of the cells was tested via a trypan blue assay and was routinely 80-95% alive.

2.2. Characterization of ASCs

The ASCs were characterized according to the International Federation for Adipose Therapeutics and Science (IFATS) and the International Society for Cellular Therapy (ISCT) standard by an immunofluorescence multicolor flow cytometry strategy (Accuri C4, BD Biosciences, San Jose, CA). The positive stem cell markers were APC

anti-human CD13, CD34, CD36, CD73, CD90 and CD105 and the negative stem cell markers were PE anti-human CD31, PE anti-human CD45 and APC anti-human CD106 (BioLegend (San Diego, CA)). Cells were seeded in 6 well plates at a density of 10^4 cells/well and were subsequently detached using TypLE, spun down and reconstituted in PBS and 10% FCS. After conducting a cell count, the cells were equally distributed in each tube and mixed with the appropriate stem cells marker antibodies and incubated for 25-30 minutes. The cells were then washed with PBS and spun down. This washing process was repeated three times and the cells were re-suspended in PBS with 10% FCS. The cells were then characterized by flow cytometry under the FL1, FL2 and FL4 channels.

2.3. Development of organotypic human skin wound models

The skin cultures were obtained under an IRB approved protocol by collaborators at the Miami Valley Hospital. The wounds were created by punch biopsy from abdominoplasty and brachioplasty skin fat specimens. Full thickness 2 or 3 mm punches extending from the epidermis into the fat were made in the center of the 8 mm skin flaps. These wound models were maintained in the central chamber of a Millicell® (EMD Millipore, Billerica, MA) hanging from the sides, without touching the bottom of the well. This created an air-liquid interface for the skin cultures in the millicell where the bottom part of the wound was exposed to the medium, in the well and the top part was exposed to air. The wound models were fed with the ASC medium (DMEM-F12, 10% FCS and 1% ABAM). Medium in the wells was changed every 48 hours. Survival of the wound model system was tested periodically by MTT assay.

2.4. MTT viability assay on skin model

Test wound model (supplemented with ASC medium) and control wound model (fixed in 4% paraformaldehyde for 2 hours) were used to study the viability of the tissue. The wound models were washed with PBS, and then 100µl of MTT in 1:10 dilution was added to the base of the transwell containing the wound models and incubated at 37ºC for four hours in the dark. After 4 hours, the wound models were observed for purple color formation and imaged under the microscope.

2.5. Infusion cloning

In an Eppendorf tube, 1.5 µl of the VEGF gene (100 ng) synthesized by Integrated DNA Technology was incubated with 1 µl of the linearized AAV5-CMV-IRES-GFP or AAV5-CAG-IRES-GFP plasmid along with 2 µl of the 5 X Infusion enzymes and 5.5 µl of water for 15 minutes at 50ºC and was then kept on ice. After cooling, 2.5 µl of the above reaction mix was incubated with Stable competent cells on ice for 15 minutes. The mixture was then heat shocked for 55 seconds at 42°C and cooled on ice for 5 minutes. Next 250µl of SOC medium was added to the mixture and placed on a shaker for 1.5 hours and then plated on Ampicillin and Gentamicin/Ampicillin plates and incubated overnight at 37ºC for colony formation.

2.6. Restriction Digestion

In an Eppendorf tube, 1.5 µg of the plasmids were mixed with 1.5 µl of the specified restriction enzyme(s), 2 µl of buffer, 2 µl of 1 X BSA and water. This solution was then incubated at 37ºC for 1.5 – 2 hours. For double digestions, the plasmids were digested with *SalI* and *BamHI* and for single digestion, the plasmids were digested with

MscI or *XmaI*. To evaluate digestion, a 10 µl volume of both the digested plasmids and the undigested plasmids were run on a 1.2% agarose gel for 30 mins at 120 V.

2.7. Plasmid DNA extraction

A single colony was grown in 5 ml of LB broth with Ampicillin overnight at 37°C. After 24 hours, 4 ml of the grown culture was transferred to a 250 ml LB broth and grown overnight at 37ºC. Next day the culture was centrifuged at 10,000 rpm for 5 minutes. The supernatant was aspirated and the pellet was re-suspended in 7ml of Buffer PR1 and mixed well. Next 7 ml of Buffer PL2 was added and gently inverted 5 – 6 times to ensure mixing and was incubated for 5 minutes at room temp. After 5 minutes, 7 ml of buffer PN4 was added and the solution was mixed by gently inverting the flask 10 times. After 10 minutes of incubation at room temperature, the solution was centrifuged at 10,000 X g for 25 minutes. The lysate was transferred into a Perfect Prep Endofree filter and the filtrate was collected in a fresh tube. 0.3 volume of isopropanol was added to the filtrate and mixed well by inverting the tube, for 5 – 6 times The isopropanol lysate mixture was added to the Perfect Prep Endofree column (equilibrated with 2.5 ml of Buffer BL and centrifuged for one minute) and centrifuged at 10,000 X g for 2 minutes. The flow through was discarded and 10 ml of buffer PW was added to the column and centrifuged at 10,000 X g for 2 minutes. This step was repeated again. Next 3 ml of absolute ethanol was added to the column and centrifuged at 10,000 X g for 2 minutes. The flow through was discarded and the column was centrifuged again at 10,000 X g for 5 minutes to remove the excess alcohol. The column was set to air dry. To elute DNA, 1 ml of Buffer PEB was added to the center of the membrane and incubated for 5 minutes. A fresh collection tube was used and the DNA was collected and stored at -20ºC for future use.

2.8. Transfection of ASCs with AAV plasmid

$6.5x10^4$ cells/cm^2 were seeded in a 24 well plate 24 hours before transfection. After 24 hours, 0.5 µg of plasmid DNA was diluted in 25 µl of DMEM high glucose and 1.5 ul of the transfection reagent was diluted in 25 µl of DMEM high glucose. The diluted transfection reagent was added to the diluted plasmid DNA and mixed well. The transfection complex was incubated at room temperature for 15 minutes. Post incubation, the medium in the wells was replaced with fresh medium and the transfection complex was added dropwise to the well and incubated at 37ºC. The medium was replaced with fresh medium the next day and the transfection efficiency was measured by comparing the number of GFP positive green fluorescent cells with the amount of non-transfected cells 24 hours post transfection.

2.9. VEGF ELISA

VEGF ELISA assay was performed on medium collected on day 3 from transduced and non-transduced cells by the VEGF ELISA kit (DY293B, R&D system). 100 µl of MαH capture antibody at a concentration of 1 µg/ml was added to the wells the previous night and sealed and kept overnight at room temperature. After 18 hours of incubation, the wells were washed with 400 µl of wash buffer three times and 300 µl of reagent diluent was added to the wells and incubated at room temperature for one hour. After one hour of incubation, the wells were washed with 400 µl of wash buffer; this washing step was repeated two subsequent times. In triplicates, dilutions of 2000 pg/ml - 31.25 pg/ml of human VEGF standard and medium from transduced and non-transduced cells were added to the wells and incubated for another two hours at room temperature after which the wells were washed with wash buffer as in the previous steps. Next 100 µl

of biotinylated GαH VEGF detection antibody were added to the wells and incubated at room temperature for two hours. After the incubation period, the wells were washed with 100 µl of Streptavidin HRP and incubated in the dark for 20 minutes and then washed with wash buffer. Next 100 µl of substrate solution were added to the wells and kept in the dark for 20 minutes for color development. Post color development, 50 µl of stop solution was added to the wells and the plate was read at 450 nm with wavelength correction at 540 nm.

2.10. Production of recombinant AAV5

AAV5-CAG-VEGF-IRES-GFP virus was made by cis acting and trans-acting Baculovirus vectors containing the AAV plasmid with the gene of interest flanked by ITR and the rep and cap genes. These vector viruses, along with the helper adenovirus, were provided by the University of Iowa Viral Vector Core. Together; these viruses were infected into SF-9 insect cells to obtain the desired AAV5-CAG-VEGF-IRES-GFP virus with a viral titer of $3.7x10^{12}$ vg/ml (batch 1), $9.11x10^{12}$ vg/ml (batch 2), $6.63x10^{12}$ vg/ml (batch 3). AAV5-CMV–IRES-GFP ($2.5x10^{14}$ vg/ml) virus was used as a control virus during subsequent experiments.

2.11. Transduction of ASCs with AAV vectors

$6.5x10^{4}$ ASCs were transduced with rAAV5-CAG-VEGF-IRES-GFP and AAV5-CMV-IRES-GFP virus (control) at a MOI of 10^{6} vg/cell in combination with 0.5 µM/ml Hoechst 33342 in ASC medium in Eppendorf tubes and incubated at 37ºC for one hour. After one hour, the cells were seeded in a 48 well plate. Medium was changed the following day to remove non-adherent cells. Non-transduced ASCs were used as a negative control. Two days after transduction, the cells were viewed under fluorescence

microscopy to observe green fluorescent cells. Medium collected from the cells after three days was used for VEGF ELISA.

2.12. Transduction of ASCs with Ad-VEGF and Ad-GFP

$1x10^5$ ASCs were transduced with Ad-CMV-VEGF or Ad-CMV-GFP at a MOI of 100 pfu/ml in Eppendorf tubes and incubated at 37ºC for one hour. After one hour, the cells were centrifuged at the supernatant was discarded. The pellet was resuspended in ASC medium and seeded in a 24 well plate. Medium was changed the following day to remove non-adherent cells. Non-transduced ASCs were used as a negative control. Two days after transduction, the cells were viewed under fluorescence microscopy to observe green fluorescent cells. Medium collected from the cells after three days was used for VEGF ELISA.

2.13. Wound healing experiment on punch biopsies

24 wound models treated with ASC-AAV5-CAG-VEGF-GFP, ASC-AAV5-CMV-GFP, non-transduced ASCs, or ASC medium (n=8) were assessed for wound healing by measuring the area of the wound punch every alternate day using ImageJ and Picture frame software. Rate of wound closure was determined by comparing the present size of the wound to the original wound area before treatment. Comparison between each group was made to assess the rate of healing conferred by each experimental group.

2.14. Cryo-OCT sectioning

Full thickness unfixed biopsies were frozen at -80ºC with tissue freezing medium in a suitable mold. When frozen, 15 µm thick sections were cut using cryostat at -27ºC. The sections were then transferred to microscope slides by gently touching the tissues to

the slide; the slides were labelled according to their respective tissue sample and stored at 4ºC.

2.15. Paraffin embedded sectioning

The tissues were fixed in 4% PFA (paraformaldehyde) or 3.7% formaldehyde for 2 hours after which the fixative was poured off and rinsed with 50% ethanol. Immediately the tissues were put in fresh 50% ethanol for one hour with 2 changes in between for 20 minutes each. Next the tissues were dehydrated in 70% ethanol, 95% ethanol and 100% ethanol for 1 hour each. After the dehydration steps, the tissues were cleared in xylene for one hour. During this, the xylene was replaced once every 20 minutes. The tissue were then infiltrated with equal volumes of xylene and molten paraffin for one hour at 60ºC. After one hour, the xylene/paraffin mix was replaced with molten paraffin and the tissues were infiltrated for three 30 minute washes. The tissues were then transferred with clean and pre-warmed forceps into their proper molds. For the future identification of tissues, embedding rings were placed on the molds and labelled accordingly. The molds were filled with molten paraffin and were allowed to set on a cold plate. Once solidified, the wax blocks containing the tissues were removed from the molds and 10 µm sections were made using a microtome. After sectioning, the ribbons were placed in a water bath at 48ºC and then were transferred to clean microscopic slides and were kept at 55ºC for 24 hours. The next day the slides were taken out and cooled at room temperature and were used for staining or were stored at 4ºC for future use.

2.16. Hematoxylin and Eosin (H&E) staining

The sections on microscopic slides were fixed in alcoholic formalin (40% formaldehyde and 95% ethanol) for one minute and then washed first in tap water

followed by distilled water. The sections were then stained with hematoxylin for 15 minutes followed by a rinse in tap water and then dipped in bluing reagent for 30 seconds. The sections were again washed in tap water and dipped in eosin for 5 minutes. Next, the sections were washed in 95% alcohol for 2 times, followed by 3 washes in 100% alcohol, and then 2 final washes in xylene. The sections were then mounted with Permount and cover-slipped and sealed along the slides with nail polish. The slides were viewed under the microscope immediately or stored at 4ºC.

2.17. Immunofluorescence staining

Cryo-OCT sectioned samples were first fixed with 3.7% formaldehyde in PBS for 15 minutes, followed by 3 rinses with PBS. Next the sections were blocked with blocking buffer (9.5 mL 10 X PBS, 0.5 mL normal goat serum and 30 µL Triton X-100 (100%) for one hour. The blocking buffer was then aspirated and diluted primary antibody (Mouse mAb CD31, Cell Signaling Technology, Inc., #3548, 1:3200 dilution; Mouse mAb Ki-67 Cell Signaling Technology, Inc., #9449, 1:800 dilution) at the required concentration was poured over the sections, which were then incubated overnight at 4ºC. The next day the sections were rinsed in PBS for three minutes. To minimize background, during the 3rd rinse, high salt PBS (50 mL 1 X PBS, 1.169 g NaCl) was used. Next, the sections were incubated in fluorochrome conjugated secondary antibody (goat anti-mouse Alexa Fluor® 488; goat anti-mouse Alexa Fluor® 568, Invitrogen) diluted in antibody dilution buffer (20 mL 1 X PBS, 0.08 g BSA, 60 µL 100% Triton X-100) for 1-2 hours in the dark and then rinsed with PBS for three times. The sections were finally cover slipped and sealed along the sides with nail polish. The slides were immediately viewed under the microscope or stored at 4ºC

2.18. Wound healing assay on cells

Wound healing assays were performed on monolayers of ASCs by creating a scratch in the cell culture with the help of a pipette tip. Cell debris was removed by washing with PBS and then replaced with medium. Scratches were created on both transduced and non-transduced cells to compare the healing rate. Cells were observed under the microscope over a period of days to determine the number of days required for the scratch to heal.

2.19. Red light exposure on ASCs

ASCs were seeded at $1x10^5$ cells per well in a 12 well plate. After two days, the cells were exposed to red light, green light or ambient light (control) for 15 minutes and were kept for 48 hours incubation at 37°C. Cells exposed to red, green or ambient light were counted two days after exposure and the count was compared to the number of cells seeded and the count before exposure to red or green LED light or ambient light to study the effect of light exposure on ASCs.

2.20. Red light exposure on wounds

1.5 mm^2 wound models were exposed to red light or ambient light for 15 minutes every other day for 20 days. Measurements on the wounds were taken throughout the experiment to study the effect of red light exposure on inducing wound closure.

2.21. Statistical analysis

All of our data are expressed as mean ± S.D. Statistical analysis was done using GraphPad Prism. Two way ANOVA followed by Bonferroni test was used to find significant differences. p value < 0.05 was considered significant.

Chapter 3: Organotypic wound model

3.1. Rationale

Chronic wound healing is a complex process. Most of the studies for the treatment of chronic wounds have been performed on mice models which are physiologically and hormonally different from humans. Often studies in mice cannot be replicated in humans, and are thus an inadequate chronic wound model system, creating a major barrier to understanding the mechanism of wound healing in humans (Nuutila *et al*., 2014). We proposed to develop a novel organotypic multidimensional wound model culture system that will replicate the complex tissue environment of human wound *in vivo* and thus help in developing a therapeutic approach that will accelerate the healing of a wound.

Previous studies in our lab showed that the skin biopsies do not retain the structure if maintained in a well plate without a support. We hypothesized that skin biopsies would retain their structure if held in a container that would allow growth at the air-liquid interface. Moreover, we hypothesized that a smaller biopsy in the center of the larger biopsy would act as a wound and recapitulate wound healing in humans. Organotypic human skin cultures with a central 2mm or 3mm wound were used as the wound models. The skin cultures were obtained under an approved IRB protocol by collaborators at the Miami Valley Hospital. The structure of the wound was analyzed in paraffin embedded sections or Tissue Freezing Medium embedded cryostat sections. Histological analyses of the wound sections were performed after hematoxylin and eosin

staining. Expression of the endothelial cell marker and proliferative cells were examined by immunofluorescence assay with CD31 and Ki-67 antibody, respectively.

3.2. Results

3.2.1. Histoarchitecture of the wound

To study the structure of the wound model, cryo-OCT embedded sections of the wound models were stained with Hematoxylin and Eosin (H&E). H&E imaging revealed the structure of the wound models, showing the epidermis, dermis and the subcutaneous fat and their sublayers. Figure 7a shows an example of a wound model in culture and figure 7b the sublayers of the epidermis, with the disrupted stratum corneum on the topmost layer, followed by stratum granulosum, the prickle layer stratum spinosum and the bottommost layer stratum basale separating the epidermis and dermis. Wound models were created from three tissue types: abdominoplasty, brachioplasty, and panniculectomy (figure 8). For the biopsies to be considered healthy, we examined into criteria like survivability of wound, maintenance of structure and integrity of wound in the millicells, normal anatomy of the skin layers.

Immunostaining of the wounds with CD31 and Ki-67 demonstrated staining of a few cells within the dermis layer of the wound model. Ki-67 stained cells were observed in the epidermis layer (figure 9). Positive staining for CD31 shows that the tissues were positive for endothelial cells indicating the presence of some blood vessels. Positive staining for mitotically active Ki67 shows that the tissues were positive for proliferative cells indicating that few cells were replicating in this model system. Control staining (with no primary antibody but only secondary antibody) showed no staining for Ki67 or

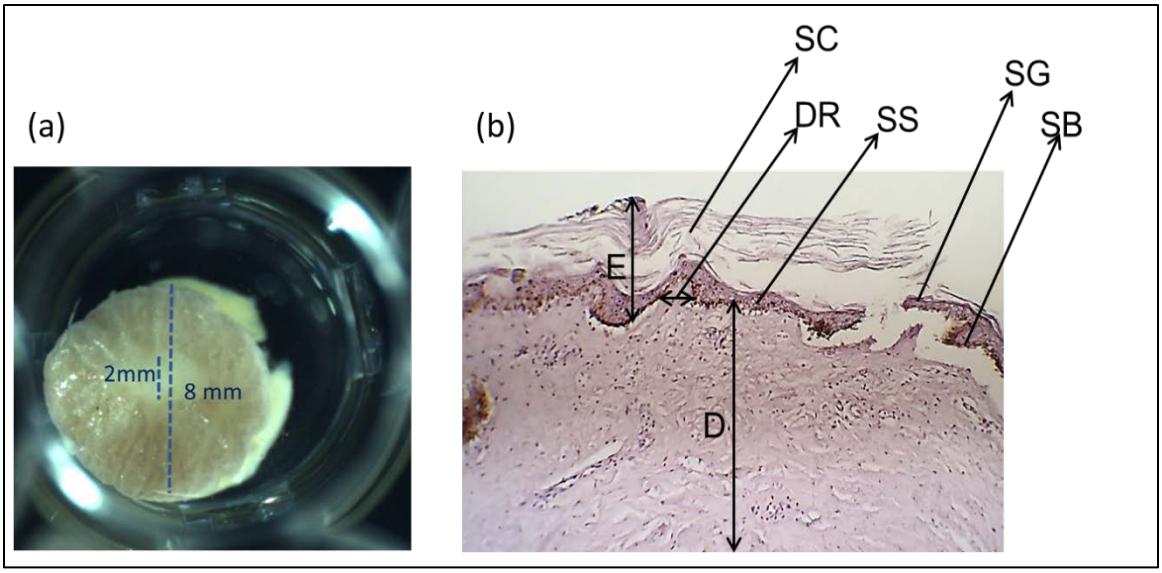

Figure 7: Architecture of the organotypic wound model system.

(a) Two month old multidimensional wound model with 8mm outer ring diameter and 2 mm inner punch (wound). Image taken at 0.63X magnification. (b) H&E staining of two month old the 2 mm wound model showing epidermis and dermis along with the sublayers. SC - Stratum Corneum, SS - Stratum Spinosum, SG - Stratum granulosum, SB - Stratum Basale, DR - Dermal ridges, E - Epidermis and D - Dermis. Images taken at 4X magnification.

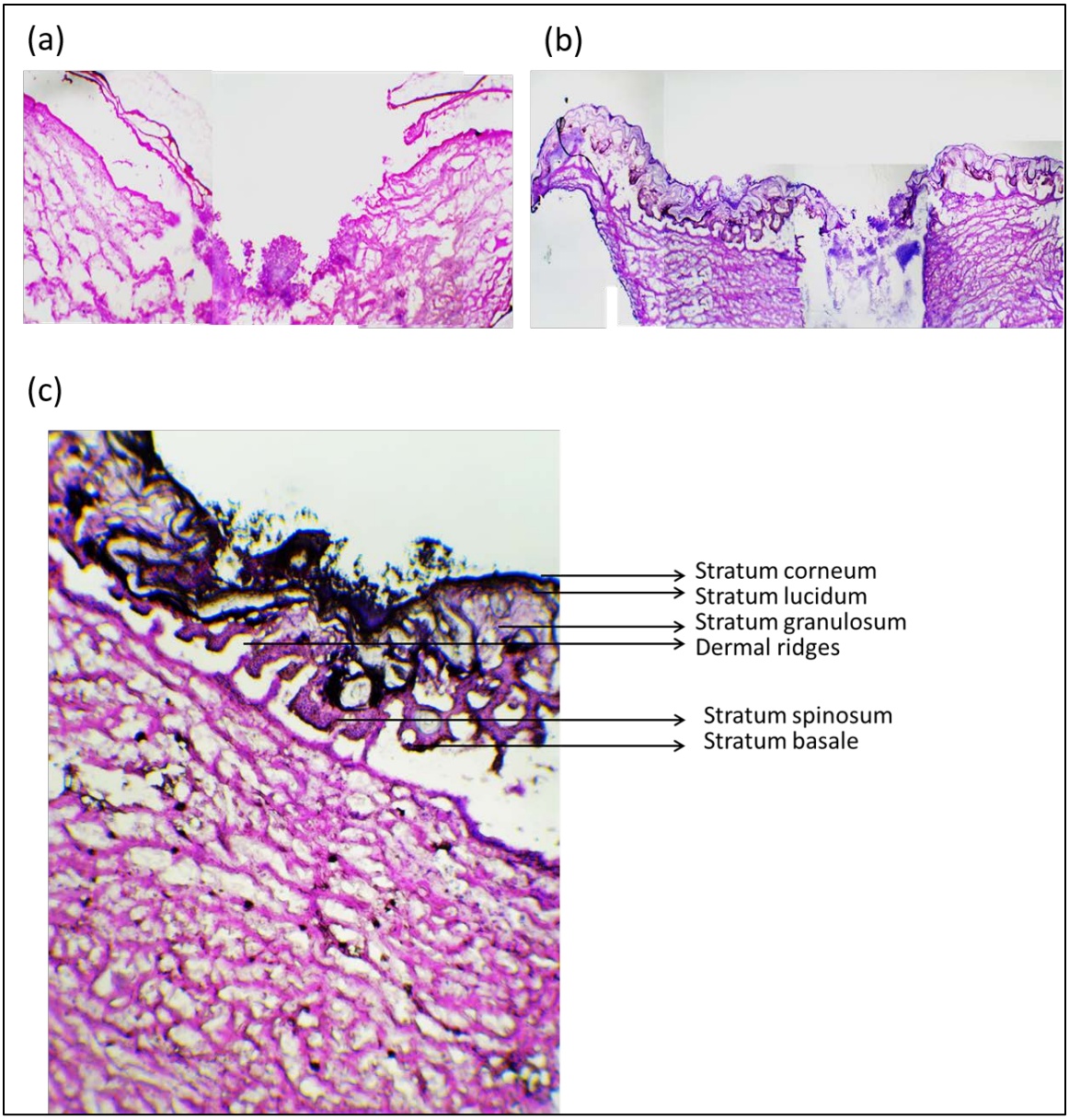

Figure 8: H&E staining of organotypic wound model

H&E staining of (a) one month old 3 mm brachioplasty partial thickness wound, (b) one month old 3 mm panniculectomy wound. Images taken at 4X magnification. (c) 10X magnified epidermis and dermis layer of a month old 3 mm panniculectomy wound.

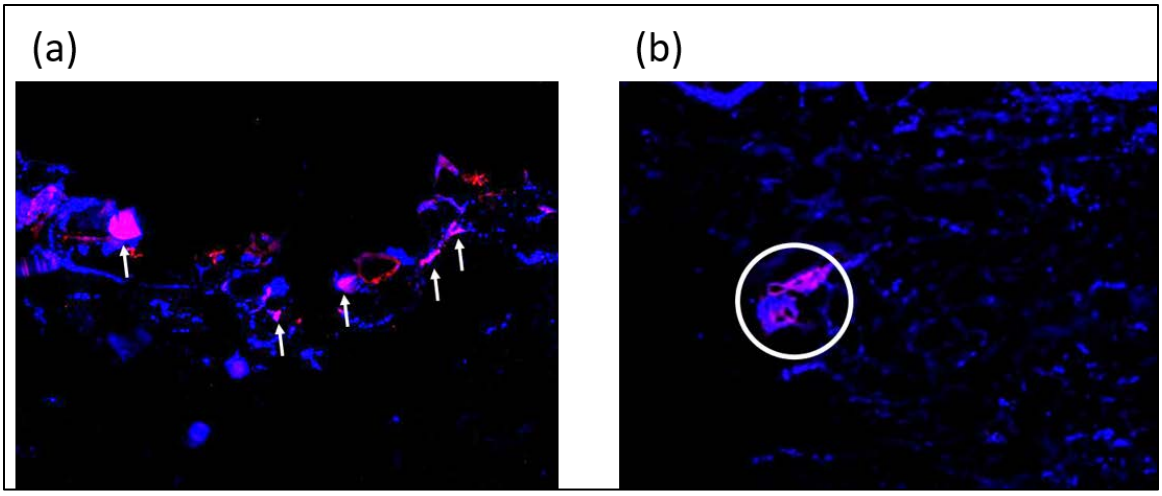

Figure 9: Immuno-characterization of wounds

Immunostaining on 2 months old 2mm wound model with (a) Ki67 antibody (in red) staining proliferative cells, (b) CD31 antibody (in red) staining blood vessels. Nucleus (DAPI) staining in blue. Images taken at 4X magnification.

CD31. Together these data suggest that the wound models were viable long term.

3.2.2. Viability of wound model:

Viability of two month old wound model was tested by MTT assay (figure 10) and evidenced by the formation of the purple color within 1 hour of addition of MTT into the wound bed. By contrast, a 4% paraformaldehyde (PFA) fixed wound did not develop color even after 6 hours of MTT addition, indicating that the PFA fixed wound model was dead. The wounds treated with MTT retained the purple color even after 6 hours of MTT addition (as shown in figure 10).

Similarly, a MTT assay was re-performed on four month old wound models previously studied for viability when the wound was 2 months old (figure 11). The minced tissue showed that within 1 hour of MTT addition, purple color darkened and it retained strong purple color till 3 days post-staining indicating that the wound model was viable after 4 months.

3.3. Discussion

In this study, we used organotypic human skin biopsies obtained by brachioplasty, abdominoplasty, and panniculectomy, as wound models. These models were maintained in millicells which provided them with sufficient support to maintain the structural integrity of the skin and wound. The wound models in the millicells were maintained at an air liquid. We expected that the wound models would require some additional growth factor like EGF or FGF or additional medium like F medium supplemented with hydrocortisone for survival of the wounds. However, it was observed that ASC medium by itself was sufficient enough to provide nutrients for survivability of wounds.

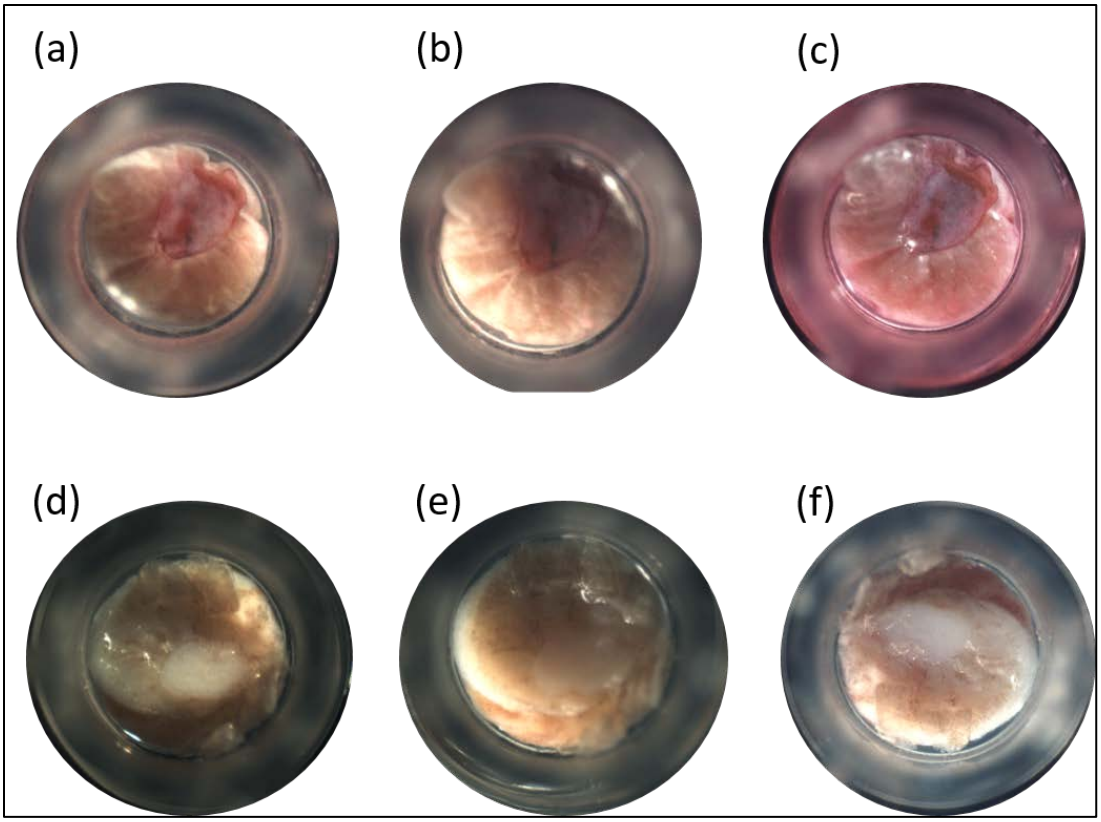

Figure 10: MTT assay to study viability of wound

MTT assay demonstrates viability of 2 month old unfixed wound model (a-c) and not 4% paraformaldehyde fixed (d-f). (a) Within 1 hour after addition of MTT to the wound a purple color began to develop in unfixed wound models and continued to intensify (b) after 2 hours and (c) after 6 hours indicating that the unfixed wounds are still viable after 6 hours of MTT addition. By contrast, no purple color formation was observed in 4% paraformaldehyde fixed wounds at (d) 1 hour, (e) 2 hours, or (f) 6 hours after MTT addition indicating that the fixed wounds are dead. Images taken at 1.25X magnification.

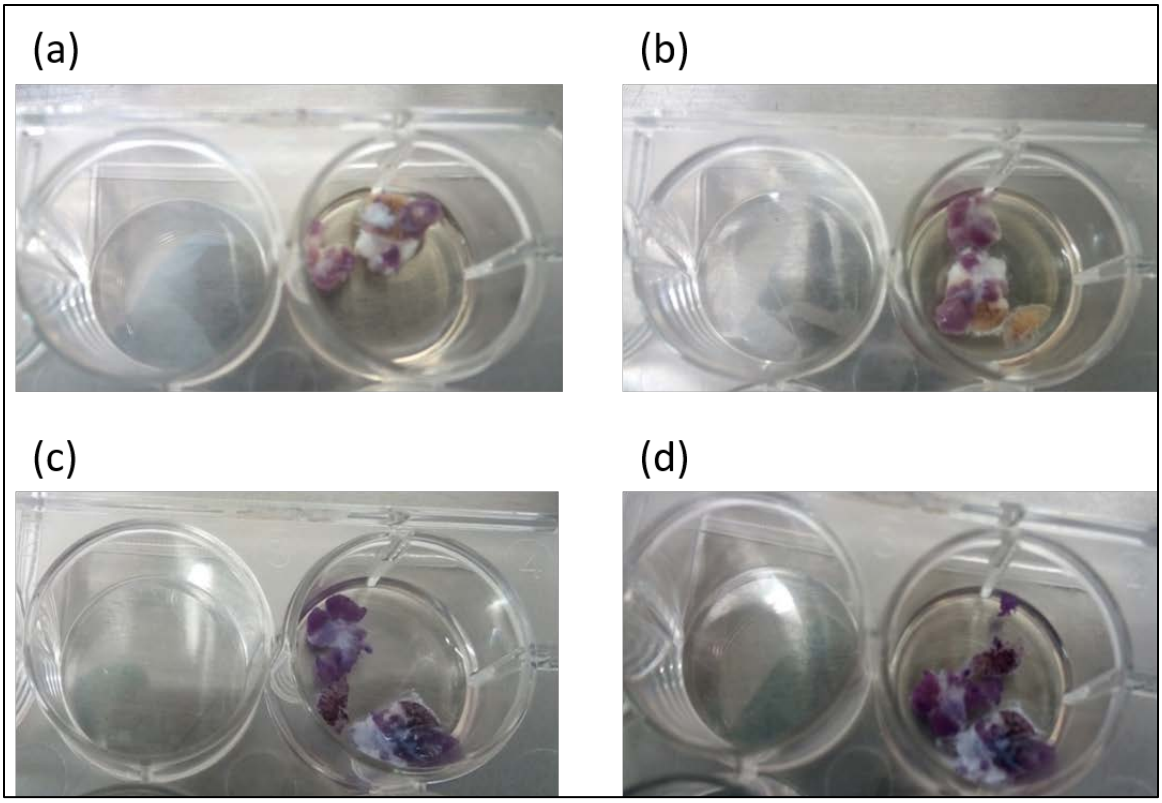

Figure 11: Viable 4 month old wound model

MTT assay re-performed on 4 month old minced wound model showed that the skin tissue and wound model is still viable. (a) at 0 hour after addition of MTT to the wound , (b) after 2 hours, (c) after 1 day and (d) after 3 days of MTT addition.

It was confirmed by MTT assay that the wound models were viable for at least four months as seen by the purple color formation in live wounds. The formation of the purple color in the live wounds was due to the breakdown of the MTT into formazan which indicates active metabolism in the live wound whereas in the control wounds fixed with paraformaldehyde, no color change was observed because the cells lost their ability to convert MTT into formazan, indicating that the wounds were not viable. Measurements taken on the wound models showed that the wounded area did not close by itself even after three months indicating that these wounds were chronic and could not heal naturally and would need additional therapies for healing.

Interestingly, these wound models derived from the skin are expected to be have a microbiome. Although we expected the antibiotics and antimycotics (ABAM) to kill the microbiome we periodically would get contamination of the medium. When the wounds were swabbed on to an agar plate in the absence of the antibiotics, bacterial colony formation was observed within 24 hours (data not shown). However, when the medium in contact with the basolateral side of the wound was plated on the antibiotic free agar plates, no colony formation was observed (data not shown) thus suggesting that the bacterial colony formation seen on the agar plate was due to the bacteria present on the skin surface of the punch biopsies. It is possible that the bacteria in the skin of the wounds are beneficial bacteria necessary for the survival of the skin. Despite the presence of bacteria, the wound cultures remained viable. Future work will explore this finding further.

H&E staining performed on the wound models confirmed the anatomy of skin model. A disrupted epidermis was observed in the wounded tissues (Figures 7, 8). It was

also observed that the epidermis of the wounds obtained from brachioplasty had a thinner epidermis than that of the abdominoplasty. Also biopsies obtained by abdominoplasty had a thicker subcutaneous fat layer than brachioplasty biopsies. The full thickness abdominoplasty wound models appears to be a better model for studying wound healing.

Immunostaining performed on the wounds with Ki67 antibody confirmed presence of mitotically active cells. CD31 staining on the wounded tissues showed a few blood vessels in the dermis region. It is expected that with the healing of the wounded tissues with VEGF treatment, more blood vessels would develop providing more of oxygen and nutrients to wound to enhance healing. However, in our models, there does not seem to be a large number of blood vessels. This could be due to the static nature of the medium (no blood flow) or insufficient cytokines to stimulate new blood vessel formation, or both. Few cytokeratin positive cells were found in the epidermis region of the wound models indicating the presence of few keratinocytes in the epidermis of the skin.

Most of the studies for wound healing are being performed in mouse models. Studies in mice cannot be replicated in human as mice genetically, hormonally, physiologically differ from human. Skin equivalents made from layering epidermis and dermis on a collagen matrix is also being studied as a model. The disadvantage of the skin equivalents is that often when epidermis stratifies, the stratum corneum spinosum layer is not formed and the statum corneum layer becomes too thin, as a result the tensile strength of these skin equivalents diminish (Sauto *et al.*, 2009). Overall, this human skin model we developed can be used to study wound healing as these models anatomically represent human skin.

Chapter 4: Adipose derived stem cells potentiate wound healing

4.1. Rationale

Chronic wounds have become a major problem in our society (Sen *et al.*, 2009). Potential treatments for chronic wounds are hyperbaric oxygen treatment, flap surgery, or amputation but these do not give a permanent solution. Thus efficient, accelerated, less invasive, personalized treatments have to be developed for millions suffering from chronic wounds. We expected to develop a cell and gene based therapy using adipose derived stem cells (ASCs) and vascular endothelial growth factor (VEGF) for treating chronic wounds. ASCs, through their regenerative properties, induce wound healing when transplanted into the wound bed. However, ASCs by themselves are not enough for the treatment of a chronic wound. We are developing a novel therapeutic strategy using an AAV to transfect the VEGF gene into ASCs in order to enhance VEGF expression to promote wound healing. We hypothesize that these VEGF expressing ASCs should then neutralize the chronic wound environment, enhance neovascularization and induce wound closure. I tested this hypothesis using in the organotypic *in vitro* wound model describe in Chapter 3.

4.2. Results

4.2.1. Construction of recombinant AAV

The construct for expressing VEGF-165 was designed by "Snapgene" software to include a chimeric synthetic intron upstream of the Kozak consensus start sequence, a VEGF-165 open reading frame (ORF), and a 3' poly-A sequence, all flanked by NheI and EcoRI restriction sites. The VEGF-165 gene block was synthesized by Integrated DNA Technology. The VEGF-165 gene was successfully cloned into the multiple cloning site (MCS) of the two AAV backbone pAAV-CMV-GFP and pAAV-CAG-GFP (figure 12). Both of these plasmids contained a GFP gene marker that is produced independently of the VEGF-165 protein by virtue of an internal ribosomal entry site separating the two genes. Ampicillin resistant colonies were grown and purified plasmid DNA was obtained by an Endofree plasmid maxi kit (5 Prime). Digestion of the plasmids with SalI and BamHI resulted in the release of the VEGF gene at around 0.9kb, which is in agreement with the expected size of the VEGF gene, 874bp. Digestion of the plasmids with MscI and XmaI showed the expected bands (as indicated by the arrows in figure 13) for pAAV-CAG-VEGF-GFP plasmid at 1033bp, 1288bp, 2471bp, 3503bp for MscI digestion and 11bp, 1685bp , 1947bp , 4652bp for XmaI digestion, but not for pAAV-CMV-VEGF-GFP. pAAV-CMV-VEGF-GFP showed some additional, unexpected, bands and was missing some of the predicted bands indicating that the ITRs were damaged.

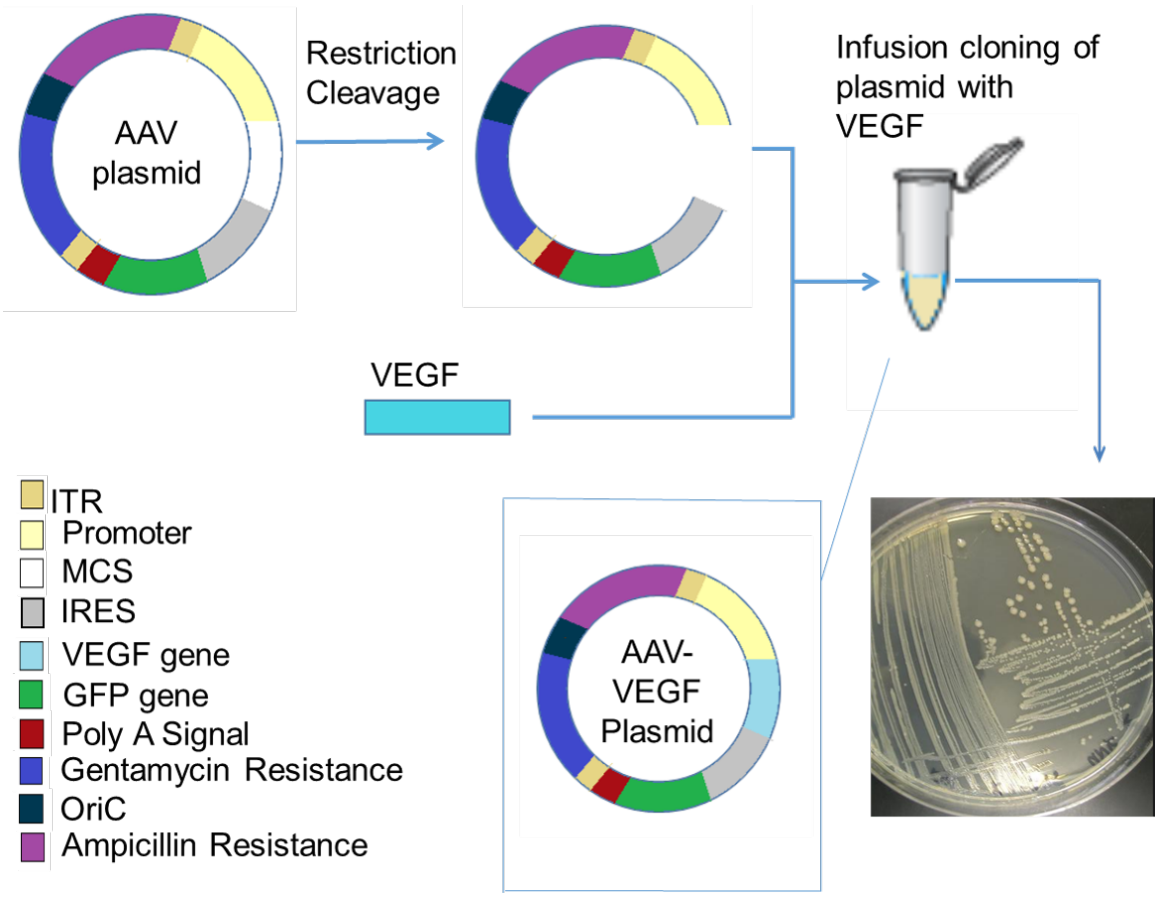

Figure 12: Cloning of VEGF into AAV plasmid

Figure represents the process for cloning the VEGF gene block into the multiple cloning site (MCS) region of AAV plasmids by Infusion cloning and production of AAV-VEGF plasmid. Different parts of the AAV plasmid are highlighted in different colors.

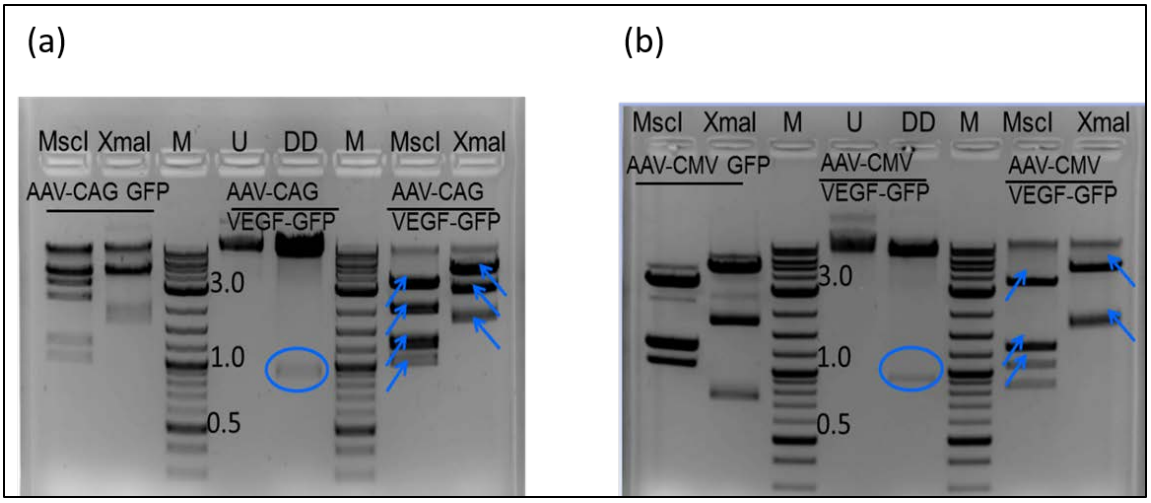

Figure 13: Restriction digestion of VEGF cloned AAV plasmid

Digestion of the (a) pFB-AAV-CAG-VEGF-IRES-eGFP and (b) pFB-AAV-CMV-VEGF-IRES-GFP plasmid with the restriction enzymes. Expected bands when digested with MscI: 1033,1288,2471,3503 bp. Expected bands when digested with XmaI: 11,1685,1947,4652 bp. DD- double digestion with SalI and BamHI, M- molecular marker. Blue arrows indicate expected bands and circle indicates the VEGF gene released at ~900 bp.

4.2.2. Transfection of recombinant AAV plasmid

The pAAV-CAG-VEGF-GFP and pAAV-CMV-VEGF-GFP plasmids were transfected into the HEK293 and ASC cells to test which promoter had a higher transfection efficiency (figure 14). pmaxGFP was used as a positive control. The CAG based promoter plasmid showed a higher and more robust gene expression of VEGF-GFP in HEK293 cells. pAAV-CAG-GFP plasmid demonstrated a lower transfection compared to pAAV-CMV-GFP, as shown in figure 14. Lower transfection efficiency was observed in the ASCs, which was expected as these cells have been previously described as being difficult to transfect.

4.2.3. Estimation of VEGF production from the transfected cells

VEGF secretion into the medium of the transfected cells was estimated by VEGF ELISA. pAAV-CAG-VEGF-GFP transfected cell medium showed higher VEGF secretion than pAAV-CMV-VEGF-GFP transfected cells, correlating with the transfection results (shown in figure 15). Only background level of VEGF secretion was obtained from the pAAV-CAG-GFP and pAAV-CMV-GFP transfected cells.

4.2.4. Production of the recombinant AAV vector

Based on the results of transfection and VEGF ELISA, purified pAAV-CAG-VEGF-GFP plasmid was used for production of recombinant AAV5-CAG-VEGF-GFP virus (with a titer of 9.11×10^{12} vg/ml (1^{st} lot); 6.63×10^{12} vg/ml (2^{nd} lot)) by the Viral Vector Core, at the University of Iowa, using the Baculovirus system. The purity of the viral vector was determined by SDS-PAGE and silver staining (figure 16). AAV5-CMV-GFP (titer 2.5×10^{14} vg/ml) virus was used as a control virus.

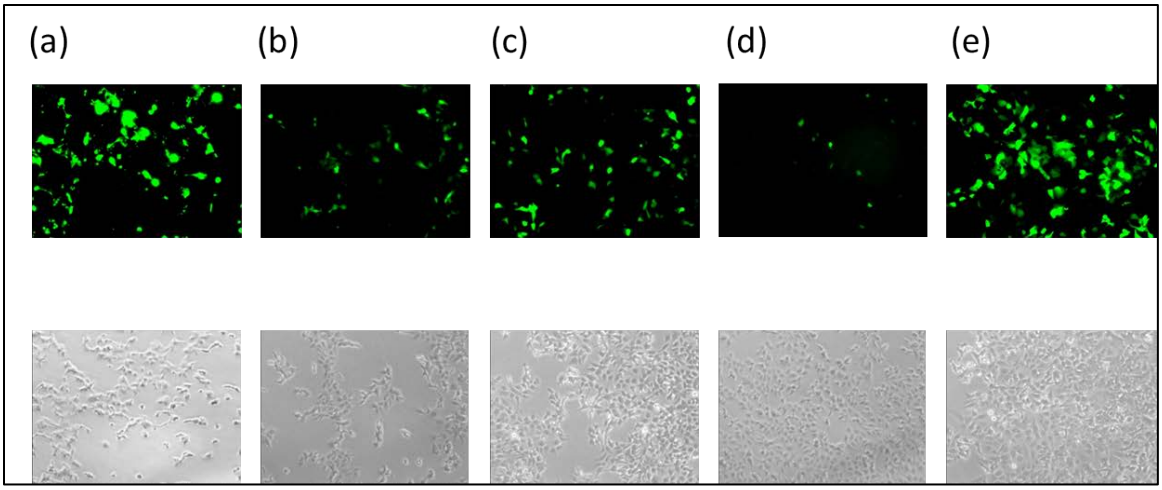

Figure 14: Transfection efficiency of VEGF cloned AAV plasmid in HEK293 cells

Transfection of the HEK293 cells with (a) pmaxGFP, (b) pAAV-CMV-GFP, (c) pAAV-CMV-VEGF-GFP, (d) pAAV-CAG-GFP, (e) pAAV-CAG-VEGF-GFP plasmid. Green cells (in the upper panel) are positive for green fluorescent protein, indicating successful transfection. Lower panel represents respective cells in the bright field. Images taken at 10X magnification using a Nikon Eclipse TE-2000-S fluorescence microscope.

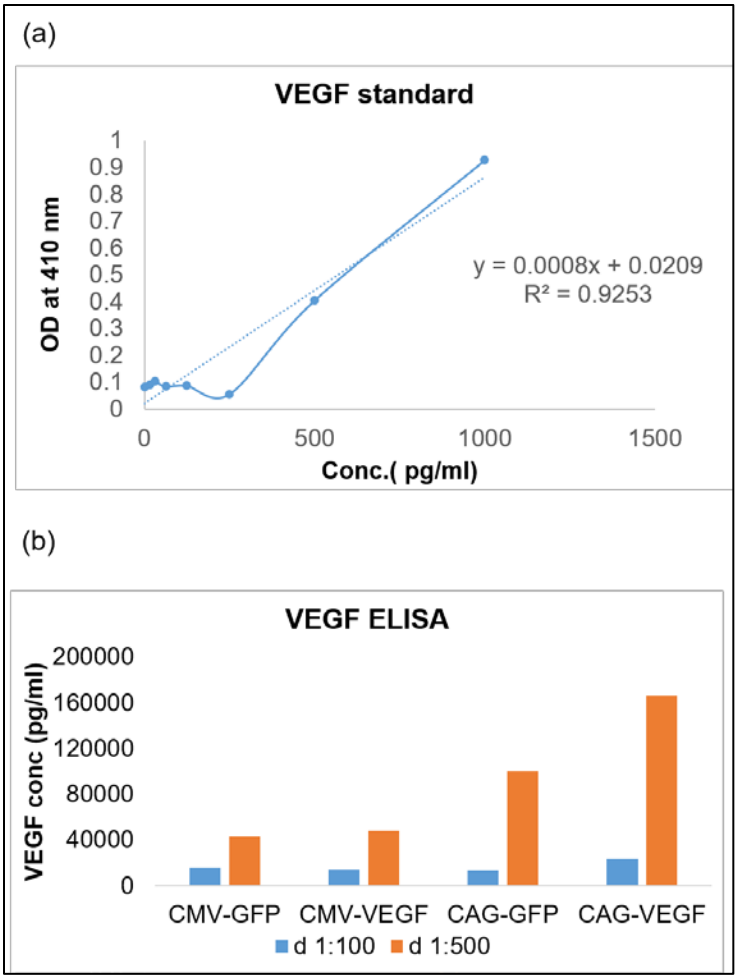

Figure 15: Estimation of VEGF secretion by pAAV-CAG-VEGF and pAAV-CMV-VEGF transfected HEK293 cells.

(a) Standard graph for VEGF ELISA. (b) Estimation of VEGF concentration secreted in the medium by the HEK293 cells transfected with pAAV-CMV-GFP, pAAV-CMV-VEGF-GFP, pAAV-CAG-GFP and pAAV-CAG-VEGF-GFP. Orange bar represents results from a 1:500 dilution and blue bar represents 1:100 dilution of medium.

4.2.5. Transgene expression of AAV5-CAG-VEGF-GFP in ASCs

ASCs transduced with AAV5-CAG-VEGF-GFP at an MOI of 10^6 vg/cell expressed green fluorescent cells positive for VEGF. A transduction efficiency of around 5-10% was obtained in the presence of 0.5 µM Hoechst 33342 owing to the low titer of AAV5-CAG-VEGF-GFP virus. AAV5-CMV-GFP showed a similar number of green fluorescent cells positive for GFP (figure 17). ASCs required a minimum of two or three days for transgene expression.

4.2.6. Transduction of ASCs with AdV5-CMV-VEGF

ASCs were transduced with AdV5-CMV-VEGF and AdV5-CMV-GFP (control virus) at an MOI of 100. Almost 70-80% of the AdV5-GFP transduced cells expressed green fluorescent protein. Since AdV5-VEGF did not have GFP transgene in its backbone, we could not estimate the transduction efficiency of AdV5-CMV-VEGF by fluorescence microscopy. The VEGF secretion by the Ad-VEGF transduced cells was estimated by VEGF ELISA.

4.2.7. Estimation of VEGF production in the AAV5-CAG-VEGF-GFP and Ad-VEGF transduced cells

VEGF secreted by the transduced cells was estimated by VEGF ELISA (figure 21). For this experiment, we included another control, an adenovirus encoding the VEGF gene (AdV5-VEGF). It is known that adenovirus is able to efficiently transduce ASCs. As expected, AdV5-VEGF showed a very high secretion of VEGF when compared to AAV5-CAG-VEGF-GFP owing to the higher transduction efficiency. Low background levels of VEGF secretion was detected from the control cells and the ASCs medium

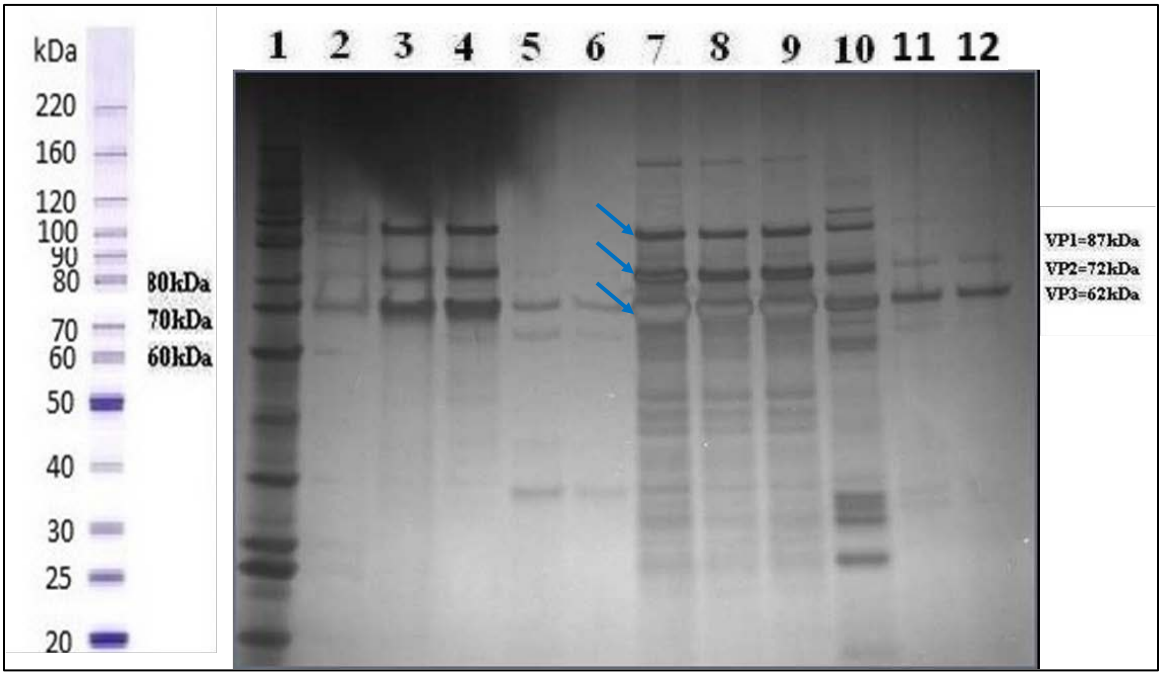

Figure 16: SDS-PAGE and silver staining on purified viral protein

The viral protein concentration as estimated by silver staining. The blue arrows indicate the AAV viral capsid proteins VP1, VP2, and VP3 are present in the expected ratio of ~1:2:10.

1- Protein Ladder, 2- AAV2/2CMVeGFP, 3- AAV2/2CMVeGFP, 4- AAV2/2CMVeGFP, 5- AAV2/2CMVCre, 6- AAV2/2CMVCre, 7- AAV2/5CAGVEGFwtIRESeGFP, 8- AAV2/5CAGwtIRESeGFP, 9- AAV2/5CAGwtIRESeGFP, 10- AAV2/5CMVCre, 11- AAV2/2CMVempty, 12- AAV2/2CMVempty.

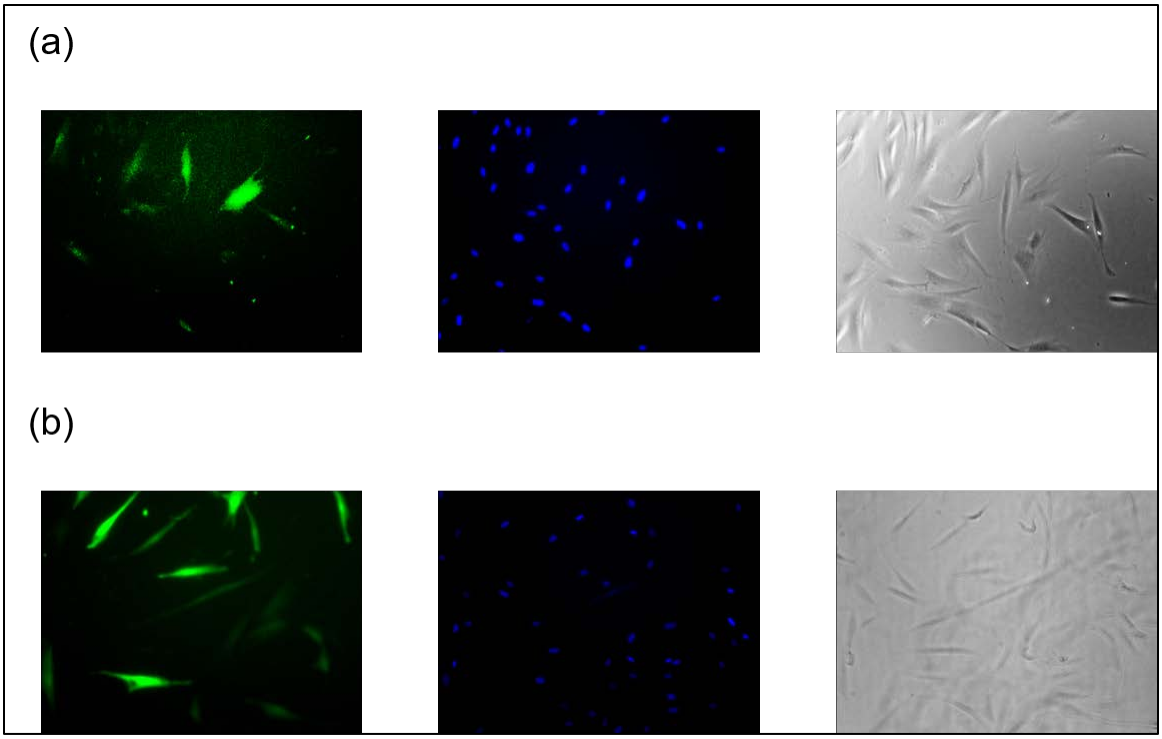

Figure 17: Viral transduction in ASCs

ASCs transduced with recombinant (a) AAV5-CAG-VEGF-GFP (top) and (b) control AAV5-CMV-GFP (bottom). Green fluorescent cells are expected to be positive for VEGF gene. Blue cells represent nuclei stained with Hoechst 33342. Images taken at 10X magnification using Nikon Eclipse TE-2000-S fluorescence microscope.

4.2.8. Characterization of transduced ASCs

ASC-AAV5-CAG-VEGF-GFP transduced and non-transduced ASCs, were characterized by flow cytometry with the selective markers according to the Gold Standard IFATS criteria. Higher than 95% of the AAV5-CAG-VEGF-GFP transduced ASC strongly expressed the ASCs stem cell markers CD13, CD44, CD73, CD90, CD105, while these cells were negative for CD31, CD45 and CD106 (endothelial cell marker, hematopoietic cell marker and vascular cell marker respectively) (figures 18 and 19), thereby indicating the transduced ASCs maintained their stem markers even after AAV5-CAG-VEGF-GFP transduction.

4.2.9. Wound healing ability of the ASCs

Monolayers of ASCs were transduced with AAV5-CAG-VEGF-GFP (n=3) ASC-AAV5-CMV-GFP (n=3), or mock transduced (n=3). Three days later cells were close to 100% confluent and wounds were made by a pipette tip scratch (on day 0) and were analyzed over a period of three days for wound closure (figure 20). By day 1, the wounds in the mock transduced cells had started to close, but these cells required nearly 3 days for complete healing. Similar to the mock transduced cells, the ASC-AAV5-CMV-GFP transduced cells took almost 3 days to heal. Whereas for the ASC-AAV5-CAG-VEGF-GFP transduced cells, by day 1, the wound had experienced 70-75% healing. By day 2, the wound had completely healed, thus indicating that ASCs expressing VEGF are much more potent in healing chronic wounds.

4.2.10. Allogenic ASCs eluting AAV-VEGF potentiate healing in 2 mm organotypic wound model

To study the healing efficiency of heterologous ASCs in inducing wound healing,

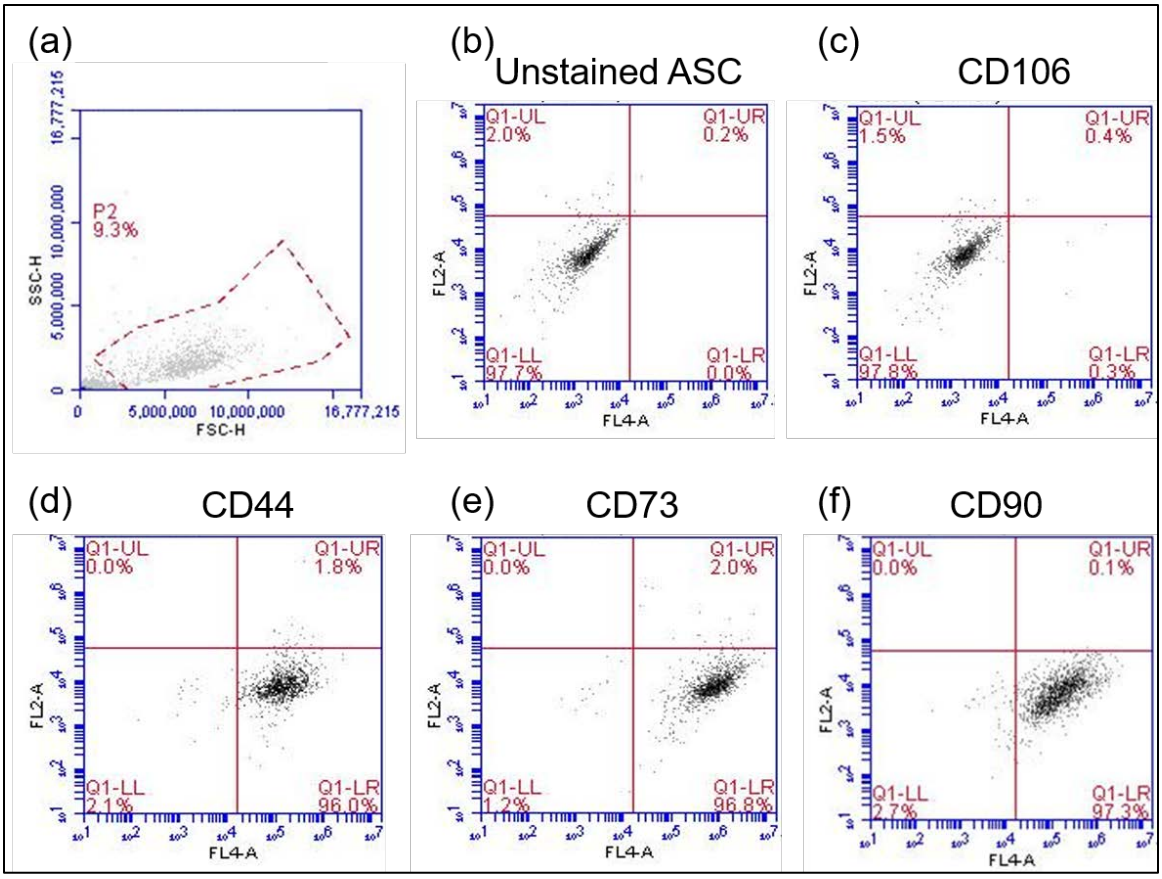

Figure 18: Flow cytometry analysis of AAV-CAG-VEGF-GFP transduced ASCs.

Flow cytometry analysis of stem cell markers show that AAV-CAG-VEGF-GFP transduced ASCs retain their stemness. (a) Representative gating of the stem cell population, (b) unstained ASCs (control), (c) CD106 is a negative stem cell marker and is not expressed. More than 98% of the ASCs express positive markers (d) CD44, (e) CD73 and (f) CD90. Data collected in collaboration with Sunishka Wimalawansa, Greg Gould and Priyanka Sharma.

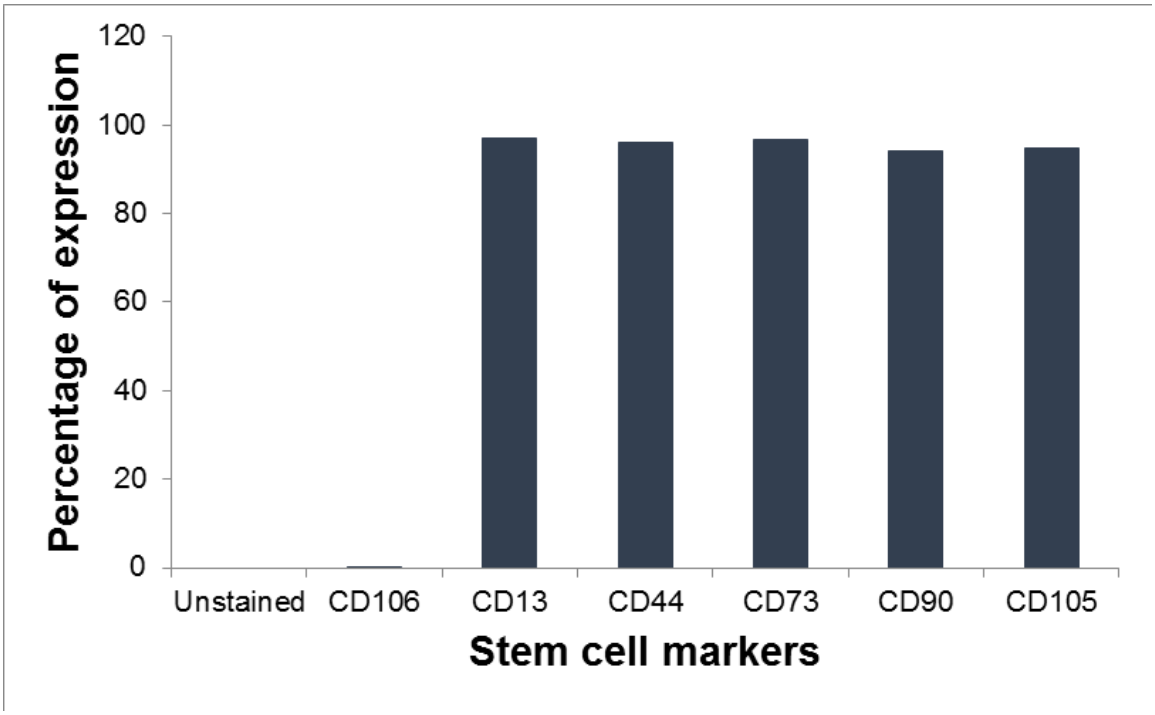

Figure 19: Stem cell marker profile of ASCs transduced with AAV-CAG-VEGF-GFP.

ASC-AAV-CAG-VEGF-VEGF (n=1) shows no expression of markers expected to be negative for stem cells (CD106) and >95% of the cells express markers expected to be positive for stem cells (CD13, CD44, CD73, CD90 and CD106).

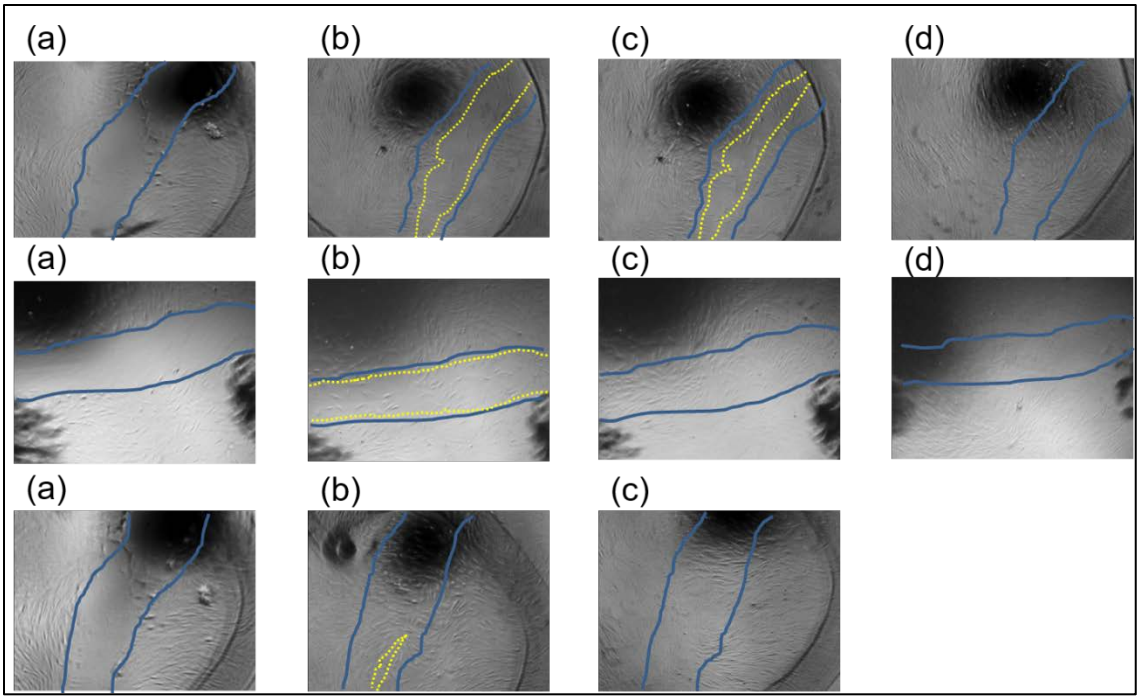

Figure 20: Wound healing assay on ASCs

Scratch assay on monolayer of non-transduced ASCs (n=3) (top panel), AAV5-CMV-GFP transduced ASCs (n=3) (middle panel) and AAV5-CAG-VEGF-GFP transduced ASCs (n=3) (bottom panel) on (a) day 0, (b) day 1, (c) day 2, (d) day 3 showing accelerated healing of ASC-AAV5-CAG-VEGF-GFP compared to non-transduced ASCs and ASC-AAV5-CMV-GFP. Images taken at 4X magnification using Nikon Eclipse TE-2000-S microscope.

ASCs were collected and infected with AAV in a small volume and in the presence of Hoechst 33342 in order to facilitate transduction. ASC-AAV5-CAG-VEGF-GFP, ASC-AAV5-CMV-GFP and non-transduced ASC were added as a cell suspension (at a cell concentration of 10^4 cells per wound every 7 days) into the wound punch of the organotypic wound model and were assessed over a month long period to compare rates of wound healing. Wounds treated with only ASC medium (n=3) were used as controls. Wounds treated with ASC-AAV5-CAG-VEGF-GFP (n= 3) healed to almost 45.18 ± 3.8 % (figure 21) over 32 days whereas the wounds treated with ASC-AAV5-GFP (n=3) and non-transduced ASCs (n=3) healed to only about 19.96 ± 2.4 % and 17.78 ± 2.3 % respectively over the same time frame. The control wounds only healed 6.19 ± 1.0 %. This indicated that ASCs expressing VEGF are more efficient at accelerating the healing of chronic wounds when compared to ASCs expressing a GFP and non-transduced ASCs. H&E staining performed on the wounds on day 2 and day 32 (figure 22), shows that compared to day 2, a significant reduction (*$p < 0.001$) in the wounded area occurred after ASC-AAV5-CAG-VEGF-GFP, ASC-AAV5-CMV-GFP or non-transduced ASCs treatment, in comparison to medium only wounds. However no significant difference in healing was observed between ASC-AAV5-CAG-GFP or non-transduced ASCs treated wounds. Ki67 staining performed on the wounds on day 2 and day 32 (figures 23 and 24) shows that the wounds were viable at the termination of the experiment on day 32. Wounds on day 2 and day 32 were stained with CD31 antibody to detect blood vessels (figure 25 and figure 26).

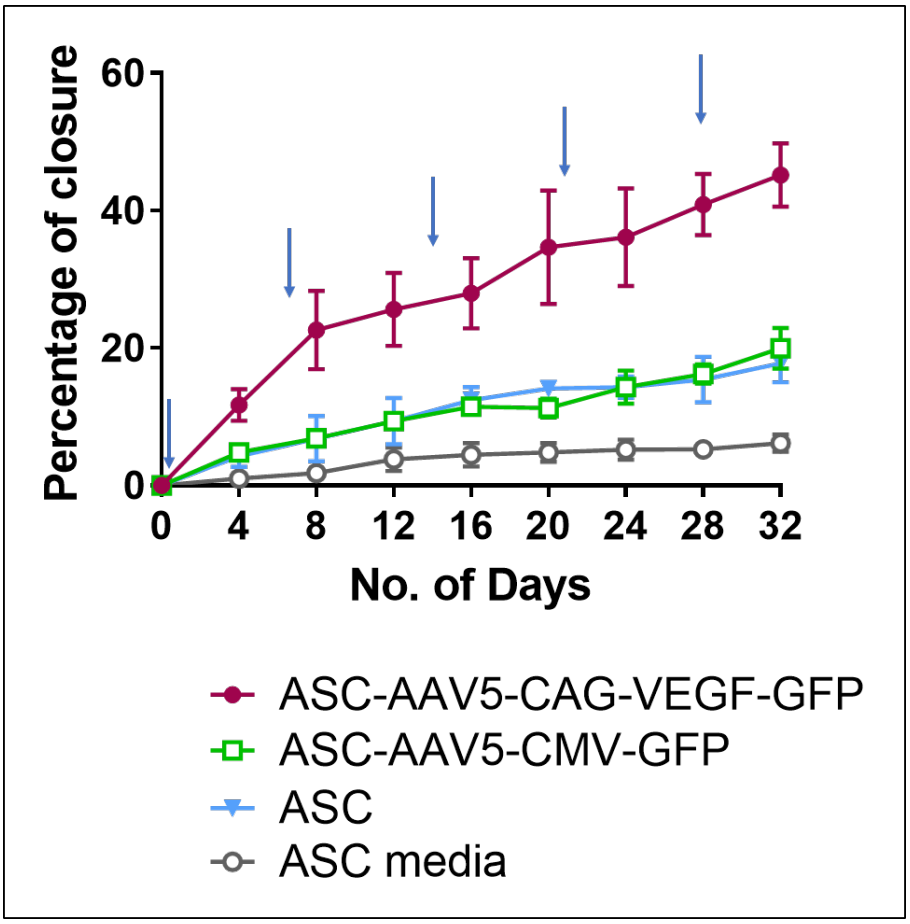

Figure 21: Effect of allogenic ASCs secreting AAV5-CAG-VEGF-GFP on 2mm wound models.

ASC-AAV-CAG-VEGF-GFP treated wounds (n=3) significantly enhanced wound healing compared to wounds treated with ASC-AAV5-CMV-GFP (n=3), non-transduced ASC (n=3) or ASC medium (n=3) from day 8 to day 32 (*$p < 0.001$). Healing by non-transduced ASCs was similar to ASC-AAV5-CMV-GFP ($p > 0.05$). Blue arrows indicate ASCs addition (10^4 ASCs per wound added every 7 days on Day 0, 7, 14, 21 and 28. Error bars represent SD. Analysis performed using two way ANOVA followed by Bonferroni test to obtain the p value.

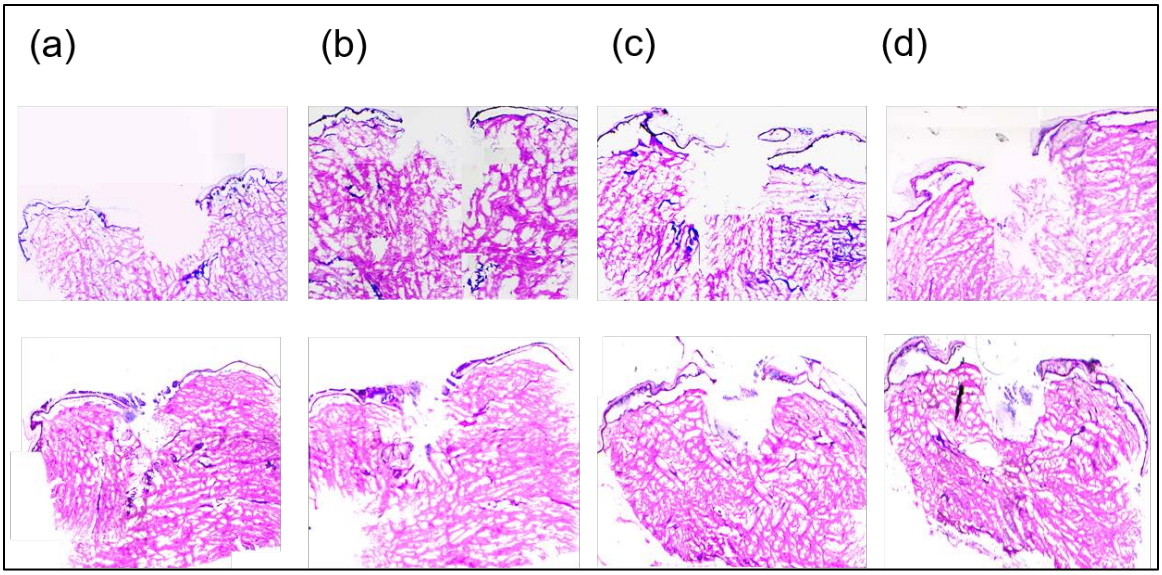

Figure 22: Histo-analysis of allogenic wounds treated with ASC-AAV5-CAG-VEGF-GFP, ASC-AAV5-CMV-GFP, non-transduced ASCs or ASC medium on day 2 and day 32.

Histological observation of allogenic wounds treated with (a) ASC-AAV5-CAG-VEGF-GFP, (b) ASC-AAV5-CMV-GFP, (c) non-transduced ASCs and (d) ASC medium on day 2 (top panel) and day 4 (bottom panel). A significant reduction in the wounded area was observed after ASC-AAV5-CAG-VEGF-GFP, ASC-AAV5-CMV-GFP, non-transduced ASCs treated wounds. Images taken at 4X magnification.

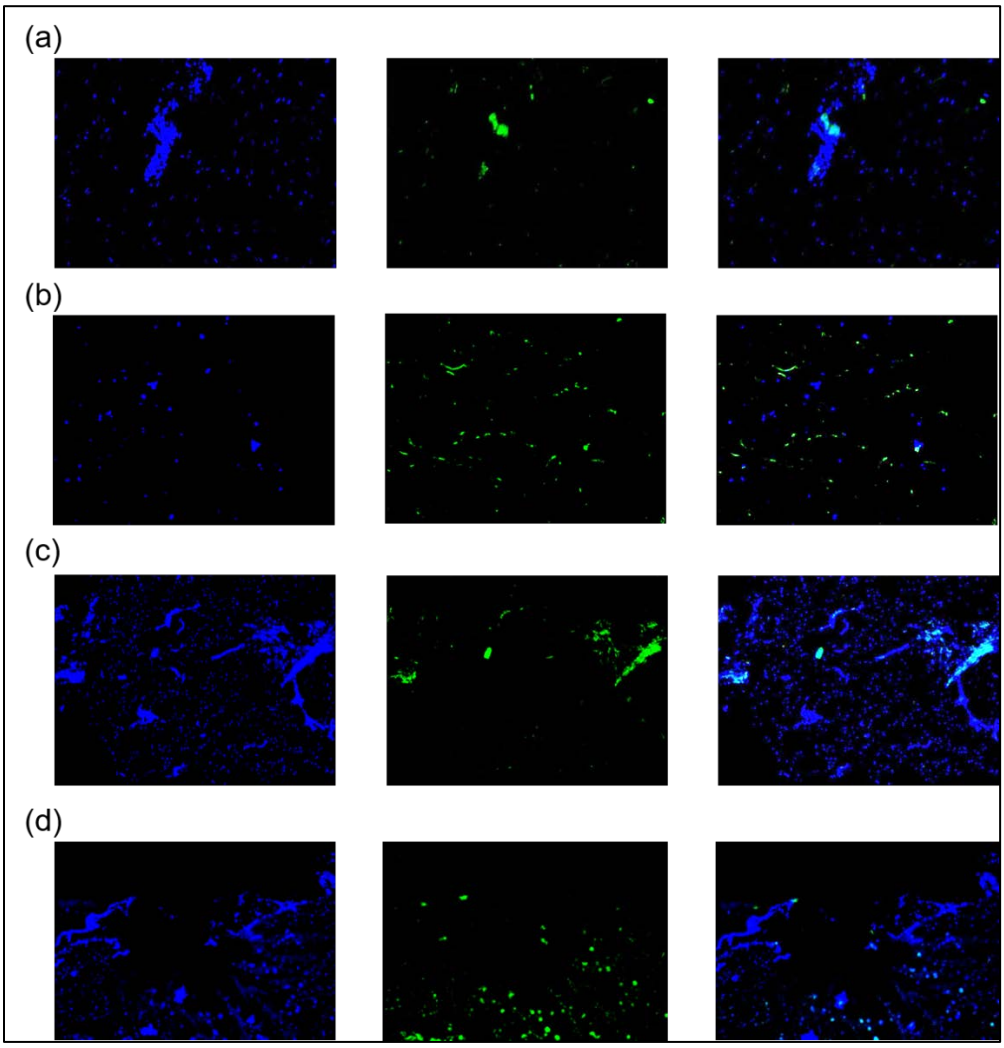

Figure 23: Ki-67 staining on 2 mm allogenic wounds on day 2 showing that the wounds are viable.

Ki67 staining (in green) on (a) ASC-AAV5-CAG-VEGF treated wounds, (b) ASC-AAV5-CMV-GFP treated wounds, (c) non-transduced ASCs treated wounds, (d) ASC medium treated wounds. DAPI staining in blue. Images taken at 4X magnification using Nikon Eclipse TE-2000-S fluorescence microscope.

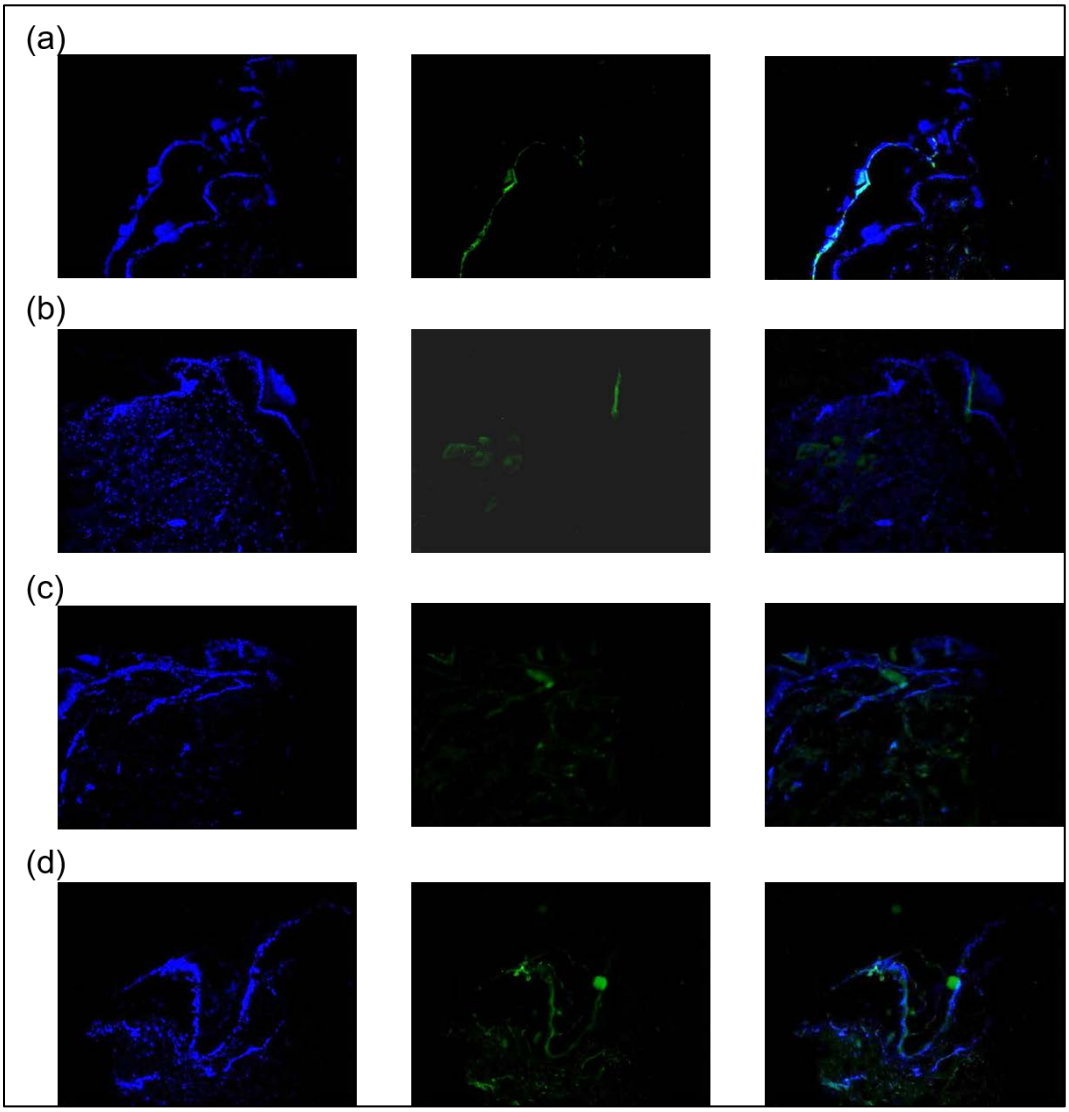

Figure 24: Ki-67 staining on 2 mm allogenic wounds on day 32 shows that the wounds are viable.

Ki-67 staining (in green) on (a) ASC-AAV5-CAG-VEGF treated wounds, (b) ASC-AAV5-CMV-GFP treated wounds, (c) non-transduced ASCs treated wounds, (d) ASC medium treated wounds. Images taken at 4X magnification using Nikon Eclipse TE-2000-S fluorescence microscope.

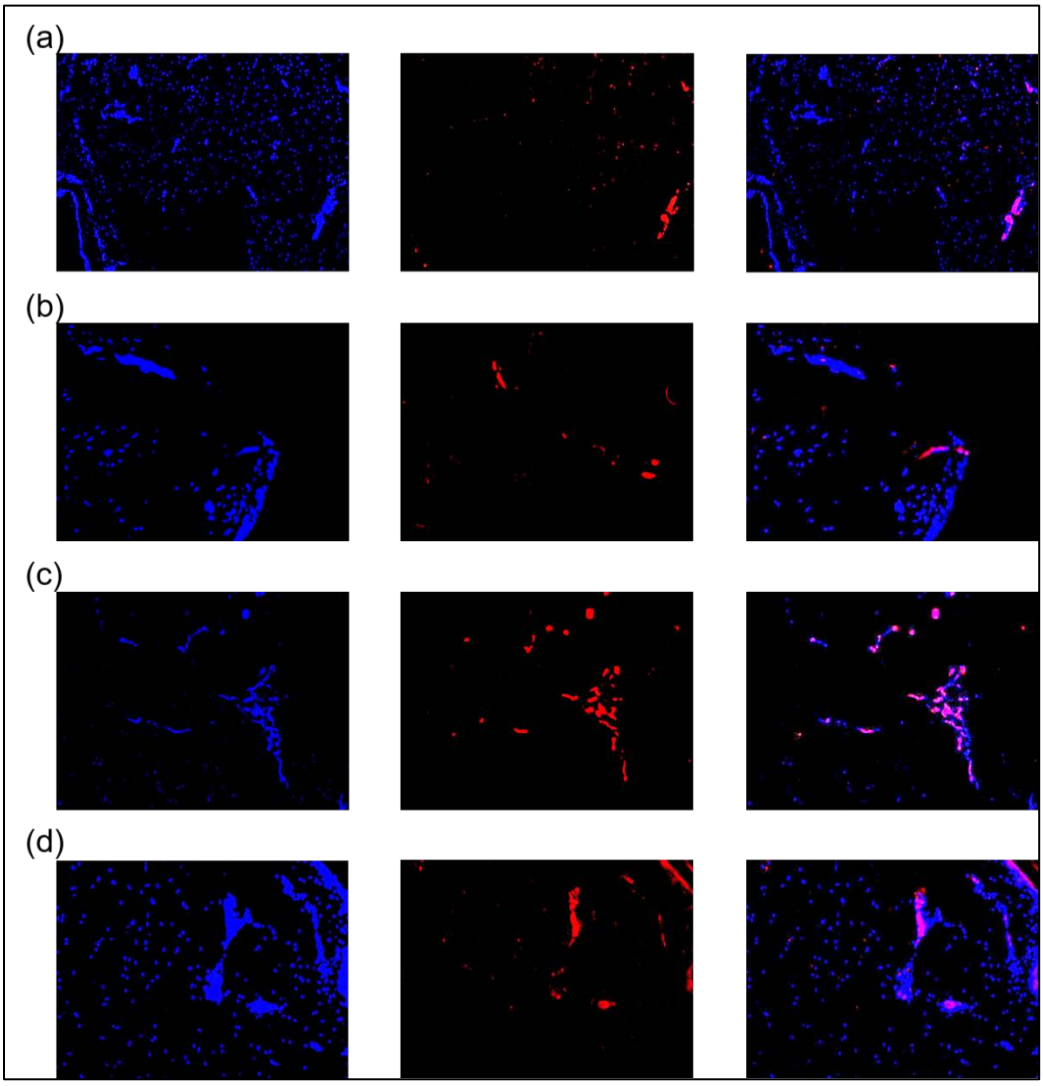

Figure 25: CD31 staining on 2 mm allogenic wounds on day 2 marking the endothelial cells.

CD31 staining (in red) on (a) ASC-AAV5-CAG-VEGF treated wounds, (b) ASC-AAV5-CMV-GFP treated wounds, (c) non-transduced ASCs treated wounds, (d) ASC-medium treated wounds. Images taken at 4X magnification using Nikon Eclipse TE-2000-S fluorescence microscope.

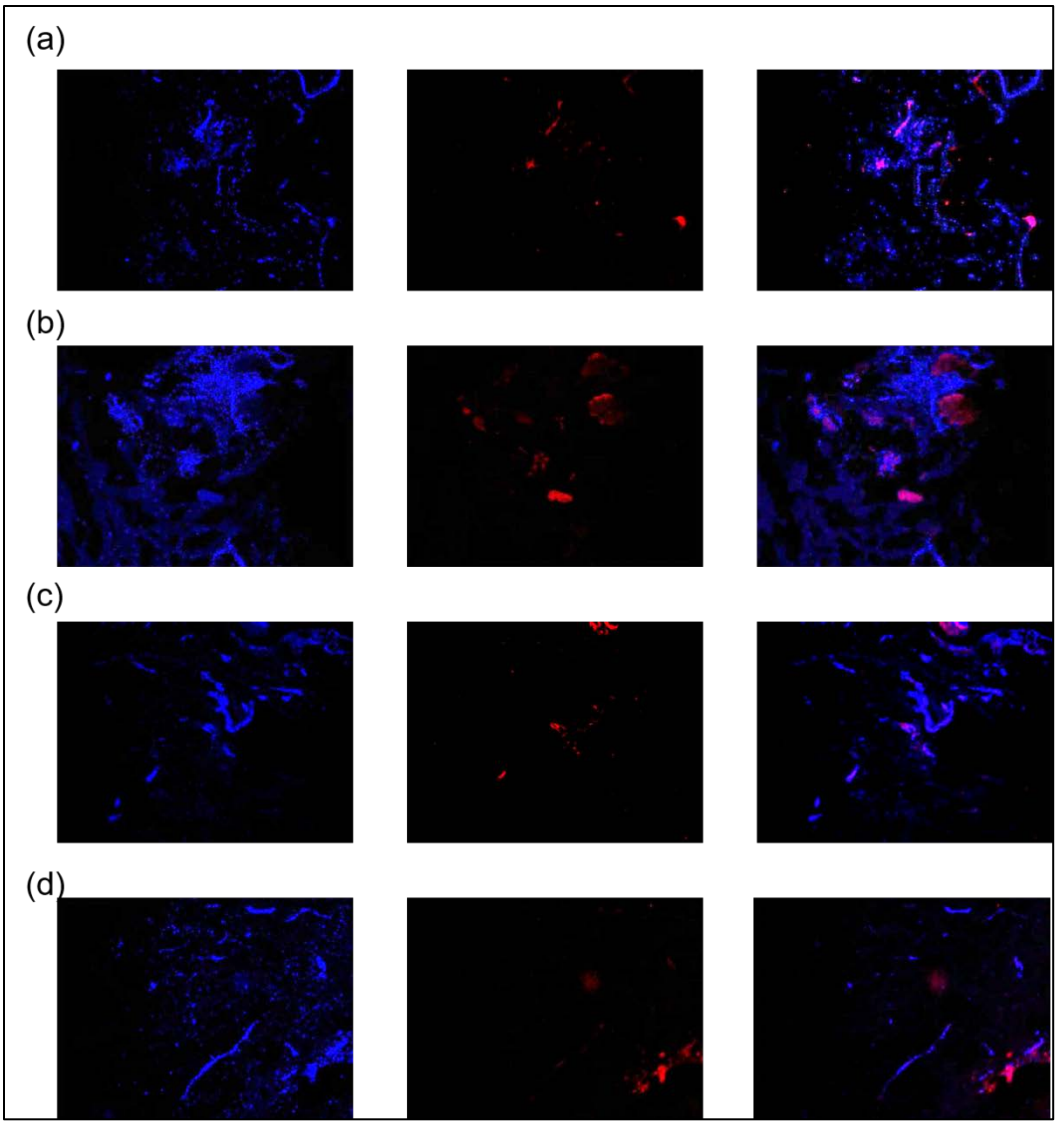

Figure 26: CD31 staining on 2 mm allogenic wounds on day 32 marking the endothelial cells.

CD31 staining (in red) on (a) ASC-AAV5-CAG-VEGF treated wounds, (b) ASC-AAV5-CMV-GFP treated wounds, (c) non-transduced ASCs treated wounds, (d) ASC medium treated wounds. Images taken at 4X magnification using Nikon Eclipse TE-2000-S fluorescence microscope.

Few endothelial cells or blood vessels were observed in the ASC-AAV5-CAG-VEGF-GFP treated wound on day 32 (shown in figure 26a). No obvious difference was observed in the formation of the blood vessels after treating the wound with ASC-AAV5-CAG-VEGF-GFP.

4.2.11. Autologous ASCs secreting AAV-VEGF enhance wound healing in 2 mm wound models

To determine the effect of autologous ASCs in potentiating wound healing, the 2 mm wound models were treated with ASC-AAV5-CAG-VEGF-GFP (n=4), ASC-AAV5-CMV GFP (n=4) (at a cell concentration of 10^4 cells/wound/7 days), or ASC medium (n=4) for a month. Though complete closure was not observed, the wound models treated with autologous ASC-AAV5-CAG-VEGF-GFP showed a closure of 49.18 ± 4.7 % (as shown in figure 27). The wound models treated with ASC-AAV5-CMV-GFP closed to about 31.38 ± 6.2 % whereas the control wounds treated with ASC medium showed only 7.65 ± 2.2 % closure. H&E staining of the sections taken at day 28 shows that ASC-AAV5-CAG-VEGF-GFP treated wound had a scarred healing with a lot of eosin-reactive (blue) deposition in the wounded area (figure 28).

4.2.12. Autologous ASC secreting AAV-VEGF enhance wound healing in 3 mm wound models

To determine the effects of ASCs secreting VEGF in healing 3mm wound models, the wound models were treated with ASC-AAV5-CAG-VEGF-GFP (n=2), ASC-AAV5-CMV-GFP (n=2), non-transduced ASCs (n=2), or ASC medium (n=2) for a period of one month. Since these were 3 mm wound models, 10^5 autologous ASCs per wound per 7 days were used for the treatment. It was observed that the wounds treated

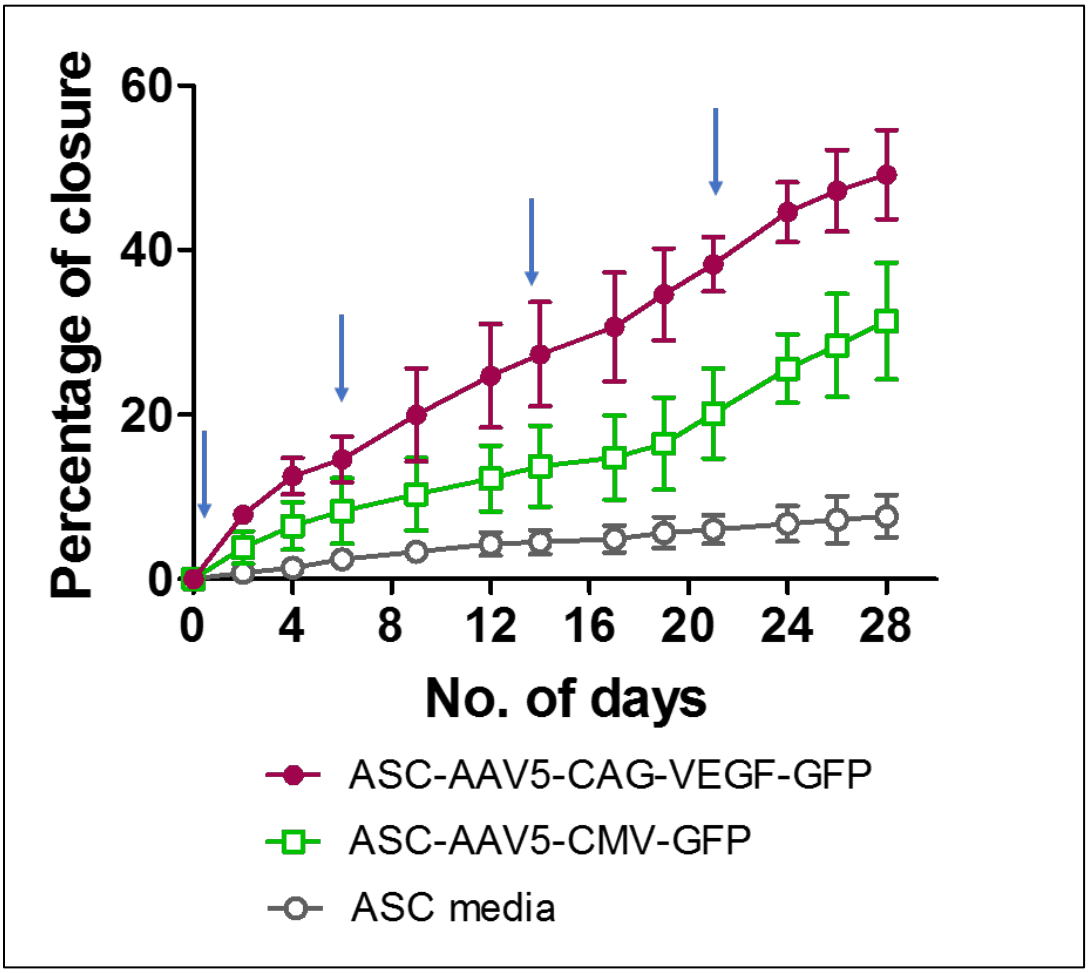

Figure 27: Effect of autologous ASCs (10^4 ASCs per wound) secreting VEGF on 2mm wound models.

Enhanced wound closure observed in ASC-AAV-CAG-VEGF-GFP treated wounds (n=4) compared to wounds treated with ASC medium (n=4) and ASC-AAV5-CMV-GFP (n=4) ($p < 0.001$).ASC-AAV5-CMV-GFP can induce healing relative to ASC medium treated wounds but not as effectively as ASC-AAV-CAG-VEGF-GFP treated wounds. Arrows indicate ASCs addition to the wounds on day 0, 7, 14, 21. Error bars represent SD. Analysis performed using two way ANOVA followed by a Bonferroni test to obtain the p value.

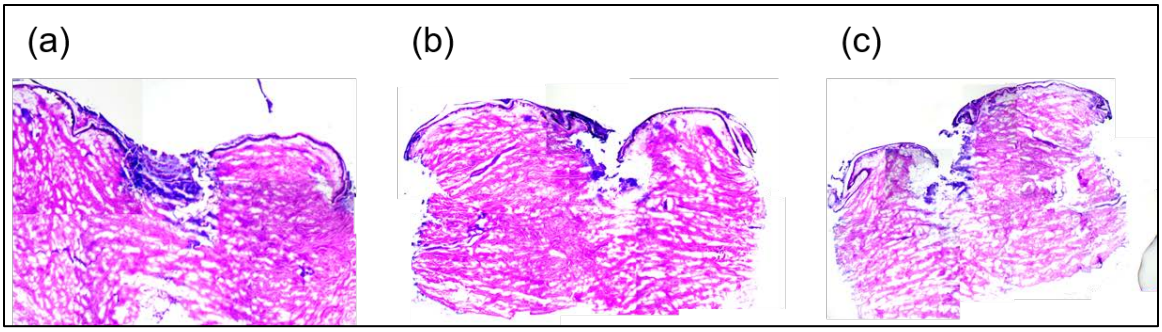

Figure 28: Histo-architecture of autologous ASC treated wounds on day 32.

H&E staining of autologous wounds treated with (a) ASC-AAV5-CAG-VEGF-GFP, (b) ASC-AAV5-CMV-GFP and (c) ASC medium on day 28. Wounds treated with ASC-AAV5-CAG-VEGF-GFP show partial healing with a lot of cellular deposition in the wounded area. Images taken at 4X magnification.

with ASCs eluting VEGF showed around 25.07 ± 1.1 % closure (as shown in figure 29) whereas the wounds treated with ASC-AAV5-CMV-GFP or non-transduced ASCs (ASCs NoT) showed about 18.01 ± 0.6 % and 16.73 ± 0.3 % healing respectively. The control wounds treated with ASC medium healed only by 8.12 ± 1.0 %.

4.2.13. Autologous ASCs secreting AdV-VEGF enhance wound healing in 3 mm wound models

Adenovirus can transduce ASCs at a higher level than adeno-associated virus and AdV-VEGF transduction yields high levels of VEGF secretion. To determine whether Ad-VEGF can induce more healing when compared to AAV5-CAG-VEGF-GFP (figures 21, 27 and 29), wound models were treated with ASC-Ad-CMV-VEGF (n=8), ASC-Ad-CMV-GFP (n=8), non-transduced ASCs (n=8) and ASC medium (control) (n=8) (figure 30). Since the VEGF secretion was much higher in the Ad-CMV-VEGF transduced ASCs when compared to AAV5-CAG-VEGF-VEGF transduced ASC, 10^4 ASC were added per wound every 7 days for the treatment of the wounds. We observed that the wounds treated with ASC-Ad-CMV-VEGF healed to around 29.00 ± 1.9 % whereas the ASC-Ad-CMV-GFP and non-transduced ASC (ASCs NoT) treated wounds healed to 22.77 ± 1.4% and 20.34 ± 1.0 % respectively. The control wounds treated with only ASC medium healed around 8.21 ± 1.2 %. ASC-AAV5-CAG-VEGF-GFP treated wound showed significant healing (*$p < 0.001$) compared to other groups. ASC-AAV5-CMV-GFP or non-transduced ASCs treated wound showed no significant difference in healing.

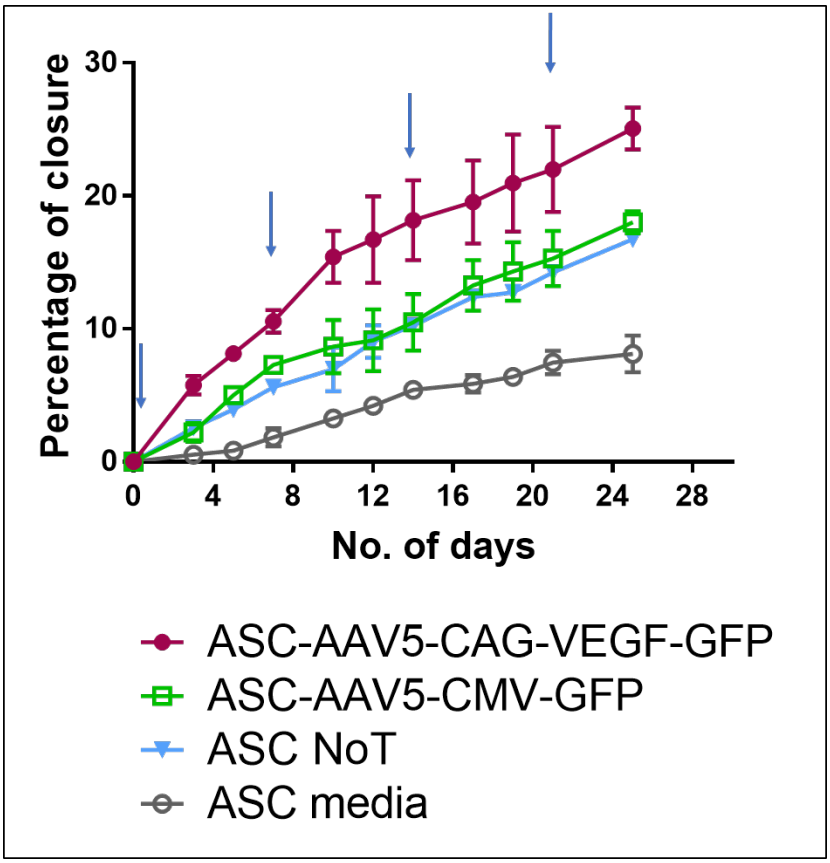

Figure 29: Effect of autologous ASCs (10^5 ASCs per wound) transduced with AAV5-CAG-VEGF-GFP on 3 mm wound models.

ASC-AAV-CAG-VEGF-GFP (n=2) significantly enhanced wound healing compared to wounds treated with ASC-AAV-CMV-GFP (n=2), non-transduced ASC (ASC NoT) (n=2) or ASC medium (n=2) starting from day 5 until day 25($p < 0.001$). ASC NoT and ASC-AAV5-CMV-GFP have similar healing efficiency ($p > 0.05$); however both show significantly three times higher healing than ASC medium treated wounds ($p < 0.001$). Arrows indicate ASCs addition to the wounds on day 0, 7, 14, 21. Error bars represent SD. Analysis performed using two way ANOVA followed by Bonferroni test to obtain the p value.

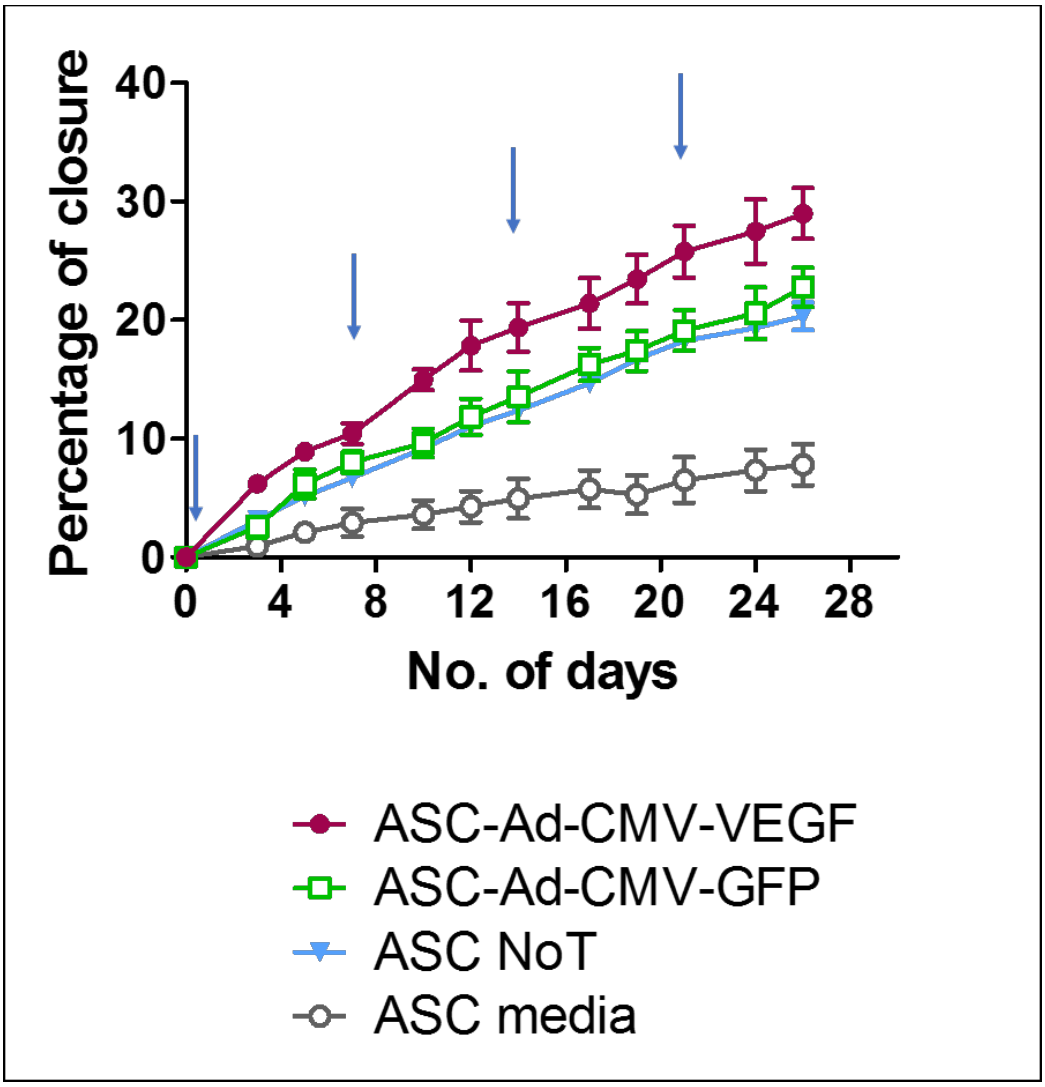

Figure 30: Effect of autologous ASCs (10^4 ASCs per wound) transduced with AdV-VEGF on 3 mm wound models.

ASC-AdV-CAG-VEGF-GFP (n=8) enhanced wound healing compared to wounds treated with ASC-Adv-CMV-GFP (n=8), ASC NoT (n=8) or ASC medium (n=8) from day 10 to day 26 ($p < 0.001$).Wounds treated with non-transduced ASCs and ASC-Ad-CMV-GFP showed the same healing efficacy ($p > 0.05$). Arrows indicate ASCs addition to the wounds on day 0, 7, 14, 21. Error bars represent SD. Analysis performed using two way ANOVA followed by Bonferroni test to obtain the p value.

4.3. Discussion

Adipose derived stem cells hold great promise as a therapy for chronic wound healing through stimulation of re-epithelialization, keratinocyte migration, capillary formation, tissue granulation, and angiogenesis (Kwon *et al.*, 2015). ASCs have the ability to differentiate into adipocytes, chondrocytes or osteocytes upon induction with respective differentiation medium (Kim *et al.*, 2007). ASCs also have the potential to secrete EGF, FGF, VEGF, PDGF, HGF, TGF-β (Park *et al.*, 2015). ASCs by themselves are not enough to induce complete wound closure, additional growth factors or cytokines are required for inducing wound closure (Kwon *et al.*, 2015).

Among the growth factors, vascular endothelial growth factor (VEGF) plays a pivotal role in wound healing by promoting angiogenesis. VEGF permeates the blood capillaries and increases the blood flow into the wounded area thereby increasing the oxygen and nutrient flow into the wounds, thus accelerating wound healing (Nauta *et al.*, 2012). Thus, ASCs expressing VEGF may an important tool for potentiating wound healing. Viral vector mediated gene therapy via adenovirus, adeno-associated virus or retrovirus is one of the most effective ways for expressing VEGF in ASCs. Both retrovirus or adenovirus transduction can result in a high amount of VEGF secretion. However adenovirus mediated gene therapy can cause a robust inflammatory response (Ritter *et al.*, 2002). In the case of retrovirus, because of its integration into the chromosomes can cause insertional mutagenesis (Yi *et al.*, 2011). Although AAV has low cell transducing ability, it is one of the most effective vectors for gene expression because of its lack of pathogenicity and non-toxic nature (Deodato *et al.*, 2002).

In our study, we isolated ASCs from patients by liposuction or after abdominoplasty and expanded them in culture in DMEM F12 medium along with FBS and antibiotic and antimycotic to provide nutrients for survivability and growth of ASCs, and protection from bacterial or fungal contamination, respectively. We characterized the ASCs by flow cytometry with positive stem cell markers (CD13, CD44, CD73, CD90, and CD105) and negative stem cell markers (CD31, CD45 and CD106). The positive markers were expressed in more than 95% of the cells and the negative markers were expressed at less than 1% (data not shown) thus indicating that the ASCs cells derived from patients were indeed stem cells. ASCs were cultured up to 3rd passage before being used for cell therapy. ASCs also differentiate into adipocytes, chondrocytes, and osteocytes (data not shown) upon induction with the respective medium. ASCs maintained their stem cell nature up to the sixth passage after which they started to lose their stem nature and stopped dividing (McIntosh *et al*., 2006).

To make the AAV vector expressing VEGF, I first cloned the VEGF gene into two AAV plasmid vector pAAV-CMV-GFP and pAAV-CAG-GFP. It was observed that the CAG-based AAV plasmid had more VEGF transfection than the CMV-based plasmid as evidenced by higher VEGF secretion in the medium as estimated by VEGF ELISA. Transfection and VEGF secretion was less in pAAV-CMV-VEGF-GFP than pAAV-CAG-VEGF-GFP probably because VEGF cloning was not entirely successful into the pAAV-CMV-GFP plasmid as its cloning site might have been disrupted as evidenced by the missing bands seen in pAAV-CMV-VEGF-GFP in figure 13. Based on the higher VEGF secretion in pAAV-CAG-VEGF-GFP, we chose this plasmid for AAV vector production from University of Iowa Viral Vector core.

To make ASCs express more VEGF, ASCs were transduced with AAV-CAG-VEGF-GFP, however only around 10-15% of the ASCs were transduced. Flow cytometry analysis of the AAV-CAG-VEGF transduced cells also confirmed the stemness of the transduced ASCs as evidenced by the expression of the positive markers in more than 95% of the cells and negative markers in less than 1%. When the ASCs were transduced with AdV-CMV-VEGF more than 80% of the ASCs were transduced and very high VEGF secretion was obtained when compared to the AAV-CAG-VEGF transduced cells. However excessive VEGF secretion can lead to tumor formation thus being cancerous for tissue (Herve *et al*., 2008).

I studied wound healing ability in ASCs *in vitro* by performing a scratch assay on non-transduced ASCs and ASCs transduced with AAV-CAG-VEGF or AAV-CMV-GFP. ASCs transduced with AAV-CAG-VEGF healed the scratch wound completely within 2 days whereas the AAV-CMV-GFP transduced ASCs and non-transduced ASCs took three days to heal, thereby suggesting VEGF supplementation with ASCs can potentially accelerate healing.

Wound healing ability was then studied in 2 mm autologous or allogenic organotypic wound models. Wounds treated with 10^4 ASC-AAV-CAG-VEGF healed nearly 50%, athough they could not completely induce wound closure, whereas the wounds treated with 10^4 ASC-AAV-CMV-GFP or 10^4 non-transduced ASCs showed around 25-30% healing. The control wounds treated with ASC medium could only heal to 6-7% suggesting ASC medium by itself was ineffective in promoting wound healing. Both autologous and allogenic ASCs were effective in potentiating healing. Histochemical analysis of the allogenic wounds showed reduction in the wounded area

(on day 32) of the ASC-AAV-CAG-VEGF, ASC-AAV-CMV-GFP and non-transduced ASCs treated wounds but the control wounds showed almost no reduction compared to day 2. Immunostaining with Ki-67 showed Ki-67 positive staining (on day 32) in all the wounds suggesting the wounds were viable at the termination of the experiment. CD31 immunostaining showed few blood vessels in the dermis of the wound. We expected to see more blood vessels in the ASC-AAV-CAG-VEGF treated wounds, however, we could see only a very few which was not obviously different from day 2. When stained with cytokeratin 5 or cytokeratin 14, cytokeratin positive cells were observed in the epidermis of the healing wounds. No significant difference in the healing rate of the autologous versus allogenic ASCs was observed most probably because the wound models lack an immune system thereby reducing the chances of rejection of allogenic ASCs.

We also studied wound healing ability in 3mm allogenic wounds. Since the wound size was larger, we used ASC-AAV-CAG-VEGF, ASC-AAV-CMV-GFP, or non-transduced ASCs for treating wounds at a cell count of 10^5 per wound. Wounds treated with ASCs expressing VEGF showed around 25-30% healing whereas wounds treated with non-transduced ASCs or ASC-AAV-CMV-GFP showed around 15-20% healing while the control wounds healed to about 8-9%. This suggests that ASCs alone may have a more difficult time healing larger wounds because of the larger surface area of the wounds and probably due to inefficient migration or proliferation of the few ASCs in the wounded area.

We also used adenovirus-mediated VEGF transduced ASCs to study healing in 3mm wound models. AdV transduced ASCs at a count of 10^4 ASCs were used to treat the

wound models. We expected that due to more VEGF secretion in the Ad-CMV-VEGF transduced ASCs, accelerated healing and complete closure will be observed in the wounds treated with ASC-Ad-CMV-VEGF. However only 30% closure was obtained, suggesting that AdV-transduced ASCs secreting VEGF was not likely any better than AAV-VEGF in mediating healing. This could also be possibly because 10^4 ASCs per wound is not enough for inducing complete closure or because very high amount of VEGF secretion can limit healing by becoming cancerous to the tissue (Herve *et al*., 2008).

Though we could not obtain complete closure, we could show that VEGF supplementation along with ASCs can potentially accelerate wound healing. We expect that with supplementation of additional growth factors (EGF, FGF, TGF, PDGF or a combination of growth factors) or treatment for a longer time will induce complete wound closure.

Chapter 5: Red light exposure

5.1. Rationale

Adipose derived stem cells, when harvested from patient's fat, were passaged sequentially three times for facilitating ASCs selection from stromal vascular fraction before being used for transplantation purposes. They are the most viable between third and the fifth passage after which they start losing their viability, shape, structure, and stem markers (McIntosh et al., 2006). And by passage eight, they completely lose their stemness. Thus, the optimum use of ASCs should be within the time when they are in between the third and the fifth passage. This acts as a limiting factor for cell therapy because ASCs might not have reached sufficient numbers or need to be manipulated beyond their fifth passage for the patient specific needs. Red light therapy (660 nm) has been shown to stimulate proliferation of stem cells (Choi *et al.*, 2013). Also, red light therapy can accelerate healing of tissues by enhancing viability of ASCs and potentiating angiogenesis in an ischemic mouse model (Park *et al.*, 2015). Based on this I hypothesized that exposure of ASCs to red light will increase their proliferation and also aid in maintaining stemness beyond the 7^{th} passage. Calu3 cells, a transformed lung cancer cell line, were used as a control cell line and also allowed me to study the effect of red light on cancerous cell proliferation.

5.2. Results

5.2.1. Red light exposure increases Calu3 cell count

Calu3 cells were seeded at a count of 7.5 x 10^4 cells per well in a 12-well plate and two days later were exposed to red, green, or ambient light for 15 minutes (figure 31). Two days after exposure, a one and a half fold increase ($p < 0.001$) in the count of red light exposed cells was observed compared to the green or ambient light exposed cells. The number of the green light exposed cells was similar to that of the ambient light exposed cells. When the cell counts of the red, green or ambient light exposed cells were compared to the seeding count, nearly five-fold increase was seen in the red light exposed cells ($p < 0.001$) whereas the green light or the ambient light exposed cells showed a three-fold increase ($p < 0.001$), thereby suggesting that the red light exposure significantly enhanced the cell proliferation of the Calu3 cells.

5.2.2. Red light exposure in ASCs increases cell count

ASCs seeded at 4 x 10^4 cells per well were exposed to red (n=3), green (n=3), or ambient light (n=3) for 15 minutes two days after seeding (Day 0) (figure 32). After two days (Day 4), red light exposed cells showed a 1.2 times higher cell count ($p < 0.01$) when compared to the ambient light exposed cells or green light exposed cells. When the cell count of these red, green, or ambient light exposed cells were compared to that of the number of cells seeded, the red light exposed cells increases by almost one and a three fourth times of the seeding count ($p < 0.001$) and the ambient light or green exposed cells increased by one and a half times ($p < 0.001$).

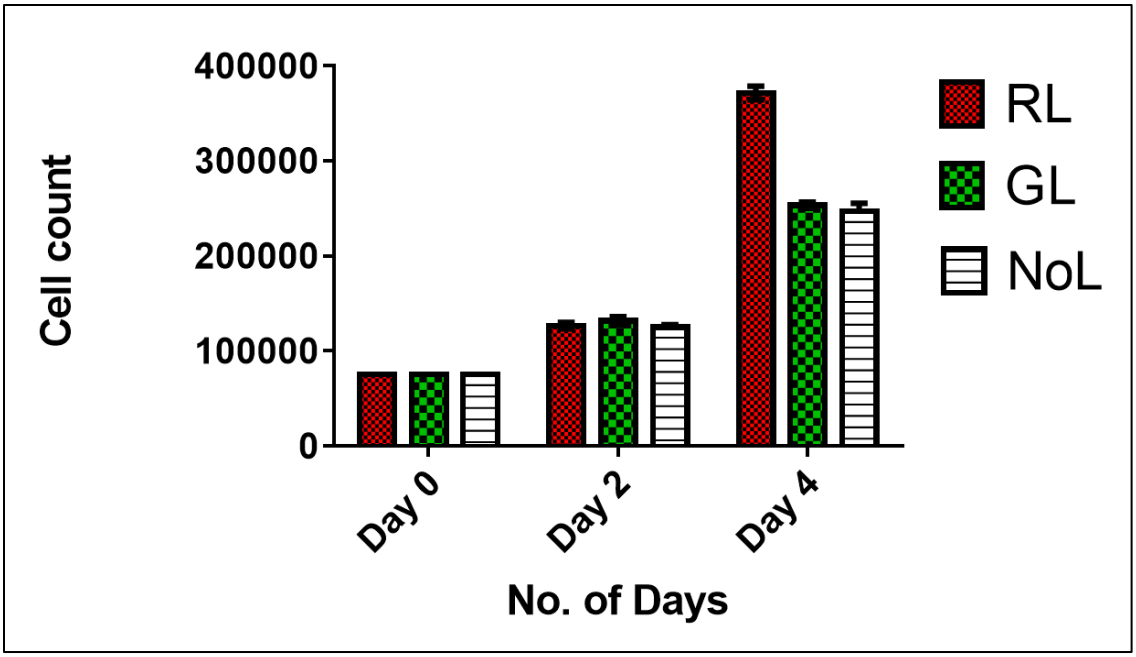

Figure 31: Effect of red light exposure on Calu3 cell growth

Exposure of Calu3 cells to red light increases the cell count by 1.5 times relative to green light or ambient light exposure ($p < 0.001$). Error bars represent SD for n=3 experiments. Analysis performed using two way ANOVA followed by Bonferroni test to obtain the p value.

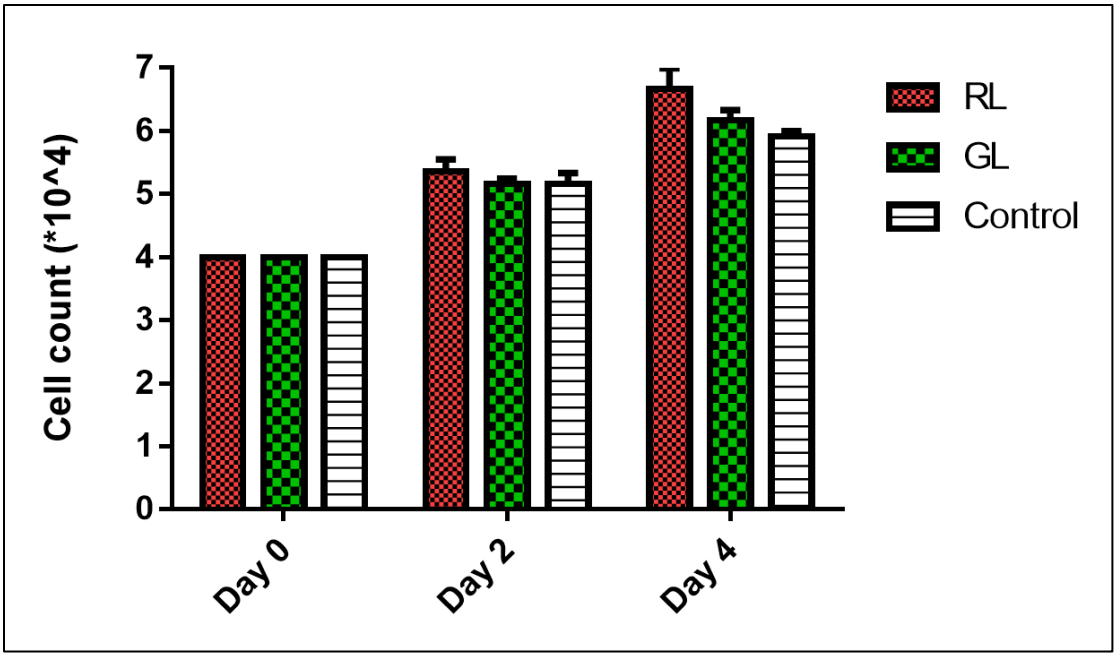

Figure 32: Effect of red light on ASCs cell count

Exposure of ASCs to red light 2 days after seeding increases the cell count by 1.2 times relative to green light or ambient light exposure, as counted on day 4 ($p < 0.01$). Error bars represent SD for $n = 3$ replicates. The experiment was repeated 3 times and data shown are from one representative experiment. Analysis performed using two way ANOVA followed by Bonferroni test to obtain the p value.

5.2.3. Red light exposed cells maintain their stemness at passage 8

ASCs not exposed to red light stopped growing at passage 7 (data not shown). By contrast, ASCs exposed to red light continued to grow and retain a stem-like morphology. To determine whether the red light exposed ASCs at passage 8 retained their stem markers, red light exposed cells (n=1) were characterized by flow cytometry with the stem markers according to IFATS standard. The ASCs showed that the positive markers CD13, CD44, CD73, CD90 and CD105 were expressed on more than 95% of the cells whereas the negative markers showed that less than 1% of the cells expressed the negative markers (CD31, CD45, CD106; figures 33 and 34), which indicated that the ASCs maintained their stem markers even after exposure to red light.

5.2.4. Red light exposure potentiates wound healing

Given the benefit of increased cell growth, I hypothesized that exposure of organotypic wound models would lead to wound closure. 1.5 mm^2 wound models were exposed to red light (670 nm) (n=3) or ambient light (n=3) every other day for 20 days. Exposure to red light from the bottom or the dermal side of the wound model caused 59.15 ± 0.3% decrease in the wound area whereas the ambient light exposed wounds only showed 4.20 ± 1.3% closure (as shown in figure 35). Given the plateau of closure by day 10, it is likely that there is a maximum amount of closure that red light can do on its own.

5.3. Discussion

Red light therapy is a successful therapeutic tool in regenerative medicine (Amid *et al.*, 2013). Exposure to red light leads to increased collagen synthesis, cytokine and growth factor secretion, increased angiogenesis, and reduced pain and inflammation (Park *et al.*, 2015).

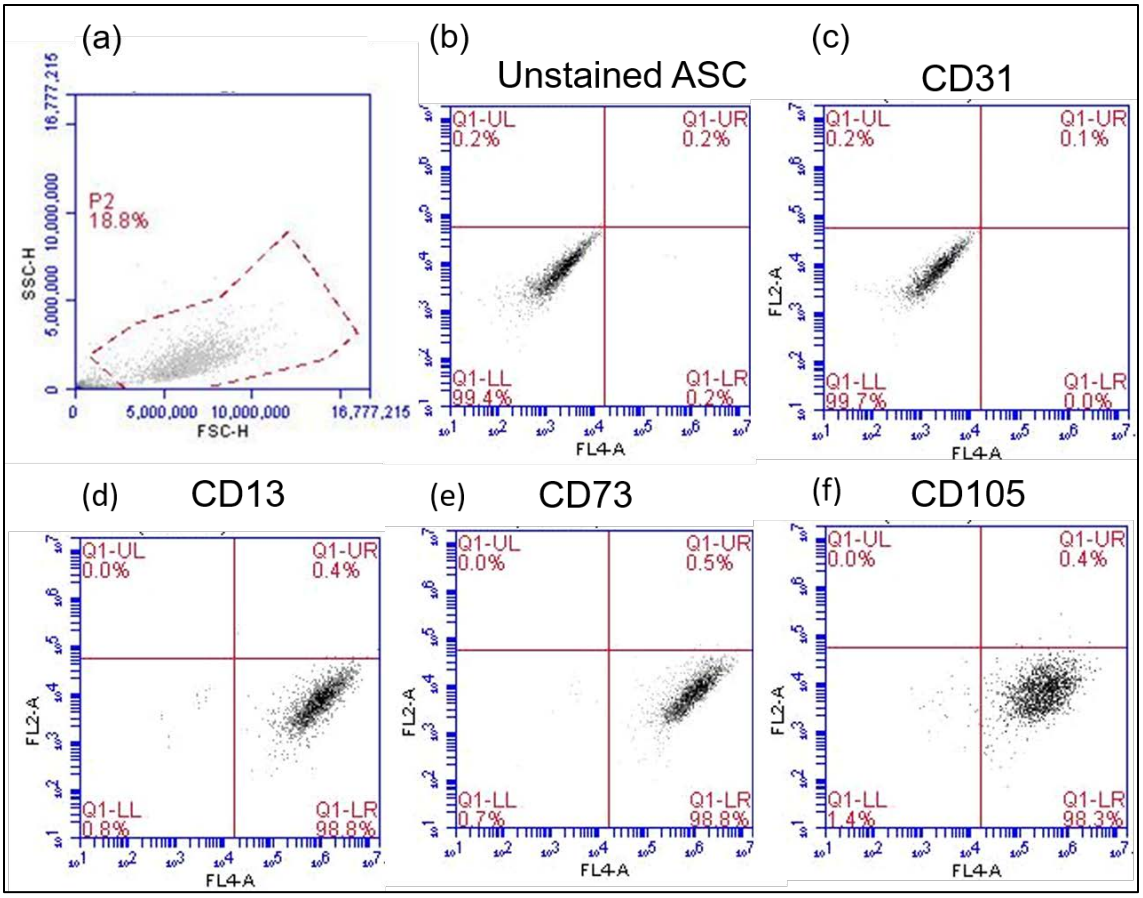

Figure 33: Flow cytometry analysis of stem cell markers show that red light exposed ASCs at passage 8 retains their stemness.

(a) Representative gating of the stem cell population, (b) unstained ASCs (control), (c) CD31 is a negative stem cell marker and is not expressed. More than 98% of the ASCs express positive markers (d) CD13, (e) CD73 and (f) CD105. N = 1 donor.

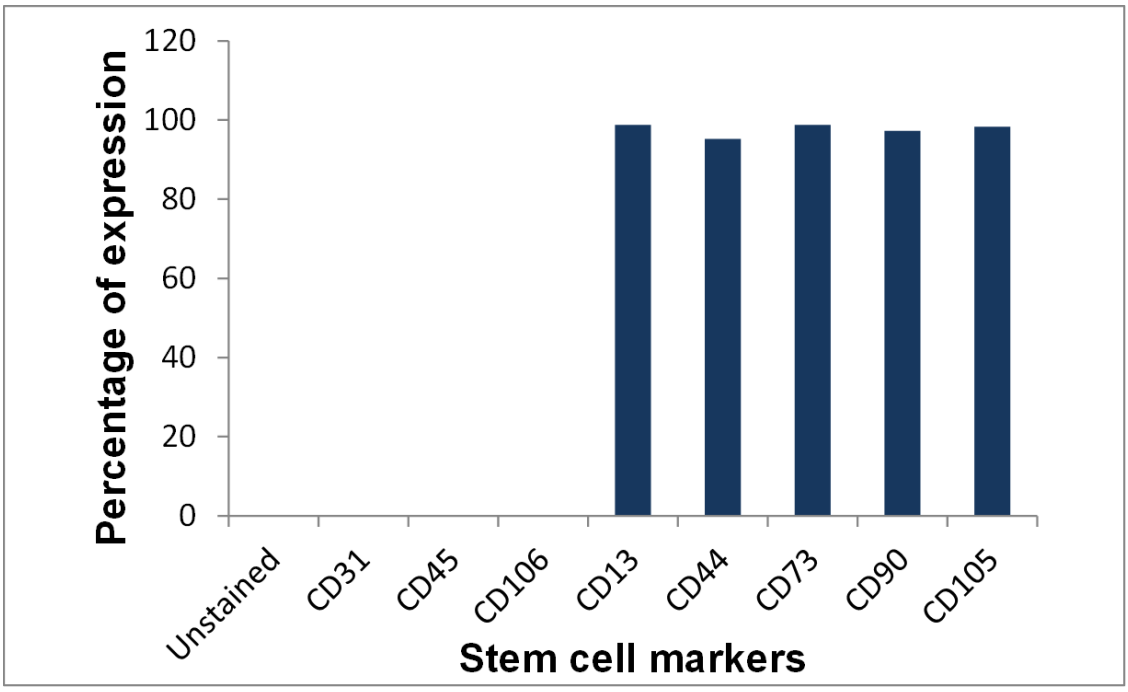

Figure 34: Stem cell marker profile of red light exposed passage 8 ASCs.

Expression of markers expected to be negative for stem cells (CD31, CD45, CD106) was less than 0.5% whereas more than 95% of the red light exposed cells (n=1) express markers expected to be positive for stem cells (CD13, CD44, CD73, CD90 and CD106). N = 1 donor.

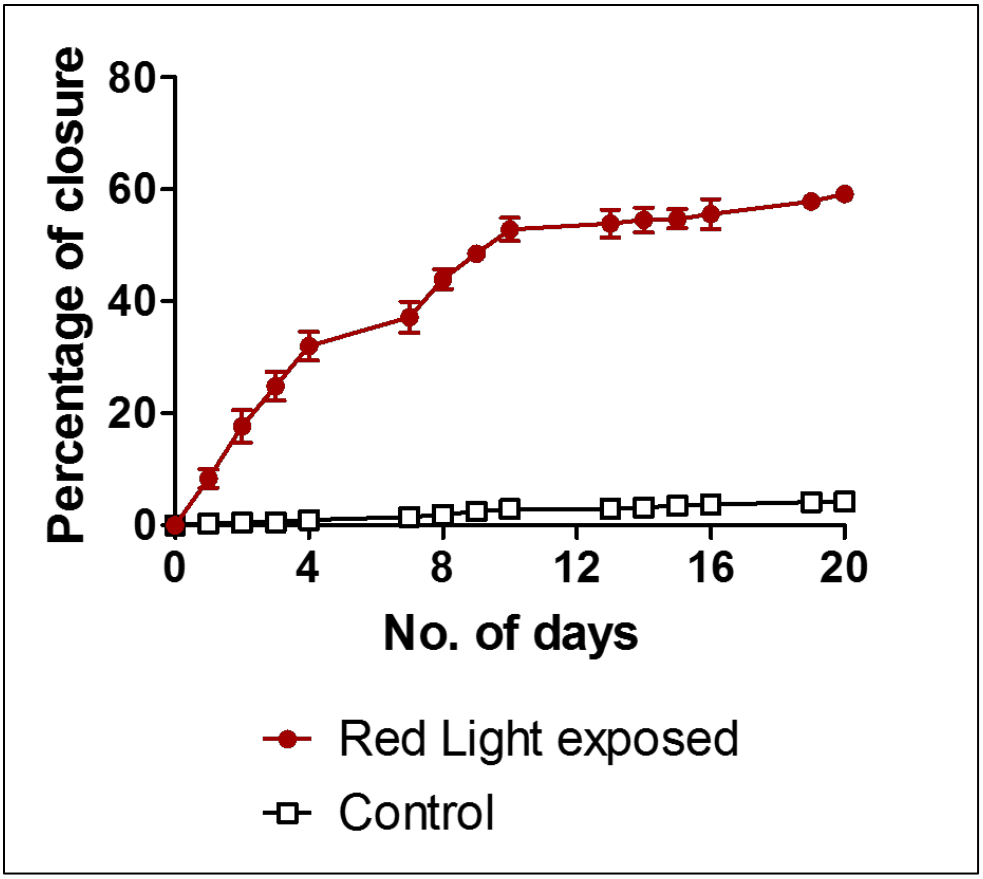

Figure 35: Red light exposure induces wound closure in organotypic wound models.

Time course of percentage of wound closure obtained in red light exposed wounds versus ambient light exposed wounds (n=3). Error bars represent SD. Red light exposed wounds show a significant difference ($p < 0.001$) in healing compared to ambient light treated wounds (control) from day 1 to day 20. Analysis performed using two way ANOVA followed by Bonferroni test to obtain the p value.

In culture, ASCs generally tend to lose their viability and stemness after the 7th passage and stem cells from elderly patients do not replicate well, thereby limiting its application in the transplantation setting (McIntosh *et al*., 2006). When ASCs beyond passage 7 were exposed to red light, an increase in viability and cell number is observed. The increase in viability can likely be attributed to a decrease in senescence or apoptosis of red light exposed cells (Park *et al.*, 2015). Also, exposure to red light leads to an increase in proliferation of ASCs compared to ambient light exposed cells. Interestingly, the red light exposed cells maintained their stem markers (with the expression of the positive stem cell markers by more than 96% of the cells and the negative markers expressed at less than 1%). This suggests that red light exposed ASCs can be used for transplantation even after the 7th passage, giving hope that stem cells from elderly patients may be responsive to red light and could be expanded for therapy. The cells exposed to green light showed a small increase in cell count when compared to the ambient light exposed cells but not statistically significant. Future experiments will test whether a combination of red light and green light may be able induce a further increase in cell proliferation. Calu3 cells proliferate at a much higher rate than the ASCs. This can be due to the fact that Calu3 cells are cancerous cells while ASCs belong to the primary cells category. Thus, cancerous cells proliferate at a much faster rate than the primary cell lines. Red light therapy is known to increase cell proliferation to a much faster rate. While this is extremely advantageous for ASCs, it is a possibility that cancerous cells would also increase their proliferative potential, posing a huge threat to the patient.

It is known that the effect of red light exposure is dose dependent, meaning low dosages of red light exposure can cause inefficient healing while high doses can have

deleterious effects and damage tissue. It can cause re-pigmentation of vitiligo and depigmentation of hyper-pigmented lesions depending on the dosimetry parameter (Avci *et al.*, 2013). Exposure to red light is known to lead to increased secretion of FGF, VEGF, and HGF. Elevated levels of these growth factors stimulate cell migration and proliferation, angiogenesis, and inhibit apoptosis (Park *et al.*, 2015). Low level light therapy (LLLT, 600-700 nm, like red light therapy but a broader band width) also induces osteoblast differentiation, proliferation and maturation (Amid *et al.*, 2013). LLLT can induce healing radiation related damages by secretion of minerals (Fernandes *et al.*, 2013).

Exposure of the wound models to red light also enhanced closure when compared to the ambient light exposed wounds. Previous studies have shown that red light has stimulatory effects on the cells in the damaged area which thereby induce wound healing by enhancing cell migration and cell proliferation in the wounds via increased secretion of growth factors like EGF, FGF , PDGF (Park *et al*., 2015) (Avci et al., 2013). However, in our model, we do not know yet what is stimulating wound closure. With Bio-plex assays, cytokines and growth factors contributing to wound closure can be determined.

Complete healing was not observed in the wound models when exposed to red light. The inefficiency in healing can be due to suboptimal dose of red light, insufficient time, and insufficient cells to divide and fill in the wound, or indicate that a combination of the red light and ASCs would be required. It is expected that a combination of red light therapy with supplementation of ASCs will lead to enhanced secretion of angiogenic growth factors, and increased cell migration and proliferation (Park *et al.*, 2015). LLLT

can induce skin rejuvenation by secretion of IL-1β and TNF-α, which thereby recruits MMPs and initiates collagen synthesis (Avci *et al.*, 2013). Thus red light therapy is a non-invasive, painless procedure which can be applied in dermatology for treatment of chronic wounds, lesions, acnes, burns, and scars (Avci *et al.*, 2013). While red light has limitations in our wound model, it may be better *in vivo* due to endogenous pools of stem cells.

Chapter 6: Discussion

Wound healing is a complex process requiring the regulation of cell migration, collagen deposition, and re-epithelialization. Studies have shown that adipose derived stem cells (ASCs), because of their ability to differentiate, regenerate, and secrete growth factors, can potentiate the process of wound healing (Kim *et al.*, 2007). Among the growth factors, VEGF has shown a pivotal role in wound healing by promoting angiogenesis. Deodata *et al.* showed that high amount of VEGF secreted by the keratinocytes in the wound bed and in migrating keratinocytes accelerated wound healing (Deodata *et al.* 2002). VEGF promotes rapid wound closure by enhancing blood and nutrient flow to the wound site, thereby facilitating healing (Nauta *et al.*, 2012). This suggests that expression of VEGF by ASCs is an important tool in wound healing. Animal studies and clinical trials have indicated that topical application of VEGF protein can lead to degradation of the protein by the time it reaches the wound site thereby requiring large doses of VEGF protein (Galeano *et al.* 2004). Viral vector mediated gene therapy using adeno-associated virus is one of the most effective ways for gene expression in cells and tissues because of the lack of pathogenicity of AAV and relative stability of AAV *in vivo* and sustained production and secretion of growth factor (Gauglitz *et al.*, 2011).

ASCs have been used in clinical trials to treat calvaria defects using SVF (stromal vascular fraction). SVF resulted in new bone formation and complete healing of the

calvaria defect (Lendeckel *et al.*, 2004). SVF fraction has also been used in clinical trial for treatment of myocardial infarction (Yoshimura *et al.*, 2008). ASCs have been used for treating scars and osteogenic defects (Mesimaki *et al.*, 2009), but clinical phase I and II trial have not been completed yet. Clinical trials for treatment of perianal fistula, Crohn's disease, GVHD, (Hassan *et al.*, 2014) have also been initiated. ASCs therapy holds much promise.

We were interested in applying ASCs to wound healing. However, *in vitro* assays are limited and it is unclear that studies in animals will truly be relevant to humans. We therefore designed and initiated the use of organotypic wound models obtained from patient skin by abdominoplasty or brachioplasty to study wound healing. These tissues are usually discarded after surgery but are a robust source of ASCs and the skin is usually healthy. We tried both 2mm or 3mm punches to create wounds in the 8 mm punch models. The 8 mm punch size was chosen because this size fits well in transwells. Transwells have semipermeable membranes and provide support the skin structure because they can then be maintained at an air liquid interface. The bottom part of the well is exposed to ASC medium, which provides nutrients to the wounds, and the top part of the transwell is exposed to air. The wound models were viable for at least four months as seen by the MTT assay (figure 11). Measurements taken on the wounds over a period of time indicated that the wounds only supplemented by ASC medium did not close by itself thus indicating that these are chronic wounds. Histoarchitecture of the wound studied by H&E staining shows that the structural anatomy of the skin contains all three layers, epidermis, dermis and fat. These wound models are advantageous over using mice or rat models because mice are anatomically, hormonally, and metabolically different than

humans. Also mice live for an average of one or two years, hence replicating the studies based on the effects seen in mice are debatable. This multidimensional wound model culture system can mimic the chronic wound environment of a human *in vivo* and therefore can be used as a model to study wound healing and help in developing a therapeutic approach to accelerate wound healing.

We isolated ASCs from patients and cultured them *in vitro* to be used for experimentation. Expression of the stem cell markers by the ASCs were characterized by flow cytometry according to the IFATS standard. The ASCs remained viable and maintained their stem cell qualities between passage three to six, after which they started losing their stem-like nature and stopped dividing. In order to preserve them long term, I exposed them to red light. I showed that red light exposure increased their viability and also helped in maintaining their stem markers, at passage 8 ASCs could then be subcultured and as long as they were exposed to red light, maintained their ability to divide and their stem-like appearance. While the ambient light-exposed ASCs at passage 9 had lost their viability and their ability to expand, red light exposed cells could continue to 15 or more passages (data not shown). This may be because red light exposure decreases the rate of apoptosis and increases rate of proliferation and regeneration (Park *et al.*, 2015), thereby increasing viability. Red light exposed cells also have been shown to secrete a larger amount of growth factors like VEGF and EGF. Future experiments will determine whether the levels of growth factors (like VEGF, FGF, EGF, PDGF, retinoic acid) change or there are other metabolic changes upon exposure to red light.

To make the ASCs express increased levels of VEGF, I transduced the ASCs with AAV-VEGF-GFP or Ad-VEGF vector. The ASCs transduced with AAV vector showed

only about 10-15% transduction efficiency whereas almost 80% of the ASCs were transduced with adenovirus. The ASCs transduced with AAV-VEGF-GFP expressed their stem markers after transduction, as shown by the flow cytometry (figure 19) indicating that transduction does not alter the ASCs stem cell profile. Though low levels of the VEGF secretion in the AAV-transduced ASCs were obtained (figure 17), it can be considered an advantage as excessive VEGF secretion can be cancerous to cells and damage them (Basu *et al*., 2009). This indicates that AAV is a suitable vector for moderate and sustainable VEGF gene expression.

We analyzed the healing ability of the AAV-VEGF-GFP transduced ASCs *in vivo* by scratch assay, performed on a monolayer of ASCs. It was seen that in the ASC-AAV-VEGF-GFP transduced cells, the scratch healed by almost 75-80% by day 1 and had healed completely by the second day. However, in the ASC-AAV-GFP transduced and non-transduced ASCs the scratch nearly took three days to heal. Whether the healing had taken place due to increased cell division, regeneration, or migration of ASCs has not yet been studied. Overall, these data indicate that ASCs secreting VEGF can potentiate wound healing *in vitro* as VEGF acts as a cell mitogen.

In our study, we tested the efficiency of ASC-AAV-VEGF-GFP in accelerating wound healing *in vivo* by comparing it to the healing rate obtained by ASC-AAV-GFP, non-transduced ASCs in both autologous and allogenic organotypic wound models. Each of the wounds was treated with 10^4 transduced or non-transduced ASCs. We showed that in the 2 mm wound models, ASCs eluting VEGF could close the wound up to around 45-50% in both allogenic and autologous wounds whereas the non-transduced ASCs or ASCs expressing GFP could only induce around 25-30% closure. The control wound

models treated with ASC medium healed only by 6-7% in a period of one month. This suggested that though ASCs by themselves can induce some closure in the wounds, they are not as potent as ASCs secreting VEGF in inducing wound closure. Also, since ASCs expressing GFP could heal the wounds to almost the same extent as the non-transduced ASCs, we can say that the healing in wounds treated with ASC-GFP is because of the ASCs, while GFP does not contribute to wound healing. This indicates that the ASCs secreting VEGF can significantly enhance wound closure when compared to non-transduced ASCs or ASC-AAV-GFP. H&E staining performed on the wound models on day 2 and day 32 showed reduction in the wound area of ASC-AAV-VEGF-GFP treated wound, while the wound size in the control group was almost equal to the day 2 time point. Immunostaining performed on the wounds with Ki67 showed mitotically active cells in the epidermis region indicating that the wounds were still alive at the termination of the experiment. However, when the sections of the wounds were stained with CD31 antibody, we did not see a significantly greater number of blood vessels in the group treated with ASC-AAV-VEGF-GFP as was hypothesized. This probably is due to the fact that the wound models do not have a network of active blood vessels and blood supply, so there was no detectable *de novo* blood vessel formation in the wounds treated with ASC-AAV-VEGF-GFP.

We did not see any significant difference in healing when we used autologous versus allogenic ASCs in the wounds. This probably is due to the fact that these wound models do not have an active immune system to cause any host versus recipient rejection or immune reaction. We also used 3mm wound models to study wound healing. Since the wound sizes of the 3mm models were bigger when compared to the 2mm models, we

increased the dosage of ASCs and hence used 10^5 ASCs per wound. We grouped the wound models in four categories, where one group was treated with ASC-AAV-VEGF-GFP, the second group with ASC-AAV-GFP, the third group with non-transduced ASCs and the fourth group as the control group treated with ASC medium. We saw that a closure of around 27-30% was observed in the group treated with ASC-AAV-VEGF-GFP while the wounds treated with ASC-AAV-GFP or on transduced ASCs healed only to around 15-20%. The control wounds treated with ASC medium alone showed very minimal healing. This could be because the wounds were bigger in size and would have probably required a larger ASCs dosage or a combination of ASCs and cytokine therapy.

We also used adenovirus transduced ASC-VEGF and ASC-GFP to investigate wound healing in 3 mm models. We had expected that with adenovirus transduction, leading to more VEGF production by ASCs (figure 34), there would be accelerated healing and complete closure of the wounds treated with ASC-Ad-VEGF. However, there was only about 30% closure in the 3 mm models, similar to what we had seen in the wounds treated with AAV transduced ASC-VEGF, which indicated that ASC-Ad-VEGF was as effective as ASC-AAV-VEGF in potentiating healing (figure 21, 27, 29). Potentially there is a threshold amount of VEGF that improves closure and levels beyond that does not help healing. It is also possible more time for closure would have made a difference, however the plateau of healing argues against this.

Red light exposure is known to increase growth factor expression, such as VEGF (Park *et al.*, 2015). We studied the effect of red light on wound healing by exposing wounds to red light and analyzing its efficacy in inducing closure compared to ambient light exposed cells. We observed closure of about 50% in red light exposed wounds in

three weeks after which the healing rate became stagnant (figure 35). However, this was in smaller wounds. Despite this, it is expected that wounds and ASCs exposed to red light led to increased secretion of growth factors, more cell migration, and proliferation (Park *et al.*, 2015). This indicates that red light exposure can potentially accelerate wound healing and complete wound closure can be achieved if a combination of red light therapy, cell therapy, and gene therapy is implemented.

Attaining complete wound closure in patients is particularly important because ineffective or partial healing can worsen the condition of the patients physically and mentally. Partially healed wounds can also be a site for infection. To attain complete wound closure, studying the conditions of chronic wounds and the factors affecting their healing have to be analyzed properly. Complete wound closure was obtained in the mouse models when treated with ASCs secreting VEGF using biodegradable PBAE (poly β-amino ester) nanopolymer within 14 days (Nauta *et al.*, 2012). This is because mice have an active blood vessel and blood supply. Supplementation of VEGF can therefore increase the blood vessel formation and also increase blood flow into the wounds, thereby providing oxygen and nutrients to wounds and facilitate wound closure. In our study, complete closure was not obtained in any of the wound models treated with ASC-AAV-VEGF or ASC-Ad-VEGF at a concentration of 10^4 ASCs per wound or 10^5 ASCs per wound. This indicated that ASCs therapy with only VEGF gene transfer potentially cannot induce complete wound closure and the healing conditions have to be more personalized. However in viable wound bed with a blood network system, VEGF may stimulate growth of blood vessels and cause increase in blood flow, and thereby potentiate wound healing process. Accelerated wound healing and a substitution of a

cocktail of growth factors to induce complete wound closure are required. Future studies will perform a Bio-plex on the medium and cells obtained from the chronic wounds, in comparison to ASC-AAV-VEGF-GFP and red light exposed, to identify the biomolecules (extra cellular matrix (ECM), collagen, keratinocytes, and fibroblasts), cytokines, growth factors, and pathways that can contribute to wound healing. Human wound healing PCR arrays can be performed to analyze the different cytokines, remodeling enzymes, extracellular matrix proteins, growth factors (like FGF, HBEGF (Heparin binding EGF like growth factor) , HGF (hepatocyte growth factor) , IGF (insulin growth factor), MIF (macrophage migration inhibitory factor) , PDGF, TGF (transforming growth factor), TNF (tumor necrosis factor), CSF (colony stimulating factor), ANGPT (angiopoietin), VEGF) expressed in the injured tissues and healing wounds. Substituting the chronic wounds accordingly with the combination of biomolecules, growth factors and cells may be the solution that mediates complete wound closure.

Contrasting to our hypothesis, VEGF could not stimulate blood vessel formation in our wound models cause of the absence of active blood network system. Thus suggesting that VEGF is not an effective growth factor for inducing angiogenesis and wound closure in the organotypic skin biopsies we developed in our lab. For our model, it appears that growth factors like EGF, FGF would work efficiently by stimulating keratinocyte and fibroblast proliferation and migration.

The wound models can be personalized according to people with different diseased conditions. Partial thickness or full thickness wound culture models can be made from each patient and studied accordingly. Wound models can be designed in such a way

to have deficiency of specific nutrients or vitamins or minerals as seen in people with similar ailments. Though treatment with autologous versus allogenic ASCs does not have an immune effect on these wound models, in humans it can cause immunogenic or inflammatory response or even rejection by the host. Thus, in patients ASCs need to be tested for compatibility before being transplanted. It is conceivable that biopsies are obtained at the same time as fat for ASC isolation and by the time the ASCs are at passage 3-4 the correct cocktail of growth factors and other molecules could have been identified for seeding along with the ASCs.

ASCs thus act as a suitable candidate for cell therapy owing to its regenerative, and paracrine signaling properties. ASCs promote wound healing both *in vivo* and *in vitro*, though when supplemented with VEGF, accelerates wound closure. Although complete closure was not obtained in the wound cultures treated with ASCs secreting VEGF, it is expected that ASCs supplemented with additional growth factors at appropriate dosages hold a promising delivery for complete healing of chronic wounds. Additionally, it is likely that red light exposure can accelerate healing when combined with cell and gene therapy. Thus this study can be personalized to develop an efficient, accelerated, less invasive or painful treatment solution for millions of people suffering from chronic wounds.

7. References

1. Alrubaiy, L., & Al-Rubaiy, K. K. (2009). Skin substitutes: a brief review of types and clinical applications. *Oman Med J, 24*(1), 4-6. doi:10.5001/omj.2009.2

2. Amid, R., Kadkhodazadeh, M., Ahsaie, M. G., & Hakakzadeh, A. (2014). Effect of low level laser therapy on proliferation and differentiation of the cells contributing in bone regeneration. *J Lasers Med Sci, 5*(4), 163-170.

3. Anson, D. S. (2004). The use of retroviral vectors for gene therapy-what are the risks? A review of retroviral pathogenesis and its relevance to retroviral vector-mediated gene delivery. *Genet Vaccines Ther, 2*(1), 9. doi:10.1186/1479-0556-2-9

4. Avci, P., Gupta, A., Sadasivam, M., Vecchio, D., Pam, Z., Pam, N., & Hamblin, M. R. (2013). Low-level laser (light) therapy (LLLT) in skin: stimulating, healing, restoring. *Semin Cutan Med Surg, 32*(1), 41-52.

5. Blanpain, C., & Fuchs, E. (2006). Epidermal stem cells of the skin. *Annu Rev Cell Dev Biol, 22*, 339-373. doi:10.1146/annurev.cellbio.22.010305.104357

6. Branski, L. K., Gauglitz, G. G., Herndon, D. N., & Jeschke, M. G. (2009). A review of gene and stem cell therapy in cutaneous wound healing. *Burns, 35*(2), 171-180. doi:10.1016/j.burns.2008.03.009

7. Branski, L. K., Pereira, C. T., Herndon, D. N., & Jeschke, M. G. (2007). Gene therapy in wound healing: present status and future directions. *Gene Ther, 14*(1), 1-10. doi:10.1038/sj.gt.3302837

8. Breitkreutz, D., Koxholt, I., Thiemann, K., & Nischt, R. (2013). Skin Basement Membrane: The Foundation of Epidermal Integrity—BM Functions and Diverse Roles of

Bridging Molecules Nidogen and Perlecan. *BioMed Research International*, *2013*, 179784. http://doi.org/10.1155/2013/179784 0.

9. Broughton, G., Janis, J. E., & Attinger, C. E. (2006). Wound healing: an overview. *Plast Reconstr Surg, 117*(7 Suppl), 1e-S-32e-S. doi:10.1097/01.prs.0000222562.60260.f9

10. Burr, S., & Penzer, R. (2005). Promoting skin health. *Nurs Stand, 19*(36), 57-65; quiz 66. doi:10.7748/ns2005.05.19.36.57.c3871

11. Chu D.H. (2008). Overview of biology, development, and structure of skin (Amid et al., 2014). *Fitzpatrick's Dermatology in General Medicine, 7*, pp. 57–73.

12. Coura, R. d. S., & Nardi, N. B. (2008). A role for adeno-associated viral vectors in gene therapy. *Genetics and Molecular Biology, 31*, 1-11.

13. Elias, P. M. (2005). Stratum corneum defensive functions: an integrated view. *J Invest Dermatol, 125*(2), 183-200. doi:10.1111/j.0022-202X.2005.23668.x

14. Falanga, V. (2005). Wound healing and its impairment in the diabetic foot. *Lancet, 366*(9498), 1736-1743. doi:10.1016/S0140-6736(05)67700-8

15. Ganceviciene, R., Liakou, A. I., Theodoridis, A., Makrantonaki, E., & Zouboulis, C. C. (2012). Skin anti-aging strategies. *Dermatoendocrinol, 4*(3), 308-319. doi:10.4161/derm.22804

16. Gauglitz, G. G., & Jeschke, M. G. (2011). Combined gene and stem cell therapy for cutaneous wound healing. *Mol Pharm, 8*(5), 1471-1479. doi:10.1021/mp2001457

17. Gille, H., Kowalski, J., Li, B., LeCouter, J., Moffat, B., Zioncheck, T. F., . . . Ferrara, N. (2001). Analysis of biological effects and signaling properties of Flt-1 (VEGFR-1) and KDR (VEGFR-2). A reassessment using novel receptor-specific vascular

endothelial growth factor mutants. *J Biol Chem*, *276*(5), 3222-3230. doi:10.1074/jbc.M002016200

18. Goncalves, M. A. (2005). Adeno-associated virus: from defective virus to effective vector. *Virol J*, *2*, 43. doi:10.1186/1743-422X-2-43

19. Guo, S., & Dipietro, L. A. (2010). Factors affecting wound healing. *J Dent Res*, *89*(3), 219-229. doi:10.1177/0022034509359125

20. Halim, A. S., Khoo, T. L., & Mohd Yussof, S. J. (2010). Biologic and synthetic skin substitutes: An overview. *Indian J Plast Surg*, *43*(Suppl), S23-28. doi:10.4103/0970-0358.70712

21. Hassan, W. U., Greiser, U., & Wang, W. (2014). Role of adipose-derived stem cells in wound healing. *Wound Repair and Regeneration*, *22*(3), 313-325. doi:10.1111/wrr.12173

22. Hervé, M.-A., Buteau-Lozano, H., Vassy, R., Bieche, I., Velasco, G., Pla, M., & Perrot-Applanat, M. (2008). Overexpression of Vascular Endothelial Growth Factor 189 in Breast Cancer Cells Leads to Delayed Tumor Uptake with Dilated Intratumoral Vessels. *The American Journal of Pathology*, *172*(1), 167–178. http://doi.org/10.2353/ajpath.2008.070181

23. Hiroyuki T., & Masabumi S. (2005). The vascular endothelial growth factor (VEGF)/VEGF receptor system and its role under physiological and pathological conditions. *Clinical science*, *109(3)*, 227-241.

24. Kanitakis, J. (2002). Anatomy, histology and immunohistochemistry of normal human skin. *Eur J Dermatol*, *12*(4), 390-399; quiz 400-391.

25. Kim, H., Choi, K., Kweon, O. K., & Kim, W. H. (2012). Enhanced wound healing effect of canine adipose-derived mesenchymal stem cells with low-level laser therapy in athymic mice. *J Dermatol Sci, 68*(3), 149-156. doi:10.1016/j.jdermsci.2012.09.013

26. Koch, S., & Claesson-Welsh, L. (2012). Signal transduction by vascular endothelial growth factor receptors. *Cold Spring Harb Perspect Med, 2*(7), a006502. doi:10.1101/cshperspect.a006502

27. Laughlin, C. A., Cardellichio, C. B., & Coon, H. C. (1986). Latent infection of KB cells with adeno-associated virus type 2. *J Virol, 60*(2), 515-524.

28. McLafferty, E., Hendry, C., & Alistair, F. (2012). The integumentary system: anatomy, physiology and function of skin. *Nurs Stand, 27*(3), 35-42.

29. Nathoo, R., Howe, N., & Cohen, G. (2014). Skin substitutes: an overview of the key players in wound management. *J Clin Aesthet Dermatol, 7*(10), 44-48.

30. Nauta, A., Seidel, C., Deveza, L., Montoro, D., Grova, M., Ko, S. H., & Yang, F. (2013). Adipose-derived stromal cells overexpressing vascular endothelial growth factor accelerate mouse excisional wound healing. *Mol Ther, 21*(2), 445-455. doi:10.1038/mt.2012.234

31. Nie, C., Yang, D., Xu, J., Si, Z., Jin, X., & Zhang, J. (2011). Locally administered adipose-derived stem cells accelerate wound healing through differentiation and vasculogenesis. *Cell Transplant, 20*(2), 205-216. doi:10.3727/096368910X520065

32. Pacak, C. A., & Byrne, B. J. (2011). AAV vectors for cardiac gene transfer: experimental tools and clinical opportunities. *Mol Ther, 19*(9), 1582-1590. doi:10.1038/mt.2011.124

33. Park, I. S., Chung, P. S., & Ahn, J. C. (2015). Adipose-derived stromal cell cluster with light therapy enhance angiogenesis and skin wound healing in mice. *Biochem Biophys Res Commun, 462*(3), 171-177. doi:10.1016/j.bbrc.2015.04.059.

34. Rigotti, G., Marchi, A., Galiè, M., Baroni, G., Benati, D., Krampera, M., . & Sbarbati, A. (2007). Clinical treatment of radiotherapy tissue damage by lipoaspirate transplant: a healing process mediated by adipose-derived adult stem cells. *Plas Recon Surg, 119*(5), 1409.

35. Samulski, R. J., Chang, L. S., & Shenk, T. (1987). A recombinant plasmid from which an infectious adeno-associated virus genome can be excised in vitro and its use to study viral replication. *Journal of Virology, 61*(10), 3096–3101.

36. Schipper, B. M., Marra, K. G., Zhang, W., Donnenberg, A. D., & Rubin, J. P. (2008). Regional anatomic and age effects on cell function of human adipose-derived stem cells. *Ann Plast Surg, 60*(5), 538-544. doi:10.1097/SAP.0b013e3181723bbe

37. Silman, N. J., & Fooks, A. R. (2000). Biophysical targeting of adenovirus vectors for gene therapy. *Curr Opin Mol Ther, 2*(5), 524-531.

38. Singh, A. K., & Shenoy, Y. R. (2012). Skin substitutes: An Indian perspective. *Indian J Plast Surg, 45*(2), 388-395. doi:10.4103/0970-0358.101322

39. Tortora GJ., & Derrickson BH (2009) Principles of Anatomy and Physiology: Maintenance and Continuity of the Human Body. *Principles of anatomy and physiology*, 13.

40. Velnar, T., Bailey, T., & Smrkolj, V. (2009). The wound healing process: an overview of the cellular and molecular mechanisms. *J Int Med Res, 37*(5), 1528-1542.

41. Yi, Y., Noh, M. J., & Lee, K. H. (2011, Jun) *Current advances in retroviral gene therapy*. Curr Gene Ther (Vol 3).

42. Zhijian W., Asokan A., & Samulski RJ. (2006). Adeno-associated Virus Serotypes: Vector Toolkit for Human Gene Therapy. *Molecular Therapy, 14*, 316–327.

8. Abbreviations

Acronym	Definition
VEGF	Vascular endothelial growth factor
VPF	Vascular permeability factor
PDGF	Platelet derived growth factor
FGF	Fibroblast growth factor
HGF	Hepatocyte growth factor
KGF	Keratinocyte growth factor
TGF	Transforming growth factor
EGF	Epithelial growth factor
IGF	Insulin growth factor
HBEGF	Heparin binding EGF like growth factor
MIF	Macrophage migration inhibitory factor
TNF	Tumor Necrosis factor
CSF	Colony stimulating factor
ANGPT	Angiopoietin
ASC	Adipose derived stem cells

GFP	Green fluorescent protein
AAV	Adeno associated virus
PLGF	Placental growth factor
MAPK	Mitogen activated protein kinase
ECM	Extracellular matrix
PKB	Protein kinase B
MMP	Matrix metalloproteinases
ERK	Extracellular regulated kinase
PI3-K	Phosphatidyl inositol 3' kinase
FAK	Focal adhesion kinase
Flt-1	Fms-related tyrosine kinase 1
SVF	Stromal vascular fraction
KDR	Kinase insert domain
HIF	Hypoxia inducible factor
PBAE	poly β-amino ester
LLLT	Low level light therapy
ORF	Open reading frames

ELISA	Enzyme-linked immunosorbent assay
ABAM	Antibiotics and antimycotics